Hydrogel with Selective Absorption for Separation of Liquid Mixtures

By

Anjana Maharjan

Submitted to the Department of Mechanical Engineering and the Graduate Faculty of the University of Kansas in partial fulfillment of the requirements for the degree of Master of Science

Dr. Gibum Kwon, Chair

Committee members

Dr. Huazhen Fang

Dr. Prajnaparamita Dhar

Date defended: August 28, 2018

The thesis committee for Anjana Maharjan certifies that this is the approved version of the following thesis:

Hydrogel with Selective Absorption for Separation of Liquid Mixtures

Dr. Gibum Kwon, Chair

Date approved: August 28, 2018

Abstract

Separation of liquid mixtures is crucial in many industries including petrochemicals, mining, leather, food, steel and metal processing. Conventional separation technologies such as distillation and liquid-liquid extraction are limited by high energy consumption, the inability to separate azeotropes (constant boiling mixture) or post treatment after separation. Therefore, there is a dire need to develop an energy efficient methodology to separate liquid mixtures.

Absorption is a promising alternative that can separate liquid mixtures by selectively absorbing one phase over the other. In this work, we report a hydrophilic (water-loving) and oleophobic (oil-hating) hydrogel by copolymerizing N-Isopropylacrylamide (NIPAM) with 1H,1H,2H,2H-Heptadecafluorodecyl acrylate (F-acrylate) (F-NIPAM). Our F-NIPAM can selectively absorb polar liquids while repelling non-polar liquids. Utilizing selective absorption, we demonstrate separation of both immiscible oil-water mixtures and miscible polar-non-polar liquid mixtures including heptane-ethanol and methanol-methyl oleate. Our F-NIPAM's selective absorption can be characterized by the Flory-Huggins polymer-solvent interaction parameter (χ). The χ values of our F-NIPAM with polar liquids are ≤ 0.5 while that with non-polar liquids are greater than 0.5. Guided by the above principles, we also demonstrate separation of miscible polar-polar liquids by increasing the χ value for only one phase greater than 0.5. We also show that our F-NIPAM can release the absorbed liquid either by the application of mild heat or by submerging in an aqueous sodium chloride (NaCl) solution. Finally, we engineer an apparatus that allows for continuous separation of liquid mixtures and in situ release of the absorbed liquid from our F-NIPAM. Utilizing the apparatus, we successfully demonstrate the separation of oil-water mixtures and simultaneous recovery of the absorbed water.

Acknowledgements

I would like to extend a sincere amount of gratitude to my advisor, Dr. Gibum Kwon for his esteemed supervision, inspiring advice and enthusiastic encouragement during my time here. I am thankful for his strong belief in my abilities and for him constantly pushing me to be a better researcher and to do my personal best. I am grateful to Dr. Huazhen Fang and Dr. Prajnaparamita Dhar for agreeing to be a part of my thesis committee and for their valuable time.

Additionally, I am sincerely thankful to all faculty members in the Department of Mechanical Engineering for their time, effort, and guidance towards providing me with a quality engineering education. The financial support provided by the Department of Mechanical Engineering is appreciated. I am thankful to my colleagues in the lab for their support and technical assistance during my research work.

Last but not least, I would like to thank my family and friends for their continuous support and positive encouragement throughout my study.

Table of Contents

List of Figures

List of Tables

1. Introduction

Separation of liquid mixtures is crucial in many industries including petrochemicals, mining, leather, food, steel and metal processing[1]. By consuming about 4500 TBtu/year, separation processes account for one-fourth of in-plant energy usage in the United States[2]. The major separation technologies utilized in industries include distillation[3], evaporation[4], extraction[5], absorption[6], and membranes[7]. Among all, distillation is by far the most prevailing separation process in industries[8,9]. It is based on the difference in vaporization of mixture components[10]. Since distillation is thermally-driven process, it is highly energy intensive that accounts for about 49% of the separation energy in industries[2,11] (Fig. 1.1). Therefore, there is an immense need to develop energy-efficient alternatives for distillation. Application of energy efficient separation in industries can save billions of dollars of energy costs[12].

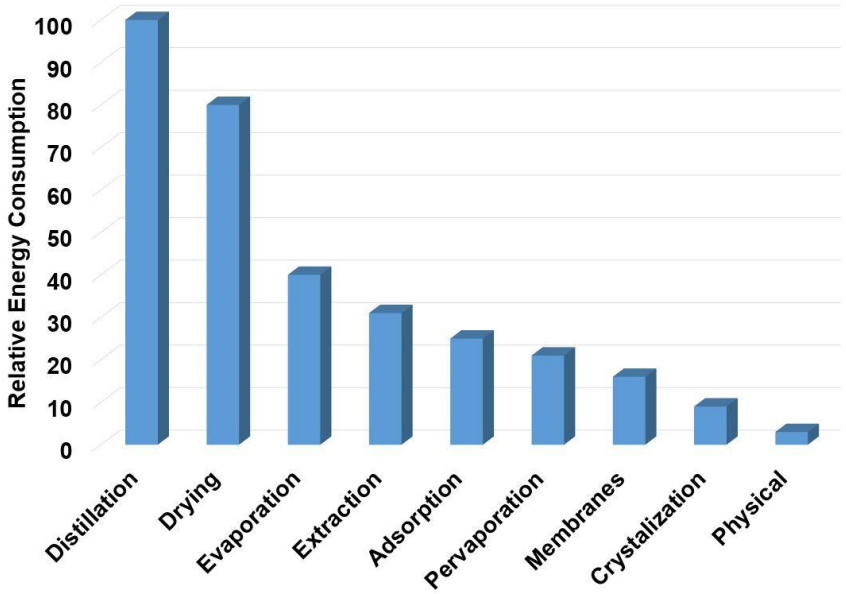

Fig. 1.1. A graph showing relative energy consumption of various separation technologies[13]. Distillation, drying and evaporation are thermally-driven processes while extraction, adsorption, membranes, crystallization are low-energy consuming methods.

Liquid-liquid extraction (LLE)[5] is a promising technology because it is relatively energy efficient and can separate azeotropes (i.e., components of a mixture have the same boiling points)[14,15]. LLE separates a liquid mixture by adding a phase separating agent (i.e. extractant) that has a different solubility for the mixture components[16]. LLE can be operated at a lower temperature and atmospheric pressure that allows for energy savings[17]. One major disadvantage of LLE is the recovery of extractant after the separation process[2]. Typically, the recovery of extractant is accomplished by energy intensive distillation.

Absorption-based techniques have the potential to improve the energy efficiency by an order of magnitude than the heat-driven separation methods such as distillation[12]. Absorption is a simple method in which an absorbing material (absorbent) can be directly submerged into the liquid mixture[6,18]. In order for effective separation of liquids using absorption, the absorbents should selectively absorb one phase over the other in a liquid mixture[19]. Such a selective absorption can be achieved when the absorbents have preferential wettability (Fig. 1.2). For instance, the absorbents that can be wet by oil (oleophilic, OL) while repelling water (hydrophobic, HP) can typically absorb oil and repel water[20,21]. As a result, such OL/HP absorbents can selectively absorb oil from an oil-water mixture[22,23]. Similar to OL/HP materials, a material can selectively absorb water (hydrophilic, HL) while repelling oil (oleophobic, OP) can also separate oil-water mixtures [24]. However, fabricating HL/OP has been considered challenging because the surface tension of water (γ_{water} = 72.1 mN/m)[25] is significantly higher than oils (γ_{oil} = 20-30 mN/m)[26]. HL/OP materials have the advantage of efficient separation of liquid mixtures with prolonged lifespan because of their antifouling properties[19,27].

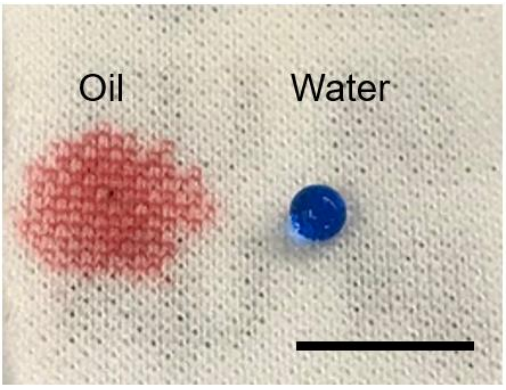

Fig. 1.2. An image showing oil and water contacting on oleophilic/hydrophobic (OL/HP) surface. On the surface, oil can wet the surface while water is repelled. Scale bar: 1 cm.

In this work, we fabricated hydrogel (absorbent) with selective wettability (HL/OP) and demonstrated that it can separate liquid mixtures by selective absorption. We fabricated our HL/OP hydrogel by copolymerizing N-Isopropylacrylamide (NIPAM) and 1H,1H,2H,2H-Perfluorodecyl acrylate (F-acrylate) resulting in hydrophilic and oleophobic F-NIPAM. The intrinsic hydrophilicity of NIPAM combined with a low surface energy material (F-acrylate) provided unique HL/OP wettability. Our F-NIPAM can selectively absorb polar liquids (e.g. water and alcohols) while repelling non-polar liquids (oils) resulting in effective separation of liquids. We also demonstrated that our F-NIPAM can selectively absorb one phase over the other from either miscible polar-non-polar liquid mixtures such as ethanol (polar)-heptane (non-polar) and methanol (polar)-methyl oleate (non-polar) or polar-polar liquid mixtures including water-DMF and water-ethanol. We also studied the relation of Flory-Huggins[28,29] polymer-solvent interaction parameter (χ) and our F-NIPAM's absorption behavior. We found that our F-NIPAM can selectively absorb one phase over the other if the χ value for the phase χ_1 is significantly lower than the other χ_2 (i.e. $\chi_1 << \chi_2$) and $\chi_1 \leq 0.5$. We further demonstrated that the absorbed liquid can be recovered from F-NIPAM by either heat or the presence sodium chloride ions. In the heat assisted method, the

absorbed water can be recovered with a mild heat treatment to increase the temperature to 33°C. As NIPAM is thermo-responsive, the absorbed water is released at a temperature (T = 33°C) above the lower critical transition temperature (LCST) (T ≈ 29°C) of our F-NIPAM. We also demonstrated that the absorbed ethanol can be released by submerging our F-NIPAM in an aqueous sodium chloride (NaCl) solution. Finally, we engineered a continuous separation apparatus that allows for simultaneous separation of liquid mixtures and recovery of the absorbed liquids.

2. Background

2.1. Fundamentals of Surface Wettability

Surface wetting is observed when a liquid droplet contacts a surface. The contacting liquid droplet can either spread or get repelled by the surface[30,31]. This surface wettability can be characterized by the contact angle between the liquid and solid surface[32,33]. The contact angle for a liquid droplet on a smooth surface is given by the following Young's relation[34]:

$$\cos\theta = \frac{\gamma_{SV} - \gamma_{SL}}{\gamma_{LV}} \tag{1}$$

where θ is Young's contact angle and $\gamma_{SV}, \gamma_{LV}, \gamma_{SL}$ refer to the solid surface energy, liquid surface tension and the solid-liquid interfacial tension, respectively. Depending on these interfacial energies between the solid surface, liquid and air, a liquid exhibits higher or lower contact angle on a surface[35]. Fig. 2.1 shows a liquid droplet contacting on a smooth surface.

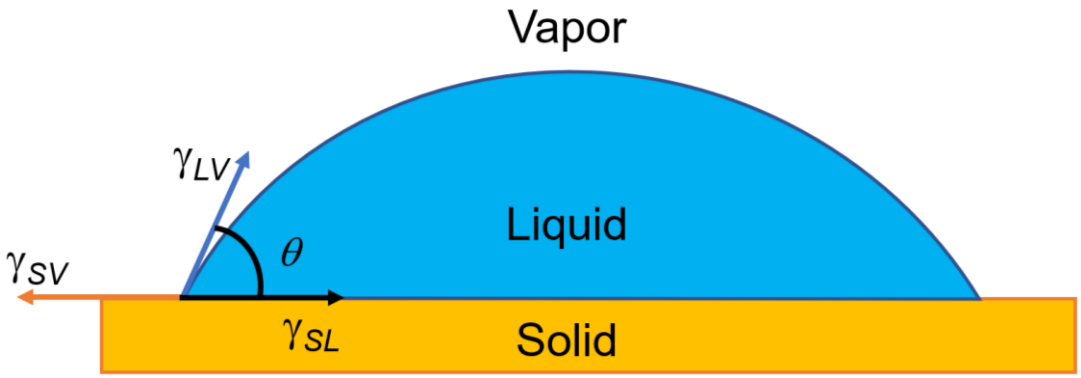

Fig. 2.1. A schematic illustrating a contact of a liquid droplet on a smooth surface.

It can be inferred from the Young' relation[34] (Eqn. 1) that the Young's contact angle (θ) increases with a decrease in the solid surface energy (γ_{SV}). The wettability of surfaces can be grouped into four categories[36] based on water contact angles: (i) superhydrophilic (SHL) when

$\theta_{water} \approx 0°$, (ii) hydrophilic (HL) when $\theta_{water} < 90°$, (iii) hydrophobic (HP) when $90° < \theta_{water} < 150°$, and (iv) superhydrophobic (SHP) when $\theta^*_{water} > 150°$ (Fig. 2.2).

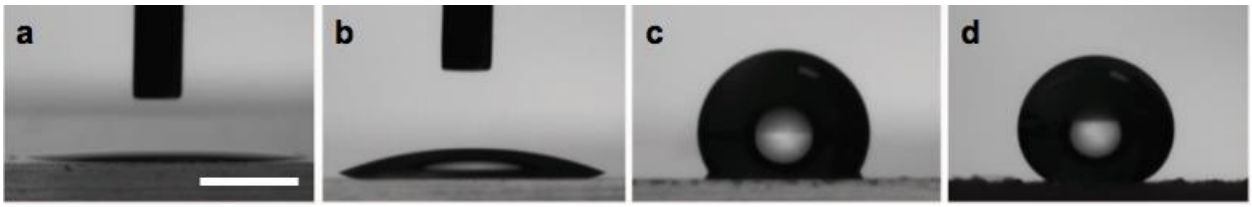

Fig. 2.2. Classification of surface based on the contact angles[36]. **(a)** Superhydrophilic ($\theta_{water} \approx 0°$). **(b)** Hydrophilic ($\theta_{water} < 90°$). **(c)** Hydrophobic ($90° < \theta_{water} < 150°$). **(d)** Superhydrophobic ($\theta^*_{water} > 150°$). Scale bar: 1 mm.

It is important to note that the Young's contact angle is the equilibrium contact angle on an ideally smooth surface. This implies that the Young' contact angle is difficult to measure experimentally[35]. Therefore the contact angles on a rough surface, apparent contact angles, are reported[37,38]. Apparent contact angles include (i) the advancing contact angle (θ_{adv}) when a liquid is spreading on a solid surface and (ii) the receding contact angle (θ_{rec}) while the droplet is being withdrawn from the wetted surface[32,39]. The advancing contact angle is typically the maximum contact angle while the receding contact angle is the minimum contact angle on a given surface[36,40]. The difference between these two contact angles is called the contact angle hysteresis ($\Delta\theta$)[41,42].

Contact angle hysteresis (i.e., $\Delta\theta = \theta_{adv} - \theta_{rec}$) is an important characteristic of the wettability of a surface[43-45]. Typically, a surface with a lower contact angle hysteresis ($\Delta\theta < 5°$) along with a very high contact angle ($\theta_{water} > 150°$) for water is considered superhydrophobic (Fig. 2.2d)[36]. Typically, a water droplet can roll off or bounce off a superhydrophobic surface[46-48].

A surface can also be classified into four groups based on the oil contact angles[36,49,50]: superoleophilic (SOL), oleophilic (OL), oleophobic (OP) and superoleophobic (SOP). A surface

is superoleophilic when $\theta_{oil} \approx 0°$, oleophilic when $\theta_{oil} < 90°$, oleophobic when $90° < \theta_{oil} < 150°$ and superoleophobic when $\theta^*_{oil} > 150°$. If a surface is both hydrophilic and oleophilic, it is called omniphilic. If a surface is both hydrophobic and oleophobic, it is called omniphobic. Similarly, if a surface is both superhydrophobic and superoleophobic, it is called superomniphobic[51].

Typically, a surface that can repel oil (oleophobic) can easily repel water (hydrophobic). This is because the surface tension of water (γ_{water} = 72.1 mN/m)[25] is significantly higher than that of oils (γ_{oil} = 20-30 mN/m)[19,52]. This can also be inferred from the Young's relation (Eqn. 1) that the higher the liquid-vapor interfacial energy (i.e. liquid surface tension, γ_{LV}), the higher would be the contact angle exhibited. On the other hand, a hydrophobic surface can be either oleophobic or oleophilic.

It can be inferred from the above discussion, developing hydrophilic (HL) yet oleophobic (OP) surface has been considered challenging. Only recently, we[53] and others[54-56] reported such hydrophilic and oleophobic surfaces utilizing the specific interactions between the surface and the contacting liquid. This results in lowering the interfacial energy between the solid and liquid (γ_{SL}). For example, when our hygro-responsive surface contacts a polar liquid such as water, it starts to reconfigure its surface chemistry to lower the overall free energy[57]. Such surface reconfiguration is known as a flip-flop mechanism[22]. Therefore, water can readily wet the surface. On the other hand, when oils (non-polar) come in contact, they are repelled by the surface (Fig. 2.3).

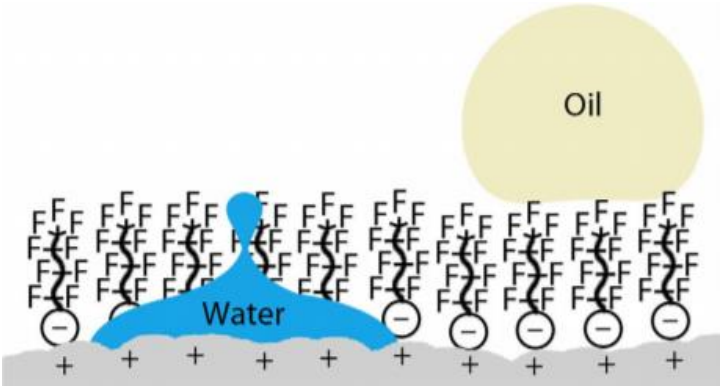

Fig. 2.3. A schematic showing the surface reconfiguration of a hydrophilic yet oleophobic (HL/OP) surface[22].

2.2. Repellent Surface Material

2.2.1. Low Surface Energy

It can be inferred from the Young's relation (Eqn. 1) that a surface with a lower surface energy (γ_{SV}) exhibits a higher contact angle for a given liquid. In order to achieve highly repellent surfaces (i.e., hydrophobic or oleophobic), surfaces are desired to possess lower surface energy[36,58]. According to previous reports[59,60], the surface energy decreases in the following order $-CH_2- > -CH_3 > -CF_2- > -CF_2H > -CF_3$. This indicates that increasing the number of fluorinated groups (CF_2 or CF_3) on the surface results in a lower surface energy, and thereby enhancing the liquid repellency. One of the most well-known fluorinated materials is Polytetrafluoroethylene (PTFE)[61]. It is also known as Teflon®. PTFE is a synthesized fluoropolymer with a very low surface energy ($\gamma_{SV} \approx 20$ mN/m). It is a chemically inert material allowing for the surface to be cleaned by solvents or submersion in chromic-sulfuric acid[61,62]. It is also stable at a very high temperature (≈ 250 °C)[62]. It is worth noting that the lowest surface energy (γ_{SV}) ever reported is about 6 mN/m using FluoroPOSS (Polyhedral oligometric silequioxane cages)[63,64].

2.2.2. Surface Roughness

The apparent contact angle θ^* on a rough surface is significantly different from the contact angle on a smooth surface (i.e., the Young's contact angle θ)[65,66]. A liquid droplet contacting a rough surface can take one of the following two configurations to minimize the overall free energy: the 'fully wetted' Wenzel state[67] or the 'composite' Cassie-Baxter state[68]. In the Wenzel state, the liquid droplet penetrates the surface texture and fully wets the surface. On the other hand, in the Cassie-Baxter state, the liquid droplet does not fully wet the surface texture and attains its equilibrium with the air pockets trapped underneath (Fig. 2.4).

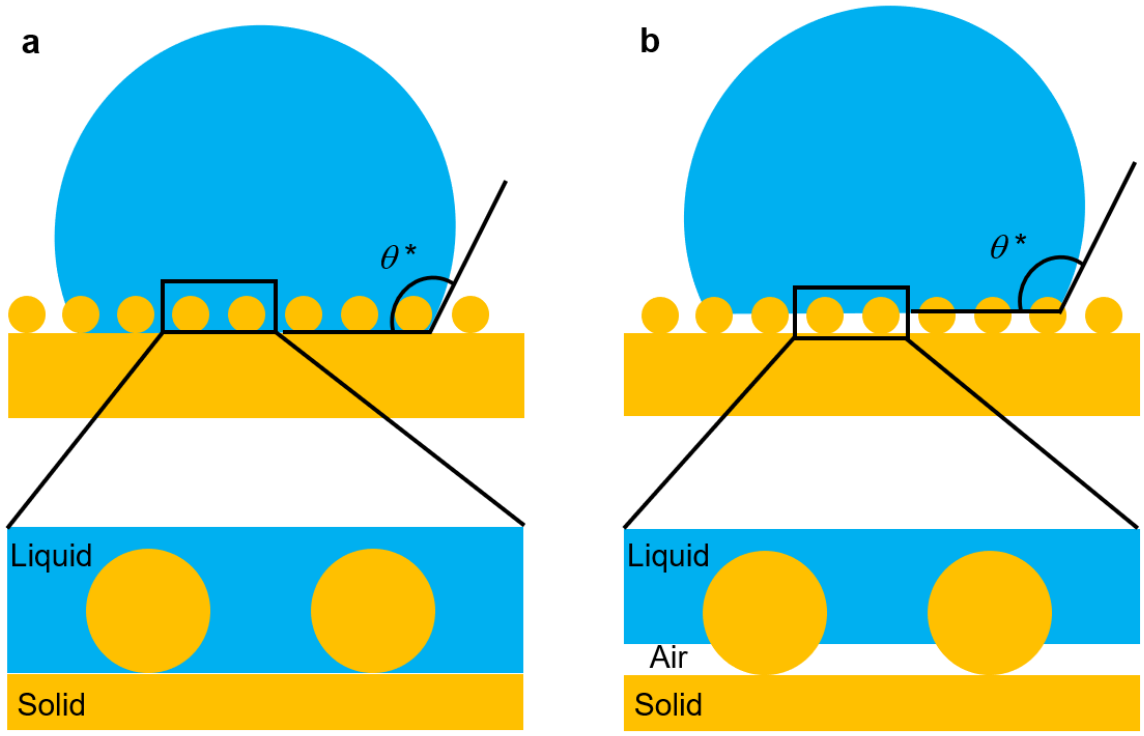

Fig. 2.4. A schematic showing a liquid droplet contacting a rough surface[36]. **(a)** Wenzel state. **(b)** Cassie-Baxter state.

When a liquid droplet is in the Wenzel state, the apparent contact angle θ^* is given by the following Wenzel relation[67]:

$$\cos\theta^* = r\cos\theta \quad (2)$$

where r is the surface roughness defined as the ratio of actual area to the projected area of the surface. θ is Young's contact angle. Here, the projected area is always less than the actual area of the surface leading to the value of r always greater than 1. As a result, the intrinsic wettability is always amplified. For a surface with $\theta < 90°$, the apparent contact angle $\theta^* << 90°$. Similarly, when $\theta > 90°$, the apparent contact angle $\theta^* >> 90°$. As the most surfaces exhibits $\theta < 90°$ for a low surface tension liquid such as oil (γ_{oils} = 20-30 mN/m), the apparent contact angle (θ^*) for oil is lower (i.e., << 90°).

When a liquid droplet is in the Cassie-Baxter state, the apparent contact angle is given by the following Cassie-Baxter relation[68]:

$$\cos\theta^* = f_{SL}\cos\theta + f_{LV}\cos\pi = f_{SL}\cos\theta - f_{LV} \quad (3)$$

where f_{SL} is the area fraction of the solid-liquid interface and f_{LV} is the area fraction of the liquid-air interface. It can be inferred that the Cassie-Baxter state allows for $\theta^* > 90°$ even for a liquid that exhibits $\theta < 90°$ on a surface. In addition, it is apparent that a surface would display higher apparent contact angles ($\theta^* >> 90°$) when the area fraction of liquid-vapor interface is high while the solid-liquid interface is sufficiently low. The Cassie-Baxter state can lead to a very high contact angle for a liquid with a low surface tension such as oil. Therefore, Cassie-Baxter state is preferred to develop repellent surfaces such as superoleophobic or superomniphobic surfaces.

2.3. Estimating the Solid Surface Energy

Owens-Wendt approach is used to estimate the solid surface energy (γ_{SV})[69]. According to this approach, the solid surface energy (γ_{SV}) can be divided into two kinds of intermolecular forces as:

$$\gamma_{SV} = \gamma_{SV}^{d} + \gamma_{SV}^{p} \tag{4}$$

γ_{SV}^{d} is the dispersive component that accounts for the dispersive forces while γ_{SV}^{p} is the polar component that accounts for polar forces such as hydrogen-bond or dipole-dipole interaction. Based on Owens-Wendt method, Fowkes[70] postulated the relation to estimate the interfacial energy of solid and liquid (γ_{SV}) given as:

$$\gamma_{SL} = \gamma_{SV} + \gamma_{LV} - 2\sqrt{\gamma_{SV}^{d}\gamma_{LV}^{d}} - 2\sqrt{\gamma_{SV}^{p}\gamma_{LV}^{p}} \tag{5}$$

where γ_{LV}^{d} is dispersive component of liquid surface tension accounting for dispersive forces and γ_{LV}^{p} is the polar component accounting for the polar forces. From the Young's relation (Eqn. 1), Eqn. 5 for a non-polar liquid ($\gamma_{LV}^{p} = 0$) such as oil can be rewritten as:

$$\gamma_{SV}^{d} = \gamma_{LV}\left(\frac{1+\cos\theta}{2}\right)^{2} \tag{6}$$

Eqn. 6 is utilized to determine the dispersive component of the solid surface energy. Here, the contact angle θ and γ_{LV} is the surface tension for a non-polar liquid. Now, to determine the polar component of the solid surface energy (γ_{SV}^{p}), Eqn. 5 and the Young's relation (Eqn. 1) for a polar liquid ($\gamma_{LV}^{p} \neq 0$) gives the following equation.

$$\gamma_{SV}^{p} = \frac{1}{\gamma_{LV}^{p}} \left[\frac{\gamma_{LV}\left(1+\cos\theta\right)}{2} - \sqrt{\gamma_{SV}^{d}\gamma_{LV}^{d}} \right]^2 \quad (7)$$

Finally, the dispersive and polar components determined from Eqns. 6 and 7 is substituted into the Eqn. 4 to determine the total solid surface energy.

2.4. Separation of Liquid-Liquid Mixtures

A liquid can be classified into two groups based on the polarity. A polar liquid is composed of molecules that have unsymmetrical polar bonds. A non-polar liquid consists of molecules with symmetrical polar bonds that cancel each other or contain no polar bonds. Water, alcohols, or acids are polar liquids while most oils and alkanes are non-polar.

When two or more liquids are mixed, they can be either miscible or immiscible. If the liquids form separate phases when they are mixed, it is an immiscible liquid mixture. One of the most well-known immiscible liquid mixtures is oil and water[7,71]. Such immiscible oil-water mixtures are classified[72] as free oil-water, dispersion or emulsions. Free oil-water is a simple form of oil and water with the dispersed phase diameter $d > 150$ μm. If $150\ \mu m \geq d \geq 20\ \mu m$, it is called dispersion. When an oil-water mixture shows $d < 20$ μm, it is called an emulsion.

In order to fabricate a stable oil-water emulsion, surfactants can be used. The surfactant molecules surround the dispersed phase and prevent coalescence of dispersed phase droplets. When oil is dispersed in water, it is called oil-in-water (O/W) emulsion. If water is dispersed in oil, it is called water-in-oil (W/O) emulsion. To produce O/W emulsion, water-soluble surfactants such as sodium dodecyl sulfate (SDS) is used. W/O emulsion can be prepared by using oil-soluble surfactant such as span80. Other forms of emulsions also exist such as oil-in-water-in-oil (O/W/O)[73] and water-in-oil-in-water (W/O/W)[74].

Unlike immiscible liquid mixtures, miscible liquid mixtures show two liquids forming a completely homogeneous phase when they are mixed. Typically, two liquids of the same polarity (i.e. polar-polar or non-polar-non-polar) are miscible. Alcohol-water, acetone-water, benzene-cyclohexane and chloroform-hexane are the examples of such miscible liquid mixtures. Polar and non-polar liquids can also form a miscible mixture including alkane-alcohol and ester-alcohol.

Separation of miscible liquid mixtures is critical in practical applications. For instance, in petroleum refining industries, sulfur, nitrogen and metal compounds need to be separated from the crude oil[75]. Biofuel (i.e. biodiesel and bioethanol) production requires separation of miscible byproducts such as methanol from the final fuel[76,77]. In the agroindustrial sector, the organic acids need to be removed from the wastewater to prevent environmental pollution[78]. Compared to immiscible liquid mixtures, separating miscible liquid mixtures is often challenging. Distillation is perhaps the one of the most popular technique for separation[13]. It is based on the difference in the boiling temperatures of each component[3]. However, it is energy-intensive and cannot separate an azeotrope (i.e. a mixture with a constant boiling temperature of components). Therefore, there is a critical need to develop energy efficient technique to separate liquid mixtures.

2.5. Methodologies of Separation of Liquid Mixtures

2.5.1. Conventional Methodologies

To separate liquid mixtures, various technologies and methods have been adopted. Conventional methods include gravity separation[79], air flotation[80], coagulation and flocculation[81], ultrasonic separation, and distillation[72,82]. The gravity separation method is effective for separation of free oil and water. Air flotation is the process of separation based on the floating density difference. For instance, small oil droplets can be separated from water by increasing the buoyancy of oil. This

process is followed by demulsification process with chemicals and heat. In coagulation, the chemicals or coagulants are added for aggregation to enhance the separation of oil from water. Although they are effective to break emulsions (i.e. demulsification), they are energy-intensive and lead to secondary pollution.

The methods discussed above are effective in separation of immiscible liquid mixtures, however, they are not suitable to separate miscible liquid mixtures. Distillation is perhaps the most widely used separation technique, based on the difference in boiling points of the components[8,83]. Although distillation is a simple and well-established technique, it is highly energy-intensive and needs the thermal stability of compounds at vaporization points[84,85]. Moreover, the conventional distillation is not suitable to separate azeotropes[16,86]. This is because the azeotropic components have the same boiling points. In order to separate azeotropes, it needs to change the operating pressure or other chemicals are added to break azeotropes to form heterogeneous ternary azeotropes[87-89].

Liquid-liquid extraction (LLE) is effective to separate azeotropes, where conventional distillation cannot be used[5,14,16]. In this method, the components of liquid mixtures are separated with the help of another insoluble liquid (i.e. extractant) which has a different solubility for the components[5]. As a result, when an extractant is added into the mixtures, phase separation occurs. Effective liquid-liquid extraction can be achieved by increasing the interfacial area between the two phases and an extractant. This can be achieved by ultrasonicating or pumping the liquids through highly tortuous columns[90,91]. Emulsification can also enhance the LLE process by providing a large interfacial area between the phases and an extractant[92,93]. However, subsequent

separation of these emulsions is often challenging. Further, post-treatment to recover the extractant and clean the residual liquid is needed.

2.5.2. Membrane-Based Separation

It is apparent that the conventional separation methods including distillation[3], liquid-liquid extraction[5] are limited by either a large energy consumption, excessive cost, or secondary pollution. Membrane-based separation techniques are versatile and relatively energy efficient (i.e. in the order of thousands of times more energy efficient) than heat driven distillation[85].

Membranes can separate liquid mixture by allowing one phase to permeate through while the other phase is retained[13]. The phase that passes through the membrane is called as the permeate while the phase that is retained by the membrane is called as the retentate. In the membrane-based separation, the mass transfer occurs with the help of a driving force that acts individually to the phases of the mixture[94]. This driving force can be a pressure gradient, temperature, concentration difference or electrical potential[94]. The separation based on pressure gradient including microfiltration, ultrafiltration, and reverse osmosis are commonly used[95,96]. Recently we[53] showed that membranes should possess selectivity for one phase over the other for an effective separation. Such selectivity can be achieved by selective wettability (either hydrophilic/oleophobic or hydrophobic/oleophilic)[97-99]. The hydrophilic/oleophobic membranes allow water (polar liquid) to permeate through while repelling oil (non-polar liquid)[100]. On the other hand, hydrophobic/oleophilic membranes allow oil to permeate through while repelling water. We[53] and others[27,101] found that hydrophilic/oleophobic membranes exhibit highly resistance to fouling by oil.

2.5.3. Absorption

Absorption is the process that a liquid enters to an absorbent (solid) and gets retained[102,103]. As it can be performed at ambient conditions (i.e. room temperature and one atmospheric pressure), it allows for energy-efficient separation of liquid mixtures. One advantage of absorption-based separation technique is that an absorbing material (absorbent) can be directly applied to the liquid mixture, unlike the membrane-based filtration where a liquid mixture needs to be passed through the filtration apparatus[104]. Moreover, membrane-based separation requires both a special apparatus to mount the membranes and an external driving force (e.g., pressure gradient, concentration difference, and potential difference) to force the feed liquid mixtures through the membrane[94]. Compared to membrane-based separation, absorption is a simple and straightforward process.

Different forms and types of absorbent materials have been studied for separating liquids[18,105-107]. Natural materials (cotton, floss, kapok, and wool), minerals (zeolites, clay, aerogels, graphite and activated carbon) and polymers (polyurethane forms, rubbers, and polypropylene) are used. The absorbents can be in the form of porous media, particles, gels, and nanocomposites. For an effective separation of liquids, the absorbents should selectively absorb one phase over the other in the liquid mixture[23,108,109]. Such selective absorption can be achieved by possessing preferential wettability.

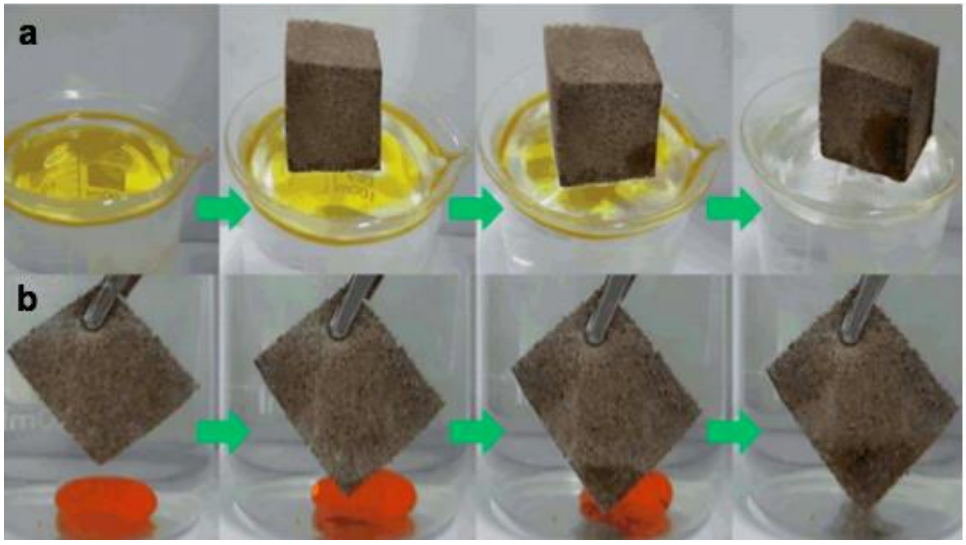

Fig. 2.5. Hydrophobic/oleophilic melamine sponges for oil-water separation. **(a)** Removal of hexane from the water. **(b)** Removal of dichloromethane from the water[110].

For instance, hydrophobic and oleophilic absorbents can absorb oil while repelling water that can lead to an effective separation of oil-water mixtures. Lei et. al[110] reports hydrophobic and oleophilic sponges that can selectively absorb oil from the oil-water mixture with high separation efficiency (Fig. 2.5). The sponges were melamine polymers that were submerged in alkali lignin and carbodiimide-modified diphenylmethane diisocyanate to obtain highly hydrophobic yet oleophilic wettability.

Although there are numerous reports of hydrophobic and oleophilic (HP/OL) absorbents for separating oil-water mixtures, hydrophilic and oleophobic (HL/OP) absorbents have been considered challenging to fabricate since water surface tension (γ_{water} = 72.1 mN/m)[25] is significantly higher than that of oil (γ_{oil} = 20-30 mN/m)[26].

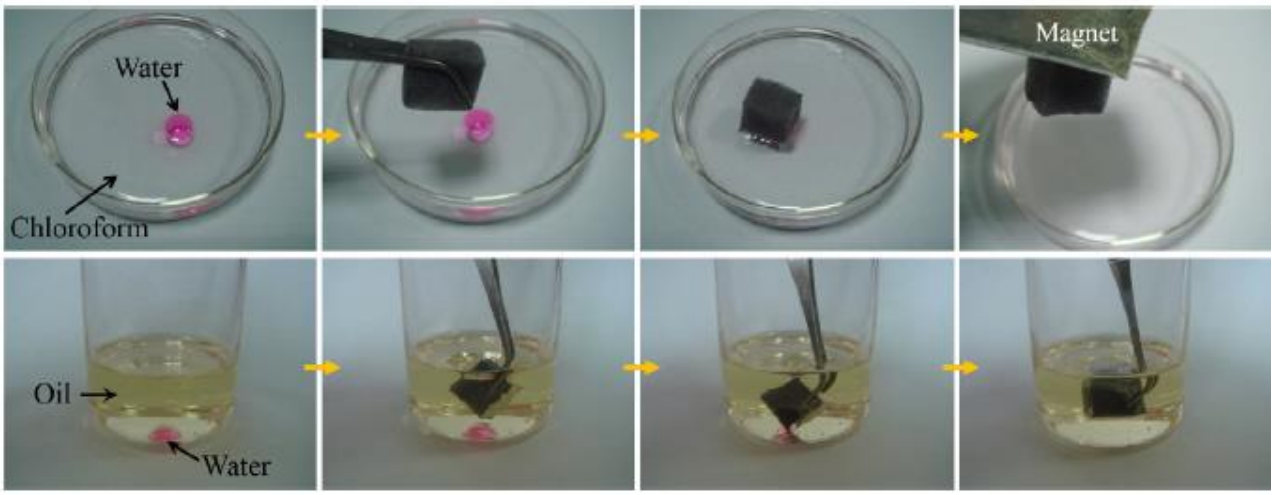

Fig. 2.6. Hydrophilic and oleophobic sponge selectively absorbing water from the oil-water mixture[24].

Only recently, a few groups fabricated hydrophilic and oleophobic absorbents[19,24]. Fig. 2.6 shows that hydrophilic and oleophobic sponge can effectively separate an oil-water mixture by selectively absorbing water. The absorbent was prepared by dipping the melamine sponge in a perfluorinated solution. The motion of hydrophilic/oleophobic (HL/OP) sponges could be easily controlled by a magnet.

Recently, there has been a development of smart absorbents that can switch their wettability in response to pH change[111], electric-field[112], magnetic-field[113] or light[114]. However, these absorbents have been limited to separation of immiscible liquid mixtures such as oil and water. Separating miscible liquids such as heptane-ethanol or azeotropes is far difficult than separating immiscible liquid mixtures. Typically, separation of miscible liquids is accomplished by distillation which requires an elevated temperature or high operating pressure. To our knowledge, there are no reports of separation of miscible liquids such as ethanol-water and the azeotropes at ambient conditions (i.e. room temperature and one atmospheric pressure) using selective absorption.

2.6. Hydrogels

Hydrogels are three dimensional, cross-linked networks of polymer that can swell extensively without dissolving in polar liquids (e.g. water)[115]. Hydrogels have the ability to retain the absorbed liquid (water) in their cross-linked network. This is different from the sponges which readily may lose the absorbed liquid. Hydrogels can easily conform to the shape of that they are applied. Therefore, they can be prepared in different shapes and sizes (either micro- or nano-)[116]. In addition, their biocompatibility and intrinsic hydrophilicity allow them to be used in a wide range of different applications including drug delivery[117], separation[118], contact lenses[119], superabsorbents[120], and wound dressings[121].

Hydrogels can be classified into physical or chemical gels depending on how their networks are crosslinked[116,122]. In physical gels, the networks are held together either by polymer chain entanglements or by physical interactions such as hydrogen bond, ionic bond or hydrophobic-hydrophobic interactions. On the other hand, chemical gels possess network cross-linked by covalent bonding. Hydrogels can also be divided into natural or synthetic hydrogels[122,123]. Examples of natural hydrogels include proteins like collagen and polysaccharides like chitosan and dextran. Examples of synthetic hydrogels include acrylamide, ethylene glycol, and lactic acid.

2.7. Thermo-responsive Hydrogel

Thermo-responsive hydrogels are unique because they can undergo conformational (shape) changes with changes in temperature[124,125]. N-Isopropylacrylamide (NIPAM) is perhaps the most extensively studied thermo-responsive hydrogel that can transition from coil to globule structure in response to change in temperature[125]. The temperature at which the transition takes place is

called the lower critical solution temperature (LCST)[125,126]. It is well-known that the LCST of NIPAM is about 32°C[127-129]. When the temperature is below the LCST, NIPAM can absorb water and swell. When the temperature is above the LCST, NIPAM releases the absorbed water and shrinks[130].

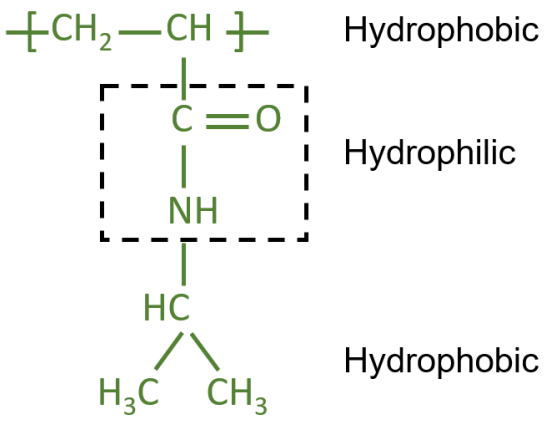

Fig. 2.7. A schematic of NIPAM molecular structure indicating its hydrophobic and hydrophilic groups.

Fig. 2.7. shows the chemical structure of NIPAM. NIPAM possesses both hydrophilic amide group (-CONH) and hydrophobic isopropyl group (-CH(CH_3)$_2$). When NIPAM contacts water below its LCST (≈ 32°C)[127], it hydrogen bonds with water through its amide group[131,132]. Simultaneously, the isopropyl group involves in hydrophobic hydration[133]. Such hydrophobic hydration allows water to form a cage (i.e. hydration shell) around the isopropyl group. Forming hydration shell is energetically favorable since water molecules form stronger hydrogen bonds with NIPAM than when they are freely located[134]. When the temperature increases above the LCST, the hydrophobic interaction between the isopropyl groups driven by entropic contribution prevails resulting in the polymer collapse releasing water from the network[127,135].

Swelling behavior of hydrogels can be determined by the Flory-Huggins polymer-solvent interaction parameter (χ)[28,29]. The χ parameter, a measure of the strength of repulsive interaction between a polymer and solvent, can characterize the tendency of swelling a hydrogel in a solvent[136]. For example, a lower value of χ with a solvent indicates a good solvent for the hydrogel[137]. It is known that the limiting value of the χ parameter for a 'marginal solvent' is 0.5[136]. When $\chi \leq 0.5$, a polymer is soluble in a solvent in all compositions, which is also true for the swelling hydrogels[136,138].

The interaction parameter χ can be estimated by Hansen solubility parameters[137] as:

$$\chi = \alpha \frac{V}{RT}\left[\left(\delta_{D2} - \delta_{D1}\right)^2 + 0.25\left(\delta_{P2} - \delta_{P1}\right)^2 + 0.25\left(\delta_{H2} - \delta_{H1}\right)^2\right] \quad (8)$$

where δ_D, δ_P, and δ_H are the Hansen solubility parameters accounting for dispersive, polar and hydrogen bonding interactions respectively. V is the molar volume of the solvent, R is the universal gas constant, T is the absolute temperature. α is a correction factor, typically 0.35. It is apparent from Eqn. 8 that the χ value is smaller when the Hansen solubility parameters between the polymer and solvent are closer. It is also reported that similar solubility parameters between a polymer and a solvent indicate extensive swelling of a hydrogel in a given solvent[139]. The Hansen solubility parameters can be determined from the group contribution method of Hoftyzer and Van Krevelen[140,141] as:

$$\delta_D = \frac{\sum F_{di}}{V}, \delta_P = \frac{\sqrt{\sum F_{pi}^2}}{V}, \delta_H = \frac{\sqrt{\sum E_{hi}}}{V} \quad (9)$$

where F_{di}, F_{pi} and E_{hi} are the group contributions to the dispersion, polar and hydrogen-bonding respectively. The group contributions (F_{di}, F_{pi} and E_{hi}) for different structural groups are given in Table 2.1.

Table 2.1. A table showing the group contributions for different structural groups for Hoftyzer-Van Krevelen method[141].

Structural groups	F_{di} $(\sqrt{\mathbf{MJ/m^3}}\,\mathbf{/mol})$	F_{pi} $(\sqrt{\mathbf{MJ/m^3}}\,\mathbf{/mol})$	E_{hi} **(J/mol)**
-CH_3	420	0	0
-CH_2-	270	0	0
>CH-	80	0	0
=CH_2	400	0	0
=CH-	200	0	0
=C<	70	0	0
>C<	-70	0	0
-F	220	-	-
-Cl	450	550	400
-Br	550	-	-
-CN	430	1,100	2,500
-OH-	210	500	20,000
-O-	100	400	3,000
-COH	470	800	4,500
-CO-	290	770	2,000
-NH-	160	210	3,100

>N-	20	800	5,000
$-NO_2-$	500	1,070	1,500

2.8. Absorption and Swelling Behavior of Hydrogel

Swelling is a unique phenomenon of hydrogel[115]. It is a continuous process that occurs from the combined effect of solvent transport and polymer network deformation. It depends on the interaction between a polymer and solvent. When a hydrogel contacts a thermodynamically compatible solvent, the solvation of polymer chains causes the network to expand. As a result, the solvent molecules are absorbed into the polymer network. The solvent transport in the network is favored by osmotic pressure difference. On the other hand, it is opposed by the elastic retraction force due the presence of covalent or physical cross-linking junctions in the network. Balancing of these osmotic and retraction forces allows the hydrogel to reach an equilibrium swelling state[142].

Different models have been presented to describe the kinetics of hydrogel swelling[143,144]. In most of the cases, swelling kinetics can be described by the first-order rate equation. This is a simplified form of the rigorous and formal equation provided by Li and Tanaka[144-147]. In the first order kinetics, the swelling at any given time (t) is proportional to the remaining uptake of swelling medium at that particular time[148].

$$\frac{dU}{dt} = k\left(U_{eq} - U\right) \tag{10}$$

where U_{eq} is the equilibrium uptake of a solvent in the hydrogel, U is the uptake at any given time (t), k is the rate constant. The solution of Eqn.10 is:

$$U = U_{eq}(1 - e^{-kt}) \tag{11}$$

Eqn. 11 gives the uptake of a solvent at a particular time as a function of equilibrium uptake and the rate constant. The swelling ratio (*S.R.*) is defined as:

$$S.R. = \frac{U}{W_s} = \frac{W - W_o}{W_s} \tag{12}$$

where W is the hydrogel weight at a given time (t), W_o is the original hydrogel weight, and W_s is the weight of the polymer in the hydrogel (i.e. without water). Combining Eqns. 11 and 12, the following relation can be obtained:

$$S.R. = S.R._{eq}(1 - e^{-kt}) \tag{13}$$

First order kinetics can accurately describe the swelling of different hydrogels in water as well as their shrinkage. There may be some deviations when hydrogel extensively swells[148]. For a gel of thickness, h, remains constant during the diffusion with diffusion coefficient, D, occurring perpendicular the thickness, and the time taken for swelling is sufficiently large, the rate constant (k) can be given as[148]:

$$k = \frac{\pi^2 D}{h^2} \tag{14}$$

During the swelling process, the hydrogel transforms into softer and rubbery gels as the solvent molecules dilute the polymer network. The local viscosity is reduced resulting in a slow increase of the diffusion coefficient (D). Therefore, when the swelling of polymer is extensive, increase in D is compensated by the increase of h^2. Since the diffusion coefficient (D) increases less than h^2, there is declination of k. This may lead to a small deviation from the first order kinetics when the polymer swelling is extremely high[148].

The swelling behavior of a hydrogel can be altered by the presence of salt ions[149,150]. Typically, hydrogels deswell in the presence of the salt ions. Ions can be ranked in the Hofmeister series, which is based on the capability of ions to precipitate out proteins from an aqueous solution[150]. It is reported that anions can affect water molecules associated with the hydrogel network[151]. The anions can polarize water molecules that are hydrogen bonded with amide groups resulting in a decrease of hydrogen-bonded water with hydrogel. In addition, the anions can affect the water molecules involved in hydrophobic hydration around isopropyl groups resulting in disruption of water cage formed around the isopropyl groups. This leads to the deswelling of the hydrogel.

3. Experimental Details

3.1. Materials and Equipment

Photocuring of the hydrogel (i.e. light-induced cross-linking) was conducted using the UVGL-55 handheld ultraviolet (UV) lamp. N-Isopropylacrylamide (NIPAM, chemical formula $C_6H_{11}NO$) was purchased from Alfa Aesar, N,N'-Methylenebisacrylamide (MBAA, chemical formula $((CH_2=CHCONH)_2CH_2$) and 2-Hydroxy-2-methyl-propiophenone (darocur 1173, chemical formula $C_6H_5CO(CH_3)_2OH$) were purchased Sigma-Aldrich. 1H,1H,2H,2H-Heptadecafluorodecyl acrylate (F-acrylate, chemical structure $H_2C=CHCO_2CH_2CH_2(CF_2)_7CF_3$) was purchased from Acros Organics. Sylgard® 184 silicone elastomer kit (base and the curing agent) was purchased from Dow Corning Corporation.

Contact angle measurements were conducted using Ramé-hart 190-U1 contact angle goniometer. Liquids n-hexadecane (Alfa Aesar), dodecane (Acros Organics), n-heptane (Fisher Scientific), ethanol (Fisher Scientific), and deionized (DI) water filtered from Milli-Q® Advantage A10® System were utilized. Glass slides were purchased from Fisher Scientific. Various alcohols including methanol (Fisher Scientific), butanol (Acros Organics), pentanol (Alfa Aesar), hexanol (Alfa Aesar) and heptanol (Alfa Aesar) were used for the absorption experiments. Surfactants sodium dodecyl sulfate (SDS) and span80 were purchased from Fisher Scientific and TCI (Tokyo chemical industries) America respectively. The refractive index measurements were performed using r^2i300 automatic refractometer purchased from Reichert Technologies. Experiments at elevated temperatures were performed using the Ramé-hart hot plate (contact angle analysis) and Fisher Scientific Isotemp (absorption experiments).

3.2. Methodologies

3.2.1. Fabrication of Fluorinated NIPAM (F-NIPAM)

NIPAM monomer, MBAA cross-linker and darocur 1173 photo initiator were mixed in the weight ratio of 97:1:2. DI water was added to the mixture making the total concentration of 200 mg/mL. The mixture was then stirred for 30 minutes to make a monomer solution. Next, F-acrylate solution was prepared by dissolving the F-acrylate in ethanol with the total concentration same as monomer solution. The resulting F-acrylate and monomer solution were mixed in the desired proportion and stirred vigorously for 30 minutes to make F-NIPAM solution. Of note, the solutions were prepared in dark to prevent light exposure and unexpected cross-linking.

F-NIPAM solution of a given volume was pipetted out and exposed to ultraviolet light (UV-A, λ = 365 nm) for the cross-linking. The cross-linked F-NIPAM was prepared either as a thin film or a cubic block of the hydrogel.

3.2.1.1. Preparation of a Smooth F-NIPAM Film

F-NIPAM films were prepared by drop casting of F-NIPAM solution in a glass slide. 300 μL of F-NIPAM solution was drop casted on a 2 cm × 2 cm glass slide. The solution on the glass slide was then exposed to UV-A for 10 minutes to allow the cross-linking process to occur. The distance between the UV-A lamp and glass slide was set to 10 cm. We found that the thickness is about 100 μm.

3.2.1.2. Preparation of F-NIPAM Blocks

F-NIPAM blocks were prepared by pouring F-NIPAM solution in a cubic polydimethylsiloxane (PDMS) mold. 1 mL of F-NIPAM solution was pipetted out and carefully poured into the cavity

of the PDMS molds. The solution in the PDMS molds was then exposed to UV-A for 15 minutes for cross-linking.

3.2.2. Characterization of F-NIPAM

Chemical, thermal and surface properties of F-NIPAM were characterized using various methods. Differential scanning calorimetry (DSC) was performed to investigate the effect of F-acrylate on the lower critical solution temperature (LCST) of F-NIPAM, Fourier transform infrared spectroscopy (FTIR) was performed to ensure copolymerization of NIPAM with F-acrylate. Scanning electron microscopy/Energy-dispersive x-ray spectroscopy (SEM/EDS) was performed to study the surface chemistry of our F-NIPAM.

3.2.2.1. Differential Scanning Calorimetry (DSC)

Differential scanning calorimetry (DSC) is an analytical technique for investigating the thermal properties of a material. It measures the difference in heat flow between a sample and a reference as a function of temperature. When a sample of a known mass is heated or cooled, the DSC records the changes in heat capacity from the differences in heat flow and temperature. As a result, it allows for the identification of phase transition temperature, glass transition temperature, and a melting point of the sample.

TA Instruments Q200 Differential scanning calorimeter (DSC) was used to characterize the thermal properties of our F-NIPAM. 10 mg of F-NIPAM, in average, was placed into the sample pan making sure that the sample is not contaminated. The sample pan with hydrogel was covered with a pan lid to prevent water evaporation and placed on the DSC heater. The hydrogel was then scanned at a rate of 10°C/min from 10°C to 50°C. Of note, the lower transition temperature of a neat NIPAM around 32°C[152] which is within our scanning windows. At the

transition temperature, an endothermic peak is expected in the DSC plots[135,153]. This endothermic peak provided the location of the LCST of F-NIPAM. After the scanning was completed, the weight of the sample was weighted, and it showed that there is negligible evaporation of water from the sample.

3.2.2.2. Fourier Transform Infrared Spectroscopy (FTIR)

PerkinElmer Spectrum 400 FTIR Spectrometer (FTIR) was used to identify the chemical structure of F-NIPAM and to ensure the copolymerization of NIPAM with F-acrylate. Identification of the chemical structure can be made from the characteristic peaks that represent a molecular or a chemical structure. The characteristic peak is obtained from selective absorption of infrared irradiation that is emitted to the sample. The characteristic structures present in NIPAM are C=O (amide I) with absorption band between 1,670 cm^{-1} and 1,650 cm^{-1} and NH (amide II) groups distinguishable from NH bending peaks between 1,650 cm^{-1} to 1,580 cm^{-1} [154,155]. Similarly, the absorption peak between 1,200 cm^{-1} and 1,250 cm^{-1} is expected due to the asymmetric and symmetric stretching of the CF_2 group of F-acrylate[156]. Before conducting the FTIR analysis, F-NIPAM film prepared by drop casting on a glass slide was dried to remove the water vapor present in the film. The sample was then scanned at the rate of 5 cm^{-1} resolution and the absorption peaks were monitored and compared with the absorption peaks of NIPAM and F-acrylate.

3.2.2.3. Energy Dispersive X-ray Spectroscopy (EDS)

To investigate the surface chemistry of F-NIPAM, the energy dispersive x-ray spectroscopy (EDS) was used in conjunction with scanning electron microscopy (SEM). EDS detects the x-rays emitted by a sample when it is bombarded by SEM's electron beam. During the bombardment of the sample by the electron beam, the atoms on the sample's surface eject electrons. This results in the

creation of electron vacancies in those atoms. When the vacancies are filled by electrons from a higher state, x-ray energies are emitted to balance the difference between the energies of two electron states. The x-ray energy provides the characteristics of the element from which it was emitted from. To perform the EDS analysis, F-NIPAM sample prepared by drop casting in a glass slide was dried. The sample was then sputter coated with the gold with 20 nm thickness. EDS analysis was performed from the SEM images. In the EDS, the presence of fluorine on F-NIPAM's surface is investigated from the spectrum of x-ray energy versus counts of the fluorine (F) element.

3.2.2.4. Contact Angle Measurements

The contact angle measurements were performed using Ramé-Hart goniometer to study the wettability of F-NIPAM. Here, we used 6 μL volume of the liquid droplet in all the contact angle measurements for consistency. We found that the contact angle for n-hexadecane on F-NIPAM is $\theta_{oil} = 90°$ while that on a neat NIPAM (without F-acrylate) is $\theta_{oil} = 0°$. Our F-NIPAM shows water contact angle $\theta_{water} = 0°$ when the temperature is below its LCST (T = 21°C). We found that $\theta_{water} = 90°$ when the temperature is above LCST. The contact angles were measured with a care under minimum vibration conditions.

3.2.3. Absorption Experiments

To perform the absorption experiments, the F-NIPAM blocks of 1 cm^3 were prepared by using the PDMS molds. PDMS molds were prepared from a silicon elastomer kit containing an elastomer base and the curing agent. Here, the elastomer base and the curing agent were mixed in the weight ratio of 10:1 and stirred vigorously. The mixture was then ultra-sonicated and de-gassed to remove the air bubbles trapped inside the mixture. The PDMS mixture was poured into a container of a fixed shape such that the mold has a cuboidal cavity. The container with the mixture was then

heated on a hotplate at 65°C for 6 hours for curing. The PDMS mold was then removed from the container. Fig. 3.1 shows the schematic illustrating the process for fabricating F-NIPAM blocks and subsequent absorption experiment by submerging the prepared F-NIPAM block in a desired liquid. We measured the weight of F-NIPAM before and after absorption to determine the swelling ratio (*S.R.*). *S.R.* was calculated from the weight measurements with Eqn. 12. In this equation, $S.R. = \frac{W_t - W_o}{W_s}$, W_t is the weight of F-NIPAM at a time t, W_o is the weight of F-NIPAM during preparation, and W_s is the polymer weight in the hydrogel. The polymer weight W_s is equivalent to 200 mg for 1 cm^3 of the F-NIPAM block.

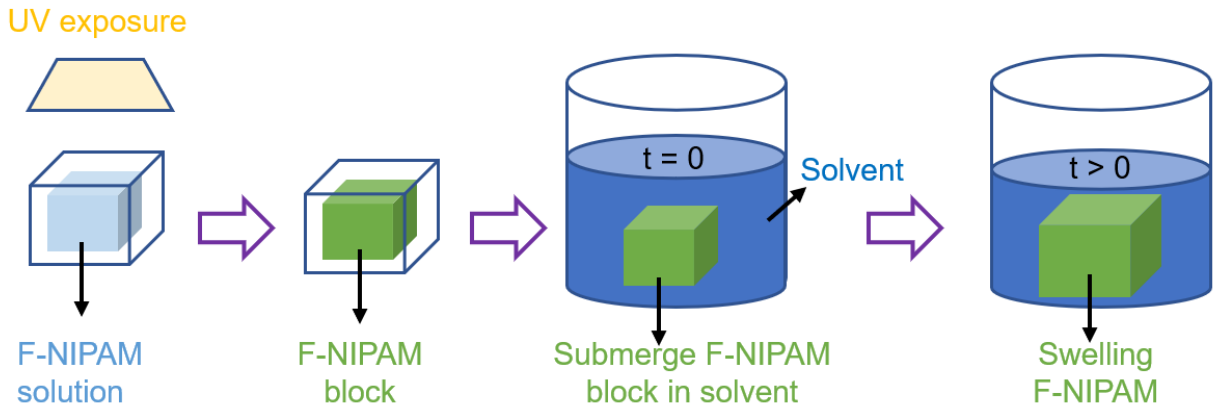

Fig. 3.1. A schematic showing preparation of F-NIPAM block by exposing F-NIPAM solution to UV-A and subsequent absorption experiment performed by submerging the F-NIPAM block in a desired solvent.

We also performed the volume measurements of the unabsorbed liquid and matched with the weight measurements. The hydrogel was submerged in a known volume of a solvent for absorption. As the hydrogel swells by absorbing the solvent, the volume of solvent in the container decreases. After absorption, the remaining solvent volume in the container was measured. The difference between the initial and the final volume of a liquid is equivalent to the absorbed liquid volume. With the known density and the absorbed volume, the weight of the absorbed liquid was

calculated from $W = \rho V$, where W, ρ and V are the weight, density and volume of the liquid, respectively. This weight was compared with the measured weight gained by the F-NIPAM block.

3.2.4. Preparing Oil-Water Emulsions

Surfactant-stabilized oil-water emulsions were prepared using sodium dodecyl sulfate (SDS) and span80 as surfactant. SDS typically allows for oil-in-water (O/W) emulsions while span80 allows for water-in-oil (W/O) emulsions. For O/W emulsions, SDS (10 mg/mL) was dissolved in water followed by mixing with hexadecane (oil). The resulting mixture was then vigorously stirred for 10 minutes. Of note, the O/W emulsion was stable during the entire absorption experiments. Similarly, for W/O emulsions, surfactant span80 was utilized. The surfactant was dissolved in hexadecane followed by mixing with water. The resulting mixture was then stirred for 10 minutes.

3.2.5. Thermogravimetric Analysis (TGA)

PerkinElmer Pyris 1 thermogravimetric analyzer (TGA) was used to determine the separation efficiency for oil-water mixtures. About 16 mg of remnant after selective absorption was heated from 25°C to 105°C with a rate of 5°C/min. The temperature was held at 105°C for 10 minutes. The weight loss by the remnant was compared with a weight loss of pure oil and pure water to determine the separation efficiency.

3.2.6. Density Measurements

Density measurements were performed to determine the separation efficiency. We measured the weight of a different volume of hexadecane-water mixtures and calculated the density by taking the ratio of measured weight and volumes. The density calibration curve is shown in Fig. 3.2. We compared the density of remnant after oil-water separation with the density calibration curve to

determine the composition of hexadecane in the remnant. The separation efficiency was determined from the composition of hexadecane in the remnant.

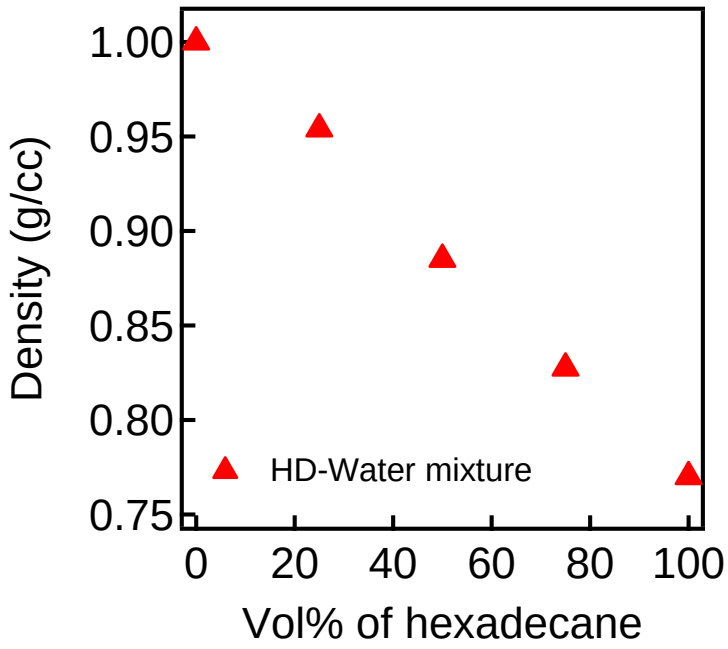

Fig. 3.2. A plot of density as a function of volume percentage of hexadecane in hexadecane-water mixtures.

3.2.7. Refractive Index Measurements

We determined the composition of miscible liquid mixtures such as heptane-ethanol, ethanol-water and DMF-water by measuring the refractive index. Figs. 3.3 - 3.5 show the plots of the refractive index of heptane-ethanol, ethanol-water, and DMF-water as a function of volume percentage of heptane, ethanol and DMF, respectively.

After selective absorption, the refractive index is measured and compared with the calibration curves (Figs. 3.3 - 3.5) to determine the composition of the remaining mixture. With this composition and the measured volume of the remaining mixture, the volume of mixture components remaining after absorption is calculated. As a result, the absorbed volume of

individual components can be readily determined from the difference of initial and the final remaining volume of the components.

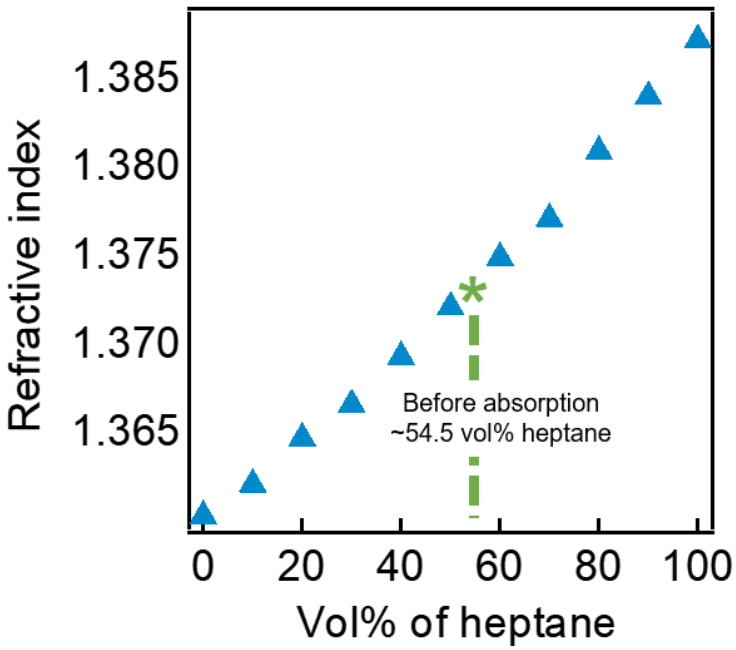

Fig. 3.3. A plot of refractive index of the heptane-ethanol mixture as a function of volume percentage of heptane. An azeotrope composition of 54.5 vol% heptane and 45.5 vol% ethanol is indicated.

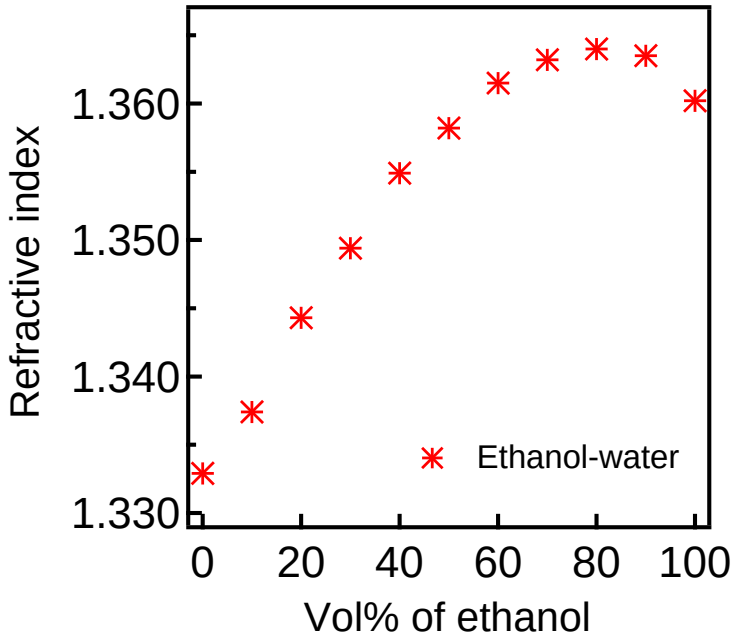

Fig. 3.4. A plot of refractive index of the ethanol-water mixture as a function of volume percentage of ethanol.

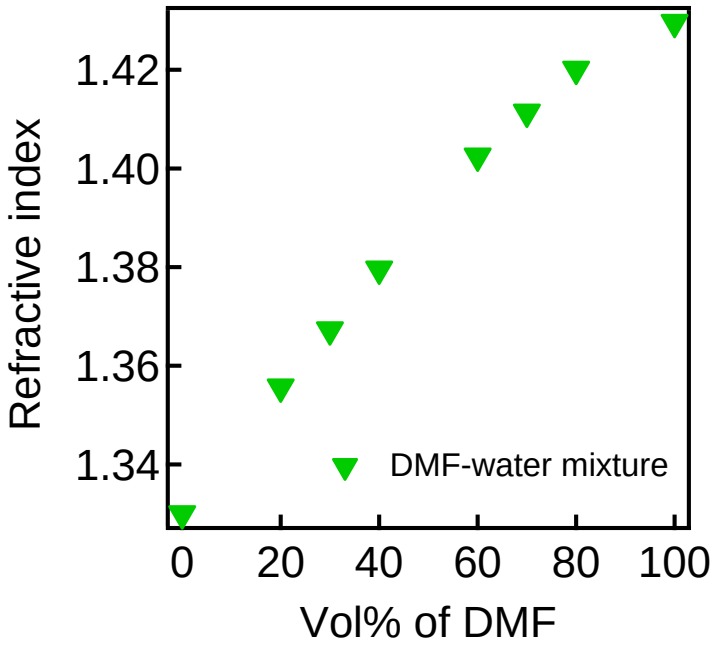

Fig. 3.5. A plot of refractive index of DMF-water mixture as a function of volume percentage of DMF.

4. Results and Discussion

4.1. Fabrication of F-NIPAM

F-NIPAM is synthesized via photocuring[157,158] of an aqueous precursor solution containing N-Isopropylacrylamide (NIPAM), N,N'-Methylenebisacrylamide (MBAA), 2-Hydroxy-2-methylpropiophenone (darocur 1173) and 1H,1H,2H,2H-Heptadecafluorodecyl acrylate (F-acrylate). The chemical structure of NIPAM, MBAA and darocur 1173 are presented in Fig. 4.1. A mixture of NIPAM monomer, MBAA cross-linker and darocur 1173 photo initiator in the weight ratio of 97:1:2 was prepared in deionized water followed by stirring for 30 minutes. The concentration of this solution was 200 mg/mL. Next, F-acrylate solution was separately prepared by dissolving F-acrylate in ethanol (200 mg/mL). These two solutions were mixed in desired proportion followed by vigorous stirring for 30 minutes to prepare a F-NIPAM solution.

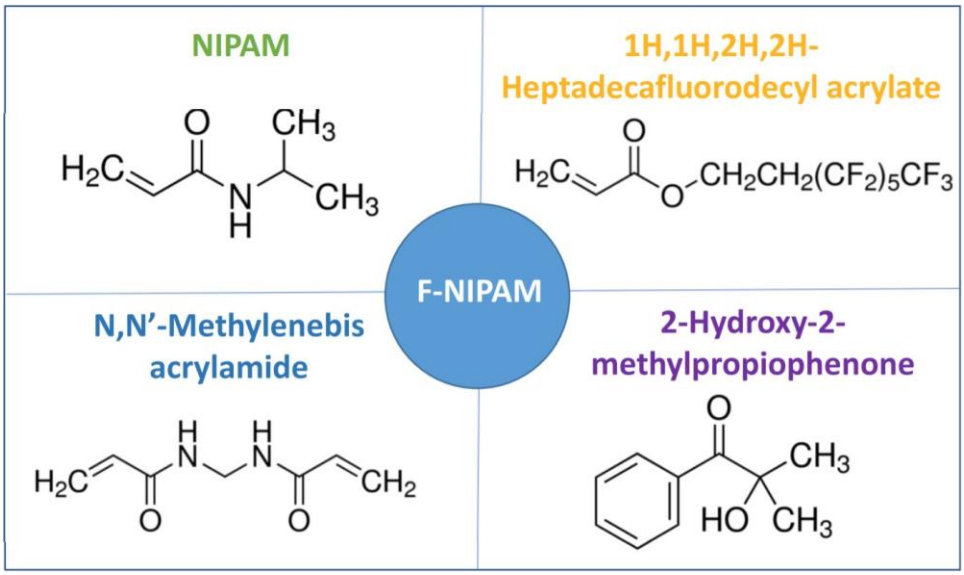

Fig. 4.1. Chemical structures of the components, N-Isopropylacrylamide (NIPAM), N,N'-Methylenebisacrylamide (MBAA), 1H,1H,2H,2H-Heptadecafluorodecyl acrylate (F-acrylate) and 2-Hydroxy-2-methylpropiophenone (darocur 1173) utilized for fabrication of F-NIPAM.

The resulting F-NIPAM solution was applied to a substrate and exposed to long-wave ultraviolet light (UV-A, λ = 365 nm) for 10 minutes for cross-linking. Upon exposure to ultraviolet light, darocur 1173 (the photo initiator) forms radicals that causes cleavage of -CH_2=CH- double bond in NIPAM (the monomer), MBAA (cross-linker) and F-acrylate (copolymer). Since NIPAM, MBAA, and F-acrylate contain similar reactive acrylic groups (-CH_2=CH-CO-) in their structures (Fig. 4.1), the final copolymer structure will consist of NIPAM, MBAA and F-acrylate[159] as shown in Fig. 4.2. As can be seen from Fig. 4.1, NIPAM and F-acrylate contain one acrylic group (-CH_2=CH-CO-) while MBAA possesses two. This implies that NIPAM and F-acrylate can form a single polymeric chain while MBAA can allow cross-linking of two polymeric chains. This will result in a cross-linked network (Fig. 4.2). Therefore, MBAA is critical to fabricate the network structure to chemically cross-link the copolymer chains.

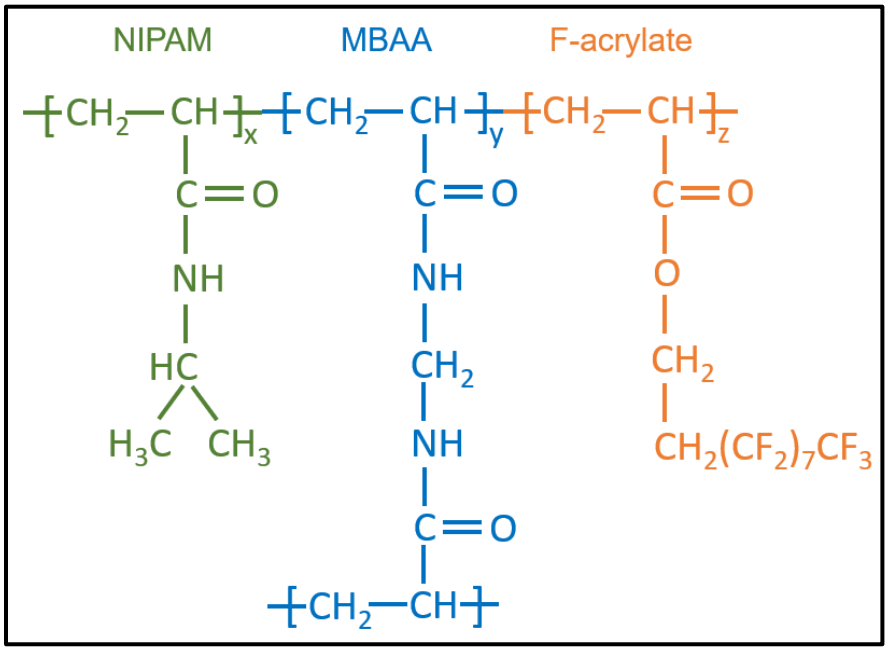

Fig. 4.2. A schematic showing the chemical structure of F-NIPAM from NIPAM monomer, MBAA cross-linker, and F-acrylate comonomer. The variables x, y, and z indicate a number that a given structure is repeated.

4.2. Characterizing F-NIPAM

DSC is used to determine the phase transition temperature (lower critical solution temperature, LCST) of our F-NIPAM. Previous reports[135,160] demonstrated that the LCST of NIPAM can be altered by copolymerization. When the added copolymer is hydrophilic, the LCST is enhanced. Similarly, if the added copolymer is hydrophobic, the LCST is lowered[135]. In this study, we copolymerize NIPAM with F-acrylate, a low surface energy material[161]. Therefore, we expect that the LCST will be lowered (T < 32°C) from copolymerization of NIPAM with F-acrylate.

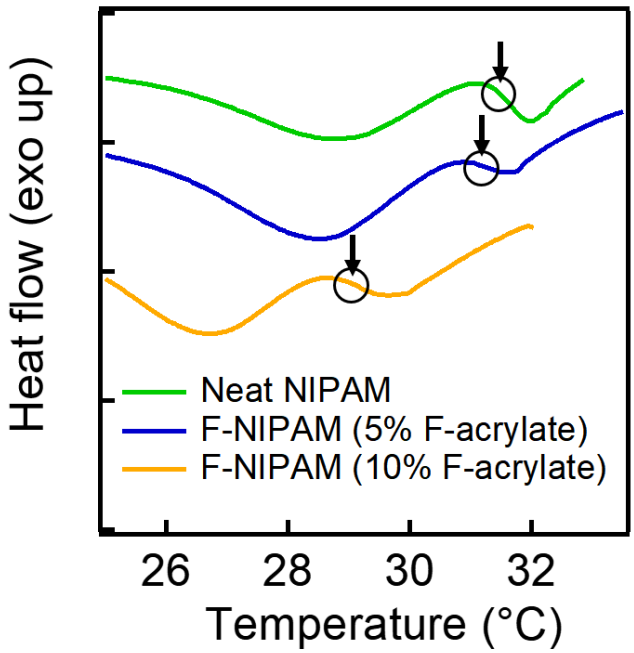

Fig. 4.3. A DSC plot for F-NIPAM for different F-acrylate concentration. Here, heat flow in F-NIPAM is plotted as a function of temperature. The endothermic peaks indicated by arrows show the LCST of F-NIPAM for different F-acrylate concentration.

Fig. 4.3 shows the DSC plot for F-NIPAM with different F-acrylate concentration. Here, the heat flow in F-NIPAM is plotted as a function of temperature. The endothermic (i.e. heat absorbing) peaks (shown by arrows) determined the phase transition temperature (LCST) of F-NIPAM. It is reported that the LCST of a neat NIPAM is 32°C, which is in good accordance with

our observation as shown in Fig. 4.3 and Table 4.1. We found that the LCST decreases with increasing the concentration of F-acrylate confirmed by the shift in the corresponding endothermic peaks to a lower temperature. This can be attributed to the copolymerization of NIPAM with hydrophobic F-acrylate. The lower value of LCST for our F-NIPAM is favorable to release and collect the absorbed liquid (water) at a lower temperature.

Table 4.1. A table with LCST values of F-NIPAM with different F-acrylate concentration.

F-acrylate wt.%	**LCST of copolymer (°C)**
0	31.8±1.0
5	31.0±1.0
10	28.9±1.0

We also characterized the chemical structure of our F-NIPAM by using FTIR. For an accurate study, the surface of F-NIPAM was thoroughly rinsed after copolymerization to remove any unbound molecules and completely dried. The FTIR spectrum was scanned in the range between 4,000 cm^{-1} and 400 cm^{-1}, at an increment of 5 cm^{-1}. Fig. 4.4 shows the absorption spectrum of our F-NIPAM. For comparison, the spectrum of a neat NIPAM is also shown.

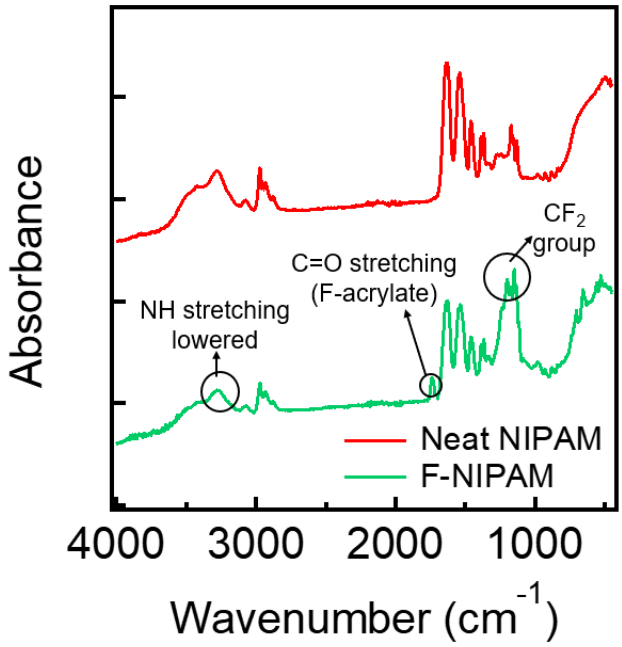

Fig. 4.4. A plot showing FTIR absorption spectrum for NIPAM and or F-NIPAM.

The characteristic structures present in NIPAM are its C=O (Amide I) and the N-H (Amide II) groups. Amide I can be distinguished by the absorption band between 1,670-1,650 cm^{-1} of C=O stretching mode[154]. The medium intensity peaks of the N-H bending around 1,650 cm^{-1} to 1,580 cm^{-1} characterize the amide II group. For the isopropyl groups (-$CH(CH_3)_2$) present in NIPAM, the absorption peaks occur at 2,800 cm^{-1}-3,000 cm^{-1}, attributed to the symmetric vibrations of CH_3 and CH_2[155]. The CH deformation peaks occur between 1,350 cm^{-1} and 1,450 cm^{-1}.

The peaks between 1,200 cm^{-1} and 1,250 cm^{-1} in F-NIPAM spectrum in the Fig. 4.4 are due to the CF_2 group from F-acrylate. Similarly, due to the presence of CF_2-CF_3 end group from F-acrylate, an absorption peak is observed at around 1,153 cm^{-1}. The absorption peak at around 1,741 cm^{-1} is attributed to the presence of C=O stretching from F-acrylate. This confirms that NIPAM and F-acrylate are copolymerized resulting in the chemical structure shown in Fig. 4.2.

The characteristic peak at 3,400 cm^{-1} due to the intense NH stretching is lowered in our F-NIPAM, indicating that NIPAM and F-acrylate are copolymerized.

The Energy Dispersive X-ray Spectroscopy (EDS) was performed to determine the surface chemistry of F-NIPAM. EDS was performed in conjunction with Scanning Electron Microscope (SEM). Fig. 4.5 shows the EDS elemental mapping on our F-NIPAM copolymerized with 10 wt.% of F-acrylate. Our F-NIPAM samples were sputter-coated with 20 nm of gold to prevent charging. Here, the entire surface of our F-NIPAM is covered by fluorine (F) (see Fig. 4.5b). Fluorine originates from CF_2 and CF_3 groups of F-acrylate. We also found that CF_2 or CF_3 groups on the surface can lower the surface free energy which is critical to achieve oil repellency (will be discussed in following sections).

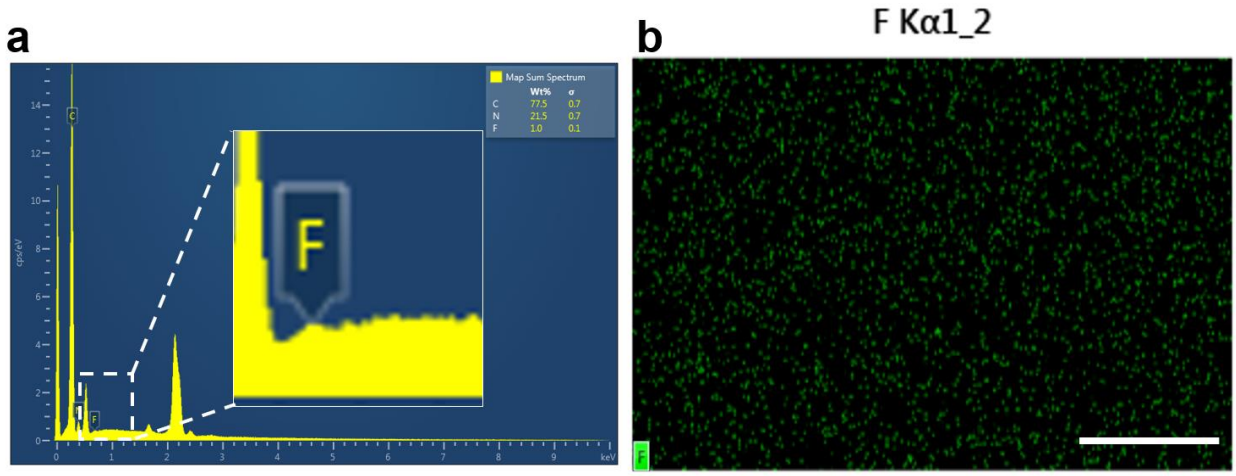

Fig. 4.5. EDS elemental analysis on F-NIPAM surface. **(a)** EDS elemental spectrum on F-NIPAM. Inset: Zoomed in the spectrum to highlight fluorine. **(b)** EDS elemental mapping of fluorine. The green spots indicate the fluorine elements. Scale bar: 100 μm.

4.3. Wettability

We characterized our F-NIPAM's wettability by using contact angle measurements. Various probe liquids including water (γ_{water} = 72.1 mN/m), hexadecane (γ_{HD} = 27.5 mN/m), heptane (γ_{HT} = 20.1 mN/m) and ethanol (γ_{EtOH} = 21.8 mN/m) were used.

4.3.1. Wettability of F-NIPAM Below LCST

Fig. 4.6 shows the polar liquids (ethanol (EtOH), water) and non-polar liquids (hexadecane (HD), heptane (HT)) on F-NIPAM at a temperature (T = 21°C) below LCST. Here, we used F-NIPAM with 10 wt.% of F-acrylate. When the temperature is below LCST, our F-NIPAM was easily wetted by polar liquids. We found that θ_{water} = 0° and θ_{EtOH} = 0° while the contact angles for heptane and hexadecane are θ_{HT} = 70°and θ_{HD} = 90°, respectively. This indicates our F-NIPAM is oleophobic. Typically, if the surface is oleophobic, it is hydrophobic. This is because the surface tension of water is significantly higher than that of oils ($\gamma_{water} >> \gamma_{oils}$). Considering the Young's relation (Eqn. 1), a liquid with a higher surface tension would exhibit a higher contact angle on a given surface. Therefore, it is considered challenging to develop a hydrophilic and oleophobic (HL/OP) surface with $\theta_{oil} > \theta_{water}$. Only recently, we[53] and others[54,55] reported such hydrophilic and oleophobic surfaces utilizing the specific interaction of such surface with contacting liquids. This results in lowering the interfacial energy of a solid and a liquid. We believe that our F-NIPAM's hydrophilic and oleophobic wettability is due to the reorganization of fluorinated moieties present on the surface when a polar liquid comes in contact. This allows the polar liquids to wet the surface.

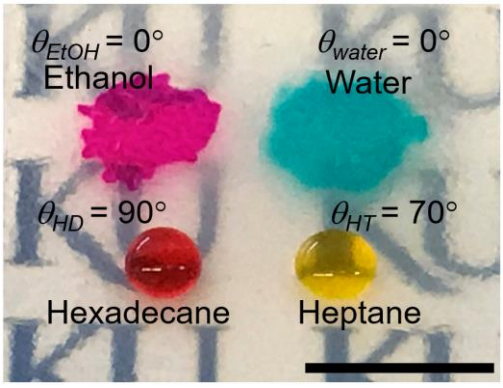

Fig. 4.6. An image showing polar (water, ethanol) and non-polar liquids (heptane, hexadecane) contacting F-NIPAM with 10 wt.% F-acrylate at 21°C (below LCST). Scale bar: 1 cm.

We systematically studied the wettability of F-NIPAM copolymerized with various compositions of F-acrylate. Fig. 4.7 shows a plot of the contact angles for various polar and non-polar liquids on F-NIPAM surfaces with different F-acrylate composition.

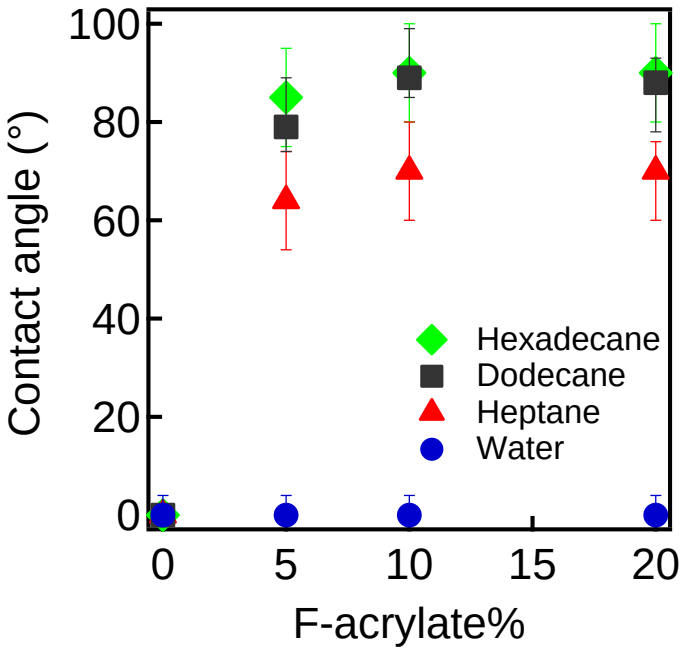

Fig. 4.7. A plot showing contact angles of water and oils on the surface of F-NIPAM as a function of wt.% of F-acrylate below LCST (T = 21°C).

We found that water contact angles are $\theta_{water} = 0°$ on the surface while the contact angles for oils (hexadecane, dodecane, heptane) increase with increasing F-acrylate composition. For example, the hexadecane contact angle on surface of F-NIPAM with 5 wt.% F-acrylate is $\theta_{HD} = 85°$ while that on a surface with 10 wt.% F-acrylate is $\theta_{HD} = 90°$. We also found that the contact angles for oils reach their maximum values on surface with 10 wt.% of F-acrylate. This can be attributed to the fact that the fluorinated moieties on the surface of F-NIPAM has reached to its maximum density when 10 wt.% F-acrylate is added to NIPAM. Therefore, further addition of F-acrylate would not result in an increase of oil contact angles. This observation is also supported from the EDS (Fig. 4.5) mapping of F-NIPAM with 10 wt.% F-acrylate surface where fluorine covers the entire surface. Therefore, we utilized F-NIPAM with 10 wt.% F-acrylate for all experiments in this study.

4.3.2. Wettability of F-NIPAM Above LCST

The wettability of F-NIPAM at a temperature (T = 40°C) above its LCST is presented in Fig. 4.8.

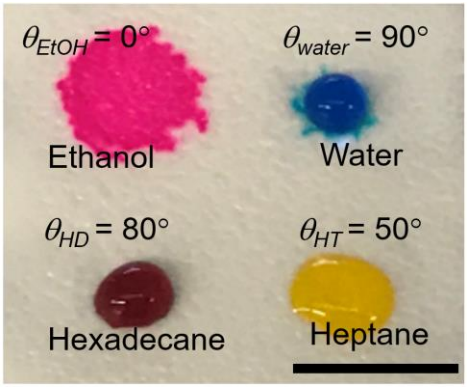

Fig. 4.8. An image showing the polar (water, ethanol) and non-polar liquids (heptane, hexadecane) contacting F-NIPAM with 10 wt.% F-acrylate at T = 40°C (above LCST).

The contact angles for hexadecane and heptane are found to be $\theta_{HD} = 85°$and $\theta_{HT} = 50°$, respectively. These values are almost the same as those observed on F-NIPAM at a temperature

below LCST (Fig. 4.8). It is also observed that the contact angle for ethanol is $\theta_{EtOH} = 0°$. By contrast, the contact angle for water is found to be $\theta_{water} = 90°$. This indicates that our F-NIPAM becomes hydrophobic when the temperature is above its LCST. Such wettability switch (i.e. HL→HP) of NIPAM upon temperature change is well documented in the literature[162-164]. It can be attributed to the hydrophilic-hydrophobic balance in the NIPAM network. NIPAM is composed of both hydrophilic (amide) and hydrophobic (isopropyl) groups. When the temperature is below its LCST, amide group and water hydrogen bond each other. When the temperature is above the LCST, the hydrogen bond is weakened and the hydrophobic interaction between the isopropyl groups increases. The prevailing hydrophobic interaction results in repelling the water when the temperature is above the LCST.

We also studied the wettability of F-NIPAM with various composition of F-acrylate at a temperature (T = 40°C) above the LCST. Fig. 4.9 shows a plot of the contact angles for various liquids on F-NIPAM surfaces as a function of F-acrylate composition at T = 40°C. We found that the contact angles for oils (hexadecane, heptane, dodecane) increase with increasing F-acrylate composition and reach a maximum value at 10 wt.% of F-acrylate. This is similar to that found at a temperature below the LCST (T = 21°C). We also found that the water consistently exhibits a contact angle $\theta_{water} \approx 90°$ independent of the composition of F-acrylate.

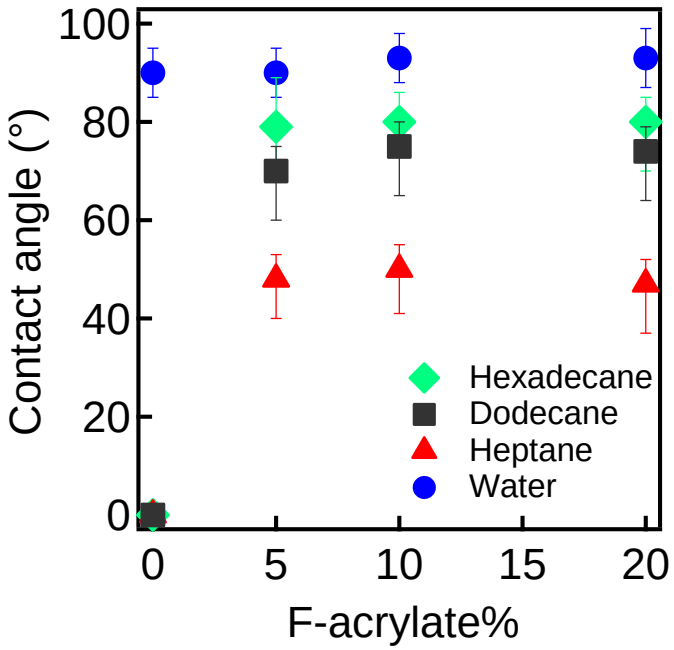

Fig. 4.9. A plot showing contact angles of water and oils on F-NIPAM above LCST (T = 40°C) as a function of wt.% of F-acrylate.

4.4. Surface Energy Estimation of F-NIPAM

The Owens-Wendt method[69] utilizes the Young's relation (Eqn. 1) and the Fowke's postulation[70] to estimate the surface energy (γ_{SV}) from the liquid contact angles (section 2.3). Adding fluorinated materials to a surface lowers the surface energy. Therefore, the surface energy of our F-NIPAM can be lowered by increasing the wt.% of F-acrylate. This results in higher contact angles for contacting liquids. We utilized hexadecane and water contact angles on F-NIPAM to calculate the surface energy. Table 4.2 lists the dispersive (γ_{SV}^{d}) and polar (γ_{SV}^{p}) components of surface energy (γ_{SV}) for our F-NIPAM with various F-acrylate composition.

Table 4.2. The surface energy of F-NIPAM with its dispersive, polar components estimated using the Owens-Wendt method.

Wt.% of F-acrylate	γ_{SV}^{d} (mN/m)	γ_{SV}^{p} (mN/m)	γ_{SV} (mN/m)
0	27.5	45.2	72.7
5	8.1	5.5	13.6
10	6.9	2.7	9.5
20	6.9	3.2	10.1

As described in section 2.3, the surface energy of a material (γ_{SV}) can be divided into a dispersive component (γ_{SV}^{d}) and polar component (γ_{SV}^{p}). To calculate the dispersive component (γ_{SV}^{d}), the contact angle (θ_{HD}) and surface tension of hexadecane (γ_{HD} = 27.5 mN/m) were used in Eqn. 6. The calculated dispersive component (γ_{SV}^{d}) along with the water contact angle were used to calculate the polar component of surface energy (γ_{SV}^{p}) using Eqn. 7. Here, the dispersive and polar components of water surface tension are γ_{LV}^{d} = 21.1 mN/m and γ_{LV}^{p} = 51.0 mN/m, respectively. The total surface energy (γ_{SV}) of F-NIPAM is calculated by summing up the dispersive and polar surface energy components.

Fig. 4.10 shows a plot of the surface energy of F-NIPAM as a function F-acrylate composition. The surface energy of F-NIPAM decreases with increasing the F-acrylate composition. This can be attributed to the fact that F-NIPAM surface is covered by -CF_2-CF_3 groups. At 10 wt.% F-acrylate, F-NIPAM is completely covered with fluorine (Fig. 4.5) leading to the minimum surface energy.

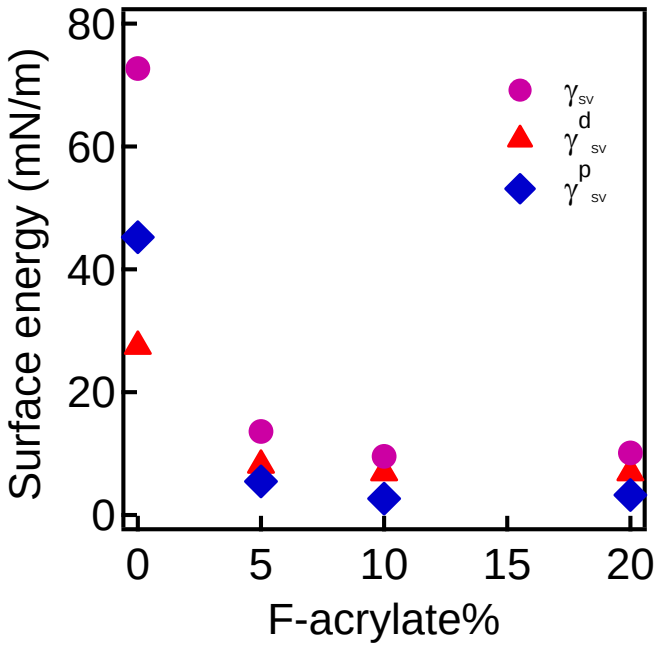

Fig. 4.10. A plot showing the surface energy of F-NIPAM as a function of wt.% of F-acrylate. γ_{SV}^{d} : Dispersive component. γ_{SV}^{p} : Polar component. γ_{SV} : Surface energy.

It is worth noting that the contact angles of water utilized in estimating surface energy of F-NIPAM (Table 4.2) are the initial contact angle (i.e., when water just touches the surface) before surface reconfiguration.

4.5. Fouling Resistance of Our F-NIPAM

Hydrophilic yet oleophobic (HL/OP) materials has been used in separation of liquid mixture which consists of a polar (such as water) and non-polar (such as oil) phases. For example, hydrophilic/oleophobic (HL/OP) membranes can selectively allow water to wet the surface and permeate through while repelling oil. Similarly, we demonstrated that our F-NIPAM can be preferentially wet by water while repelling oil at a temperature below the LCST (Fig. 4.6). We found that a water droplet can undercut the oil and consequently wet the surface. Such self-cleaning ability is critical to mitigate surface fouling.

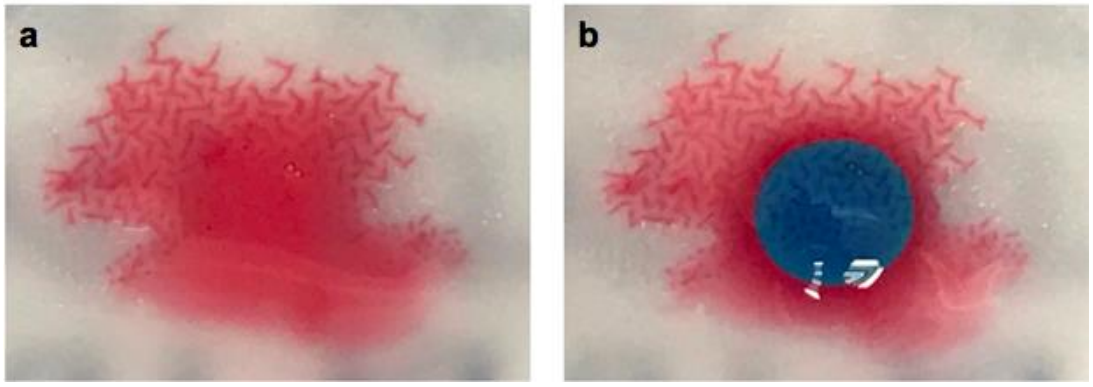

Fig. 4.11. Images showing oil fouling on the surface of hydrophilic/oleophilic (HL/OL) neat NIPAM. **(a)** Fouled by oil (hexadecane, dyed red). **(b)** Oil fouling hinder water (dyed blue) to wet the surface.

By contrast, Fig. 4.11 shows a neat NIPAM (without F-acrylate) that is fouled by oil. Here, an oil droplet (hexadecane, dyed red) with surfactant (span80, 5mg/mL) can easily spread on the surface. When a water droplet (dyed blue) comes in contact, oil hinders the water from wetting the surface and being absorbed. Therefore, it is difficult to clean the oil fouled NIPAM surface by applying water.

4.6. Absorption of Polar and Non-Polar Liquids

We studied the absorption capacity for polar and non-polar liquids of our F-NIPAM. This is critical for designing separation experiments such that we know the required dimensions of F-NIPAM to separate a given volume of a liquid mixture within a given time. To characterize the absorption capacity, F-NIPAM with a desired volume was prepared by molding in cubical polydimethylsiloxane (PDMS) mold (see Section 3.2.3). Briefly, the PDMS mold was prepared by mixing the main component and the curing agent in 10:1 ratio by weight followed by degasification in vacuum oven to remove trapped air bubbles. The mixture was then poured in a cuboidal mold of 1.2 cm x 1.2 cm base and heated at 60°C for 6 hours for cross-linking. The PDMS mold replicated the shape of the mold with the dimensions mentioned above. Subsequently, 1 mL of the

F-NIPAM solution was poured in the PDMS mold and exposed to ultraviolet light (UV-A, $\lambda = 365$ nm) for 15 minutes for photocuring. After photocuring, the cross-linked F-NIPAM gel with 1.2 cm × 1.2 cm × 0.7 cm (about 1 cm^3 volume) dimension was carefully removed from the mold.

All absorption experiments were performed using F-NIPAM with 10 wt.% F-acrylate. F-NIPAM will be referred to this composition unless otherwise stated. F-NIPAM with known weight was submerged in a desired liquid bath. The change in weight is recorded. We determine the swelling ratio (*S.R.*) of F-NIPAM using Eqn. 12 from the weight of F-NIPAM at time '*t*', during preparation and the weight of polymer in F-NIPAM (equivalent to weight of dried F-NIPAM). Similarly, the equilibrium swelling ratio would indicate the swelling ratio of F-NIPAM at its maximum swelling state. The equilibrium swelling ratio was obtained by submerging F-NIPAM in the desired solvent for seven days.

4.6.1. Equilibrium Swelling of F-NIPAM by Absorption

Fig. 4.12 shows the equilibrium swelling ratio of our F-NIPAM for various polar and non-polar liquids. It is worth noting that all the swelling experiments were performed at room temperature (T = 21°C). We found that our F-NIPAM can absorb up to 11 times the polymer weight when they are submerged in polar liquids (e.g., water and alcohols). The equilibrium *S.R.* for water is around 7.42 and that for heptanol is 10.45. On the other hand, *S.R.* values for non-polar liquids including hexadecane and heptane are almost zero indicating that our F-NIPAM barely absorbs them.

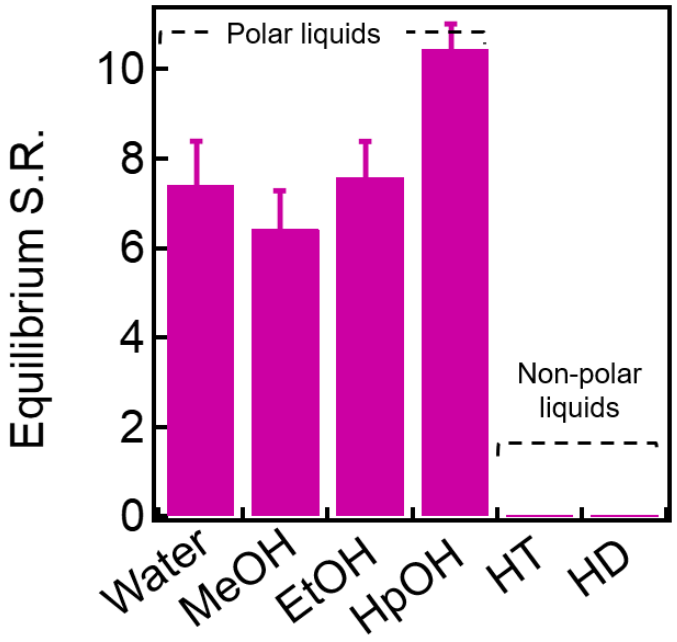

Fig. 4.12. A plot showing equilibrium swelling ratio of F-NIPAM in polar and non-polar solvents. MeOH: Methanol. EtOH: Ethanol. HpOH: Heptanol. HT: Heptane. HD: Hexadecane.

The selective absorption for polar liquid over the non-polar liquid of our F-NIPAM can be explained in the following manner. When our F-NIPAM contacts the polar liquid, the most hydrophilic (amide) parts are hydrated first (Fig. 4.13a) resulting in swelling due to interaction through hydrogen bonding. The hydration of hydrophilic parts leads to exposure of isopropyl (hydrophobic) group to water molecules, which in turn results in the interaction of the hydrophobic group with water (Fig. 4.13b). Particularly, the water molecules interact with the hydrophobic isopropyl group by forming the cage structure, called as hydrophobic hydration. After both hydrophilic and hydrophobic groups interact with the liquid, further absorption can be occurred due to the osmotic difference in the polymer network (Fig. 4.13c). At equilibrium, the driving force due to the osmotic difference is balanced by the retracting elastic force of the network. However, non-polar liquid such as heptane and hexadecane cannot form the hydrogen bond with hydrophilic

moiety or form hydrophobic-hydrophobic interaction. Therefore, our F-NIPAM barely absorbs the non-polar liquids.

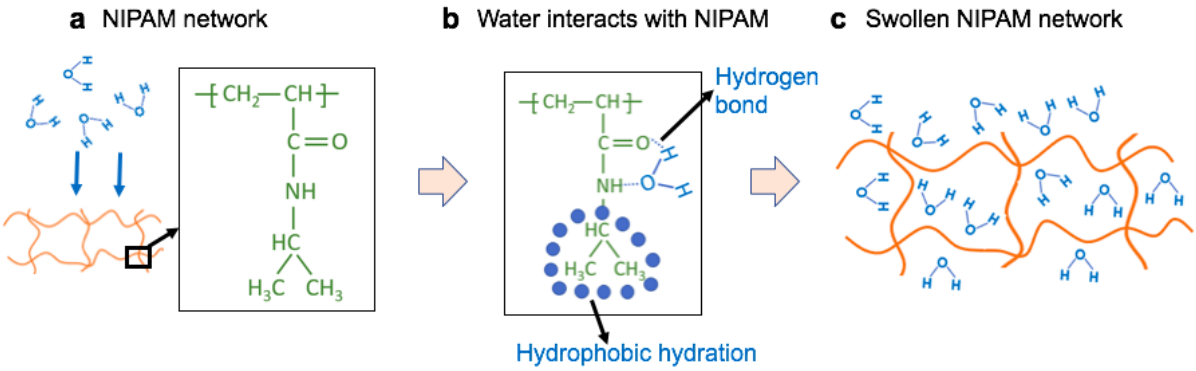

Fig. 4.13. Schematic showing absorption mechanism of NIPAM. **(a)** Water comes into contact with NIPAM. **(b)** Water hydrogen bonds with amide group of NIPAM. Simultaneously, hydrophobic hydration occurs around the isopropyl group. **(c)** After hydrogen bonding and hydrophobic hydration, water diffuses into the network of NIPAM driven by osmotic pressure.

We found that the absorption capacity of our F-NIPAM is a function of the amount of cross-linker used. This is because the cross-linking density affects the porosity of F-NIPAM which in turn affects the absorption capacity. Fig. 4.14 shows the equilibrium swelling ratio of F-NIPAM for ethanol and water as a function of cross-linker concentration. It clearly shows that F-NIPAM absorbs less amount of liquids when the cross-linker concentration is increased. This is because when the cross-linker is increased, the porosity is reduced making it difficult for F-NIPAM to absorb liquids and swell. Therefore, it is desirable to lower the crosslinker amount to achieve higher swelling ratio. However, too low cross-linker concentration (c.a. less than 1.0 wt.% MBAA) result in making it difficult to fabricate the hydrogel in a desirable shape. Herein, we used 1.0 wt.% of the cross-linker.

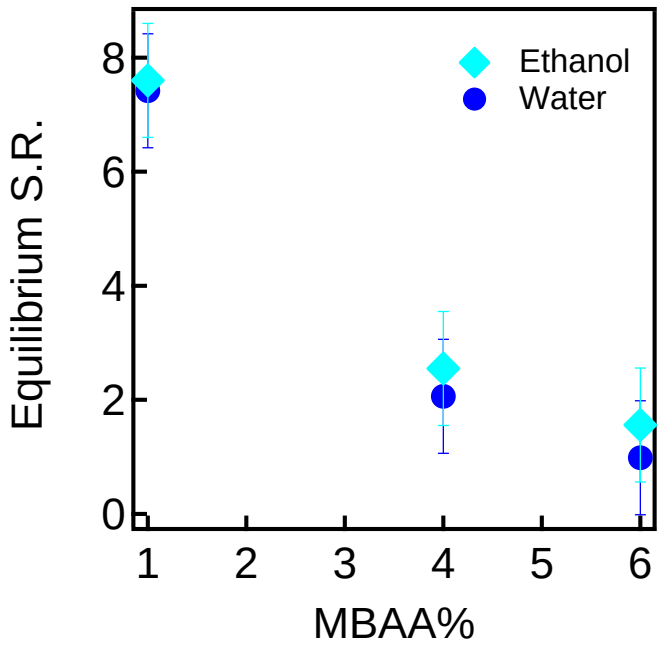

Fig. 4.14. A plot showing equilibrium swelling ratio (*S.R.*) of F-NIPAM as a function of MBAA composition.

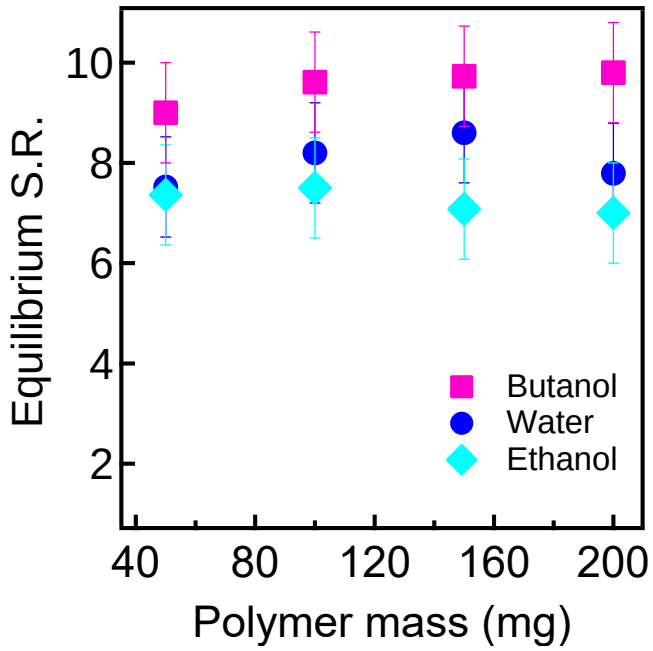

Fig. 4.15. A plot showing equilibrium swelling ratio of F-NIPAM as a function of polymer mass. It shows that the equilibrium *S.R.* for a given liquid is not altered by polymer mass.

We also performed the absorption tests using F-NIPAM with various polymer mass (Fig. 4.15). Of note, the polymer mass is the mass of F-NIPAM by excluding the solvent (i.e. water) present in F-NIPAM. This is equivalent to the dried F-NIPAM mass. We found that the equilibrium swelling ratio is almost the same for F-NIPAM with different polymer mass. This indicates that the equilibrium swelling ratio for a given liquid is not affected by the mass of the polymer.

4.7. Relation of Swelling Behavior and the Flory-Huggins Polymer-Solvent Interaction Parameter (χ)

To study the relation of swelling behavior of our F-NIPAM and the Flory-Huggins polymer-solvent interaction parameter (χ), we conducted absorption tests for various alcohols including methanol (MeOH), ethanol (EtOH), propanol (PpOH), butanol (BuOH), pentanol (PtOH), hexanol (HxOH) and heptanol (HtOH). Interestingly, we found that our F-NIPAM can absorb a larger amount of alcohols with increasing number of hydrocarbons in alcohols (Fig. 4.16). For example, the swelling ratio for methanol (CH_3OH) is about 6.43 while that for heptanol ($C_7H_{15}OH$) is 10.45.

We explain this using the Flory-Huggins polymer-solvent interaction parameter (χ). The interaction parameter χ can be related to the Hansen solubility parameters (HSP) by Eqn. 8. The relation of χ and Hansen solubility parameters (HSP) is useful because HSP values for common liquid or polymers are extensively documented.

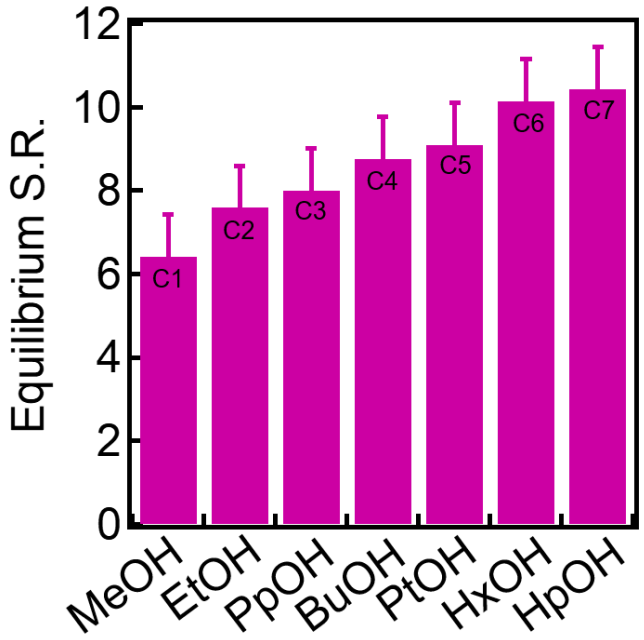

Fig. 4.16. A plot showing equilibrium swelling ratio of F-NIPAM for alcohols with various number of hydrocarbons. MeOH: Methanol. EtOH: Ethanol. PpOH: Propanol. BuOH: Butanol. PtOH: Pentanol. HxOH: Hexanol. HpOH: Heptanol.

The Hansen solubility parameters δ_D (dispersion), δ_P (polar) and δ_H (hydrogen bonding) for various alcohols are listed in Table 4.3[165].

Table 4.3. Hansen solubility parameters for alcohols[165] and their respective molar volumes.

Solvent	**δ_H ($\sqrt{MPa}$)**	**δ_P ($\sqrt{MPa}$)**	**δ_D ($\sqrt{MPa}$)**	**V (cm^3/mol)**
Methanol	22.3	12.27	15.1	40.7
Ethanol	19.43	8.8	15.8	58
Propanol	16.4	6.1	15.8	75.2
Butanol	15.8	5.7	16.0	91.5
Pentanol	11.0	4.9	16.1	108.6
Hexanol	15.9	5.8	12.5	126.17

Heptanol	16	5.3	11.7	141.4

If HSP values are not known, we can estimate HSPs by using for the group contribution method by Hoftyzer and Van Krevelen (Eqn. 9). The group contribution method assumes that the property of molecules can be estimated by adding the values contributed by each group. For example, the groups present in the structure of NIPAM is listed in Table 4.4. These contributions are added and utilized in Eqn. 9 to estimate the Hansen solubility parameters. We estimated the Hansen solubility parameters of NIPAM as δ_D = 19.15 $\sqrt{\text{MPa}}$, δ_P = 7.76 $\sqrt{\text{MPa}}$ and δ_H = 7.04 $\sqrt{\text{MPa}}$. We also estimated the Hansen solubility parameters for F-acrylate from the group contributions listed in Table 4.5. The estimated HSPs for F-acrylate are δ_D = 14.87 $\sqrt{\text{MPa}}$, δ_P = 2.74 $\sqrt{\text{MPa}}$ and δ_H = 3.97 $\sqrt{\text{MPa}}$.

Table 4.4. Group contributions corresponding to dispersive, polar and hydrogen-bonding for estimation of Hansen solubility parameters of NIPAM[141]. No. of the group indicates the number of times the groups occur in the chemical structure of NIPAM.

Groups	**No. of group**	F_{di} **(** $\sqrt{\text{MPa}}$**/mol)**	F_{pi} **(** $\sqrt{\text{MPa}}$**/mol)**	E_{hi} **(J/mol)**
-CH_3	2	420	0	0
>CH-	1	80	0	0
-NH-	1	160	210	3,100
-CO-	1	290	770	2,000
=CH-	1	200	0	0
=CH_2	1	400	0	0

Table 4.5. Group contributions corresponding to dispersive, polar and hydrogen-bonding for estimation of Hansen solubility parameters of F-acrylate[141]. No. of group indicates the number of times the groups occur in the chemical structure of F-acrylate.

Groups	No. of group	F_{di} ($\sqrt{\text{MPa}}$/mol)	F_{pi} ($\sqrt{\text{MPa}}$/mol)	E_{hi} (J/mol)
$=CH_2$	1	400	0	0
=CH-	1	200	0	0
-CO-	1	290	770	2,000
-O-	1	100	400	3,000
$-CH_2-$	2	270	0	0
>C<	8	-70	0	0
-F	17	220	0	0

Using the estimated Hansen solubility parameters, we calculated the χ values of NIPAM (χ_{NIPAM}) with various alcohols using Eqn. 8. We also calculated the χ values of F-acrylate ($\chi_{F\text{-}acrylate}$) with various alcohols. The χ values of F-NIPAM ($\chi_{F\text{-}NIPAM}$) were then calculated by considering F-acrylate a factor of 0.1 (i.e. $\chi_{F\text{-}NIPAM} = 0.9\ \chi_{NIPAM} + 0.1\ \chi_{F\text{-}acrylate}$). These χ values for F-NIPAM ($\chi_{F\text{-}NIPAM}$) for various alcohols are shown in Fig. 4.17. It is worth noting that the correction factor α utilized in Eqn. 9 is 0.35 for all the calculations.

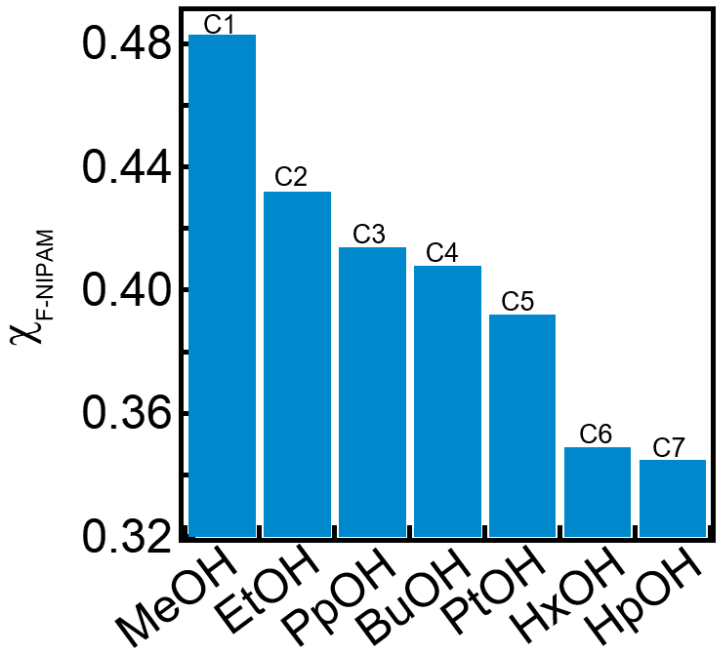

Fig. 4.17. A plot showing χ values of F-NIPAM for alcohols of various number of hydrocarbons. The χ values decrease with increasing number of hydrocarbons.

We found that the χ values for our F-NIPAM and alcohols decrease with an increase in the number of hydrocarbons in alcohols (Fig. 4.17). Since a lower χ value indicates a better miscibility between a polymer and solvent[165], heptanol is expected to exhibit the highest equilibrium *S.R.* among the alcohols. This is true because a lower χ value indicates that the Hansen solubility parameters are close for a polymer and solvent. As a result, the polymer and solvent possessing closest HSPs are expected to have higher *S.R.* values. This matches well with the results shown in Fig. 4.17, where the equilibrium *S.R.* of F-NIPAM increases with increasing the number of hydrocarbons in alcohols.

It is also important to note that the χ values of F-NIPAM with heptane and hexadecane are estimated as 0.82 and 1.39, respectively. As these values are greater than the critical parameter value ($\chi = 0.5$), heptane and hexadecane are not absorbed by F-NIPAM (Fig. 4.12). Therefore, the

Flory-Huggins polymer-solvent interaction parameter χ can be used to predict whether or not a liquid will be absorbed by our F-NIPAM.

4.8. Kinetics of Absorption of F-NIPAM

To study the kinetics of absorption, our F-NIPAM was submerged in the desired liquid and the weight change was recorded at intervals.

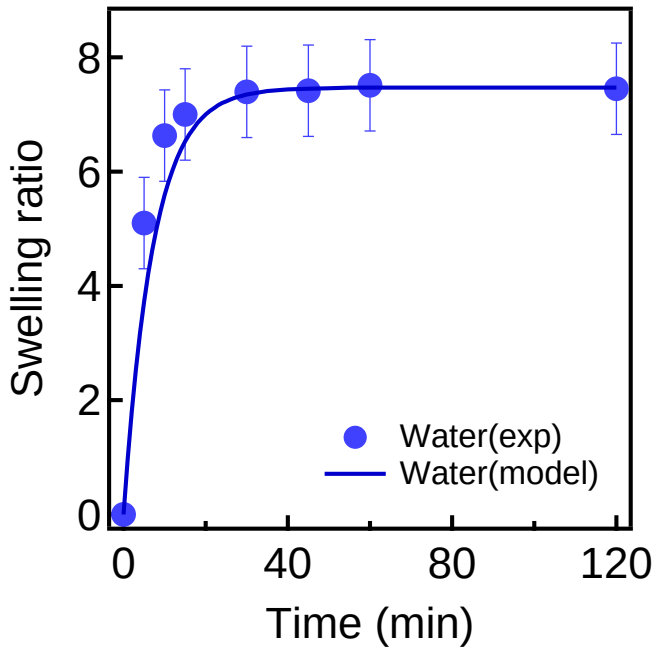

Fig. 4.18. A plot showing the swelling ratio of F-NIPAM in water as a function of time. The swelling is shown from the first order kinetic model. exp: experiment.

Fig. 4.18 shows a plot of swelling ratio (*S.R.*) for water as a function of submerging time. The absorption behavior can be explained with the first order kinetics (section. 2.8), which is a simplified form of the formal and rigorous equation provided by Tanaka et.al[144]. The first order kinetics, based on diffusion-controlled Fick's law, can accurately describe the swelling of different polymers as well as their shrinkage[148]. Here, the swelling ratio (*S.R.*) at a given time (t) is given by $S.R. = S.R._{eq}(1-e^{-k_s t})$ where $S.R._{eq}$ is the equilibrium swelling ratio and k_s is the swelling rate

constant. The rate constant (k_s) for water is found to be 0.0023 sec^{-1}. This rate constant is close to the value reported in literature[154]. The rate constant (k_s) is related to the diffusion coefficient (D) and the thickness of hydrogel (h) from Eqn. 14. Utilizing the Eqn. 14, the diffusion coefficient for water to our F-NIPAM is calculated as 7.3×10^{-4} cm^2/sec.

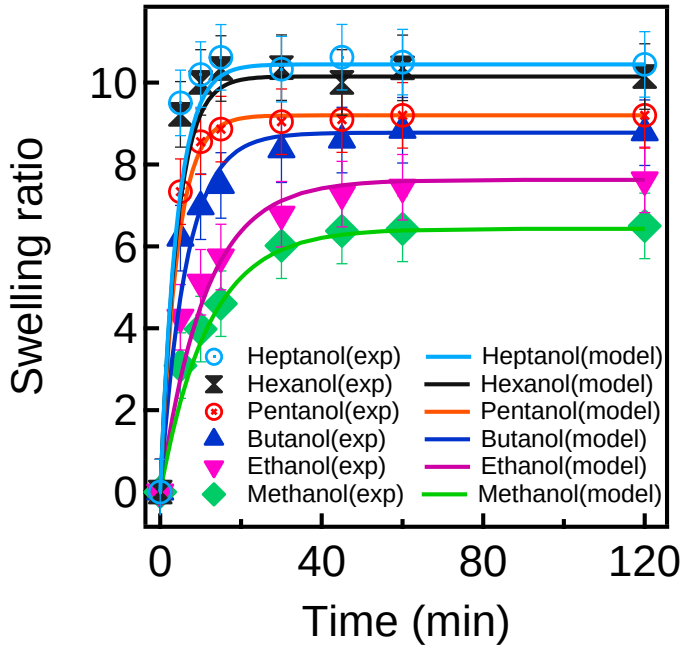

Fig. 4.19. A plot showing swelling ratio (*S.R.)* of F-NIPAM in alcohols with different number of hydrocarbons as a function of time. The swelling is shown with first order kinetic model. exp: experiment.

Fig. 4.19 shows the plots of *S.R.* values for various alcohols as a function of submerging time. Similar to water absorption, the simple first order kinetic model match well with the experimental data. The rate constants (k_s) are found as 0.0014 sec^{-1}, 0.0015 sec^{-1}, 0.0025 sec^{-1}, 0.0040 sec^{-1}, 0.0040 sec^{-1}, and 0.0040 sec^{-1} for methanol, ethanol, butanol, pentanol, hexanol and heptanol, respectively. We found the diffusion coefficient (D) values as 4.45×10^{-4} cm^2/sec, 4.78×10^{-4} cm^2/sec, 7.76×10^{-4} cm^2/sec, 12.73×10^{-4} cm^2/sec, 12.73×10^{-4} cm^2/sec and 12.73×10^{-4}

cm^2/sec respectively. The low value of diffusion coefficient for methanol is probably because of the low χ value of F-NIPAM with methanol (Fig. 4.17).

It is worth noting that the absorption can deviate from the first order kinetics when hydrogel swells extensively. This is because the solvent molecules dilute the polymer network resulting in transforming to a softer and rubbery phase. Consequently, the local viscosity decreases, and the diffusion coefficient slowly increases. The increase of diffusion coefficient (D) needs to be compensated by an increase in the polymer thickness (h) to maintain the rate constant (k_s). However, the increase of a diffusion coefficient is slower than the increase of hydrogel thickness, there is some declination in rate constant k. The rate constant (k_s) may decrease which can result in deviation from the first order kinetics.

4.9. Separation of Liquid-Liquid Mixtures

We demonstrated that our F-PNIPAM is hydrophilic and oleophobic (HL/OP) at a temperature below its LCST. We also found that the Flory-Huggins polymer-solvent interaction parameter χ of F-NIPAM with polar liquids (such as alcohols) are less than 0.5 while that for non-polar liquids (such as heptane and hexadecane) are greater than 0.5. This indicates our F-NIPAM can only absorb polar liquids while repelling non-polar liquids. Therefore, our F-NIPAM can be utilized to separate polar and non-polar liquid mixtures. The polar-non-polar liquid mixtures can be grouped into either immiscible (e.g. oil-water) and miscible (e.g. alcohol-alkane) mixtures.

4.9.1. Separation of Immiscible Liquid Mixtures

To demonstrate the separation of immiscible liquid mixtures using our F-NIPAM, hexadecane (oil)-water mixtures are used.

4.9.1.1. Free Oil-Water mixture

Fig. 4.20 shows the separation of free hexadecane and water (50:50 vol%, total volume = 6mL) mixture using our F-PNIPAM.

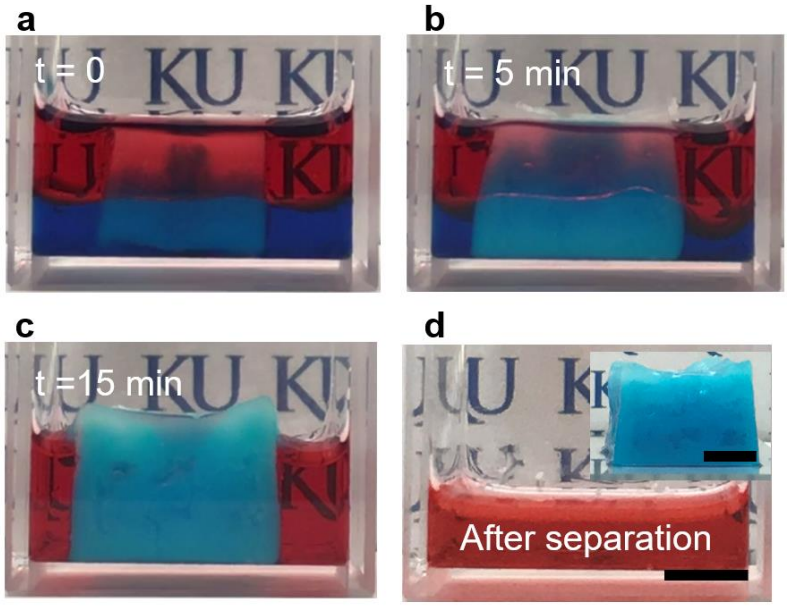

Fig. 4.20. Images showing separation of free hexadecane and water using F-NIPAM. **(a)** F-NIPAM submerged in 50:50 vol:vol of free hexadecane and water. Hexadecane is dyed red while water is dyed blue. **(b)** After 5 minutes of submerging F-NIPAM into the free hexadecane and water, the swelling of F-NIPAM by absorbing water. **(c)** F-NIPAM absorb all water within 15 minutes of submerging while repelling hexadecane. **(d)** After separation, almost pure hexadecane is left out. Inset: F-NIPAM turned blue by absorbing water. Scale bar: 1 cm.

As prepared F-NIPAM with the volume of 3 cm^3 was submerged into free hexadecane and water such that our F-NIPAM can contact both oil and water. Here, hexadecane was dyed red while water was dyed blue. The separation was performed at room temperature (T = 21°C). Based on the *S.R.* data for water (Fig. 4.12), we expect that our F-NIPAM selectively absorb all the water (3 mL) from the mixture in about 15 minutes. In fact, we found that our F-NIPAM can absorb all water and become blue.

We defined the separation efficiency by $\frac{S.R.}{S.R._{eq}} \times 100$, where $S.R._{eq}$ indicates the equilibrium swelling ratio and *S.R.* is the swelling ratio at a time (*t*). Fig. 4.21 shows a plot of separation efficiency for 50:50 vol:vol free hexadecane and water as a function of time. It can be seen that the separation efficiency reaches about 65% within a few minutes of submerging our F-NIPAM in the mixture. In 15 minutes, the separation efficiency was found to be about 99%.

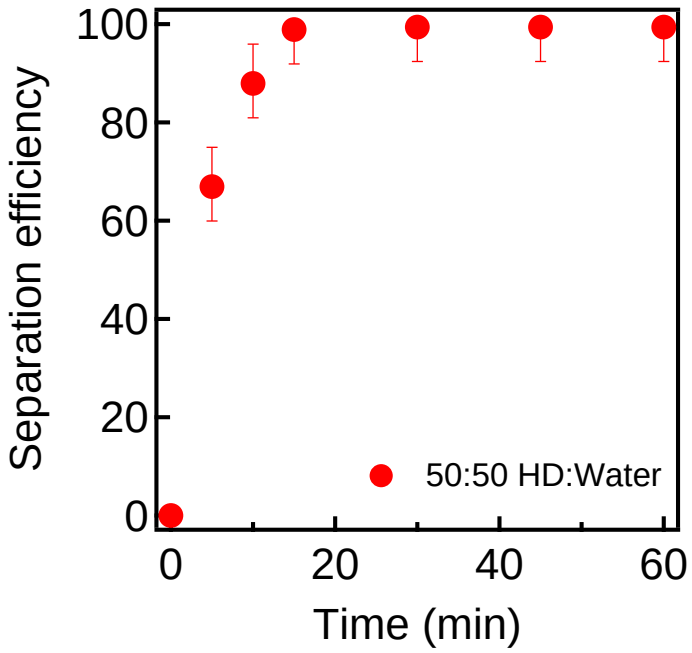

Fig. 4.21. A plot showing separation efficiency for free hexadecane and water (50:50 vol:vol) as a function of time using F-NIPAM.

We determined the separation efficiency using thermogravimetric analysis (TGA) (see Section 3.2.5). Briefly, about 16 mg of a liquid was heated from 25°C to 105°C at a rate of 5°C/min and the temperature was held constant at 105°C for 10 minutes.

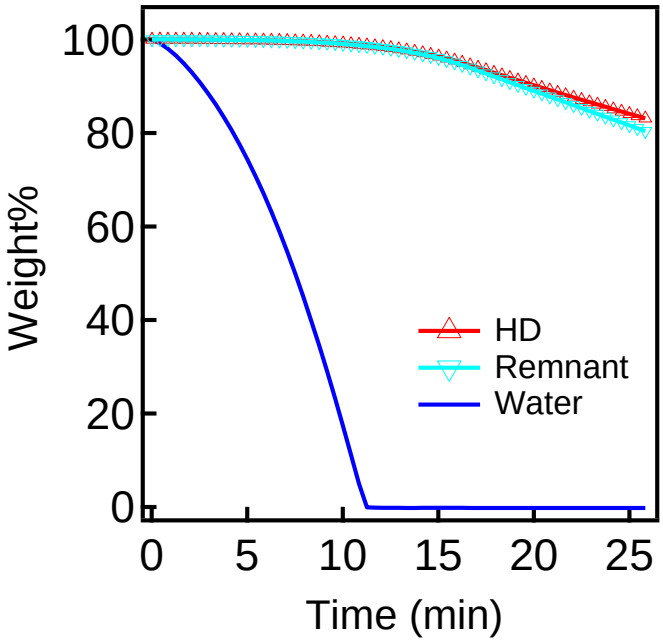

Fig. 4.22. A TGA plot for the remnant after separation of free hexadecane and water. The plots for hexadecane and water are also included.

Fig. 4.22 shows the TGA plot for remnant after free hexadecane and water separation. For comparison, TGA data for pure hexadecane and water are also shown. Here, the weight percentage of the liquid is plotted as a function of time. It is worth noting that the boiling point of water is 100°C while that for hexadecane is 287°C. The loss in weight of the remnant after separation of free hexadecane and water was compared with the weight loss of pure hexadecane and water to estimate the purity of the remnant. If the remnant is hexadecane, we expect the weight loss in remnant to be similar to that of pure hexadecane. Similarly, if the remnant has water, we expect the weight loss in remnant to be similar to that of water. From Fig. 4.22, it is apparent that the weight loss of our remnant after separation of free hexadecane and water is almost the same as that of pure hexadecane. From this comparison, we determined that the separation efficiency for free hexadecane and water mixture using our F-NIPAM is about 99%.

We also determined the separation efficiency by comparing the density of remnant after separation of free hexadecane and water with the density calibration curves (Fig. 3.2). We found that the density of the remnant after separation is 0.771 g/cm^3. Comparing this density with the calibration curves (Fig. 3.2), we found that the remnant consists of almost pure hexadecane with less than 1 vol% water.

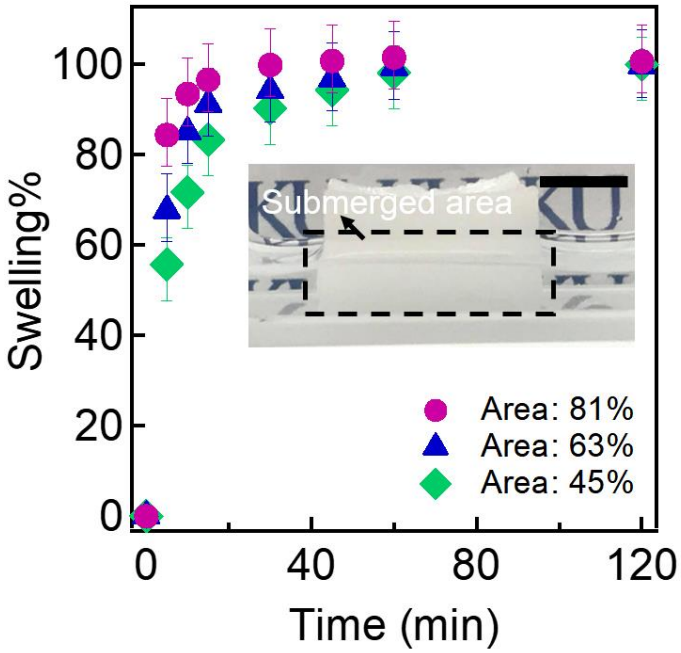

Fig. 4.23. Swelling percentage as a function of submerged time when the submerged area of F-NIPAM in water is varied. Inset: F-NIPAM submerged in water. Scale bar: 1 cm.

Fig. 4.23 shows the time-dependent evolution of the swelling percentage with a various submerged (contact) area of F-NIPAM in the water phase (see inset in Fig. 4.23). We define the swelling percentage as the swelling ratio (*S.R.*) with respect to the equilibrium swelling ratio ($S.R._{eq}$) i.e. $\text{Swelling\%} = \frac{S.R.}{S.R._{eq}}$. We found that decreasing the submerged area of F-NIPAM results in a slower swelling. This is because water is absorbed less when the submerged area is low.

Although the swelling rate is affected by the submerged area, F-NIPAMs could effectively reach to their equilibrium swelling after 120 minutes.

4.9.1.2. Separation of Oil-in-Water Emulsion:

We prepared hexadecane-in-water emulsion (30:70, vol:vol) using sodium dodecyl sulfate (SDS) as a surfactant. Fig. 4.24 shows a plot of size distribution of hexadecane droplets in the emulsion. The droplet sizes were digitally extracted from optical microscope images using 'imfindcircles' function in MATLAB. As apparent from the figure, the size of the dispersed phase (oil) is less than 20 μm indicating that the mixture is an emulsion.

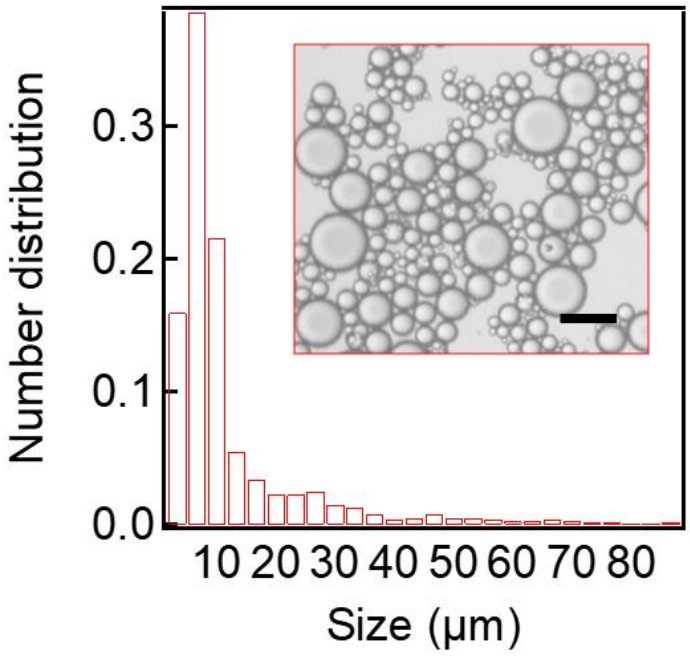

Fig. 4.24. A plot showing size distribution of hexadecane in SDS stabilized hexadecane-in-water (30:70 vol:vol) emulsion. Inset: An optical microscopic image of the emulsion. Scale bar: 100 μm.

SDS was dissolved in water such that the concentration is 10 mg/mL. Hexadecane was added to the SDS dissolved water such that the volume ratio of water and hexadecane is 70:30 followed by vigorous stirring for emulsification. We submerged F-NIPAM (1 cm^3) into 2 mL of

hexadecane-in-water emulsion (Fig. 4.25). Here, water is dyed blue and the hexadecane is dyed red. Our F-NIPAM selectively absorbs water from the emulsion. After 15 minutes, almost pure hexadecane was left indicating that almost all the water is absorbed by our F-NIPAM. We found that the separation efficiency reached around 99% in 30 minutes.

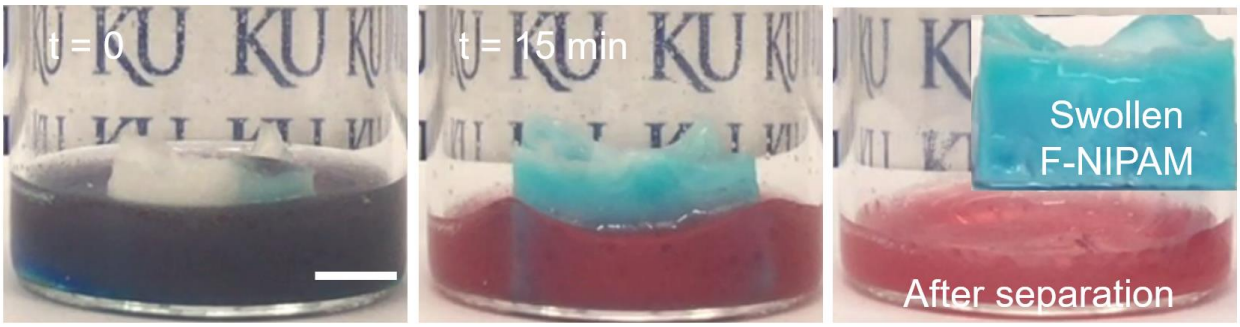

Fig. 4.25. Images showing separation of hexadecane-in-water emulsion using our F-NIPAM. Hexadecane is dyed red while the water is dyed blue. **(a)** F-NIPAM submerged in the hexadecane-in-water (30:70 vol:vol) emulsion. **(b)** After 30 minutes of submerging our F-NIPAM in the hexadecane-in-water emulsion. F-NIPAM became blue by absorbing water while the emulsion became hexadecane rich. **(c)** After separation of the hexadecane-in-water emulsion, the remnant is almost pure hexadecane. Scale bar: 1 cm.

We determined the separation efficiency for hexadecane-in-water (30:70 vol:vol) emulsion using TGA. Fig. 4.26 shows the TGA plot for remnant after separation of hexadecane-in-water emulsion along with pure hexadecane and water. We found that remnant after separation of the oil-in-water emulsion is almost same as that of pure hexadecane. From the comparison, we determined that the separation efficiency for hexadecane-in-water emulsion is about 99%.

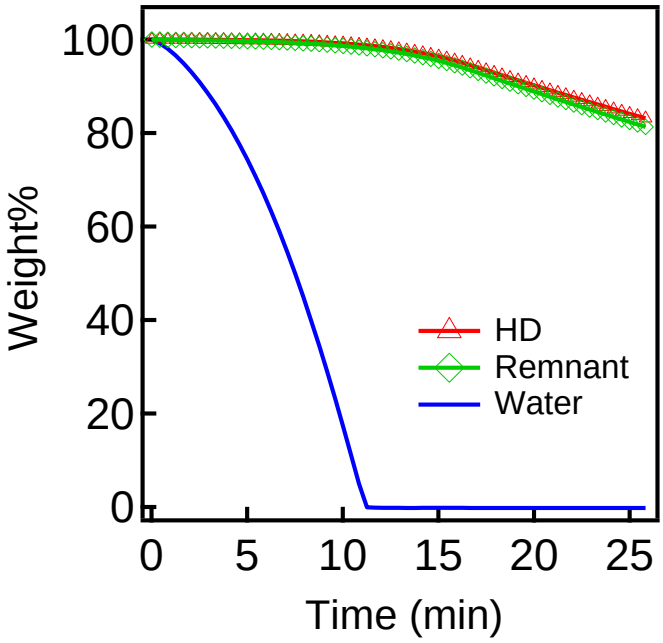

Fig. 4.26. A TGA plot for the remnant after separation of hexadecane-in-water (30:70 vol:vol) emulsion. The plots for pure hexadecane and water are also included.

The separation efficiency was also determined by comparing the density of remnant after separation with the calibration curves (Fig. 3.2). We found that the density of the remnant after separation is 0.772 g/cm^3. This is equivalent to hexadecane with less than 1 vol% water.

Fig. 4.27 shows the time-dependent separation efficiency of two different hexadecane-in-water emulsions with different oil composition (30% and 50 vol% of hexadecane). We found that an increase of hexadecane composition in the emulsions does not affect the final separation efficiency of our F-NIPAM (about 99 %). We can attribute this to our F-NIPAM's resistance to oil fouling. As our F-NIPAM is oil-repellent yet water-loving (HL/OP), our F-NIPAM can effectively repel oil while absorbing water. This can lead to a high separation efficiency even for the surfactant-stabilized oil-water emulsions. It is worth noting that separating 50:50 hexadecane-in-water emulsion is slower than 30:70 hexadecane in water emulsion. This can be attributed to

the fact that the contact area of our F-NIPAM and water is lowered due to the high concentration of oil phases.

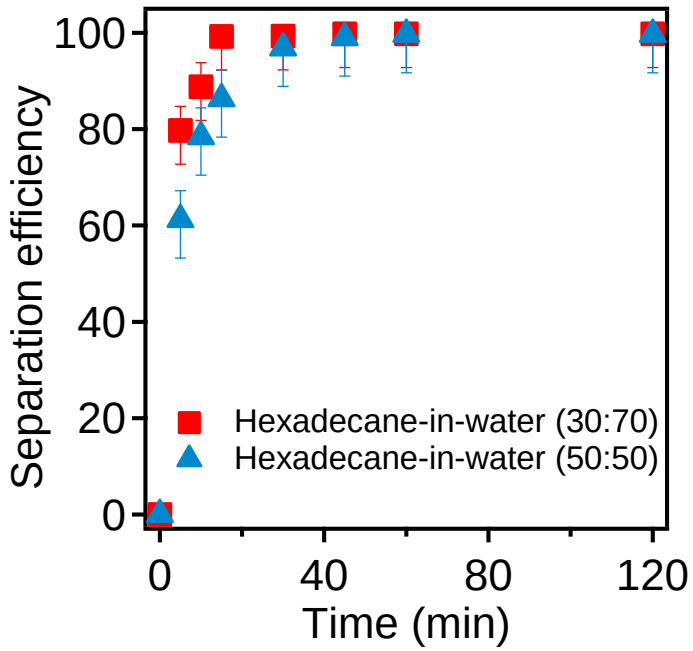

Fig. 4.27. A plot showing separation efficiency of F-NIPAM for hexadecane-in-water (30:70 vol:vol) emulsion as a function of time. The separation efficiency for hexadecane:water of 50:50 vol:vol is also shown.

4.9.1.3. Water-in-Oil Emulsion:

To further investigate the ability of our F-NIPAM to separate oil-water mixture, water-in-oil emulsion was also tested. We prepared water-in-hexadecane emulsion (50:50, vol:vol) using span80 as a surfactant. Here, span80 was dissolved in hexadecane such that the concentration of span80 in hexadecane is 1 mg/mL. Water was added to this span80 dissolved hexadecane such that the ratio of water to hexadecane by volume is 50:50. The mixture was then vigorously stirred for 10 minutes to prepare the emulsion. Fig. 4.28 shows a plot of size distribution of water droplets in the emulsion. As apparent from the figure, the majority of the dispersed water droplets is less than 20 μm in diameter indicating that the mixture is an emulsion.

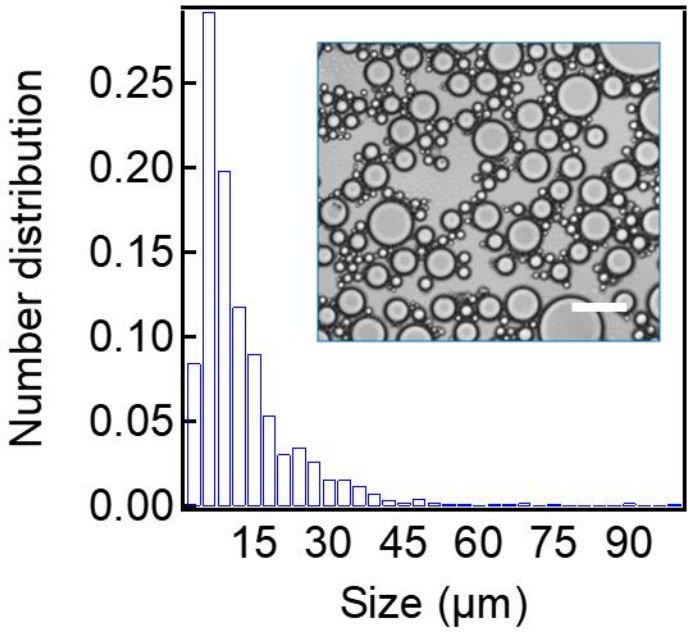

Fig. 4.28. A plot showing size distribution of water in span80 stabilized water-in-hexadecane (50:50 vol:vol) emulsion. Inset: Optical microscope image of the emulsion. Scale bar: 100 μm.

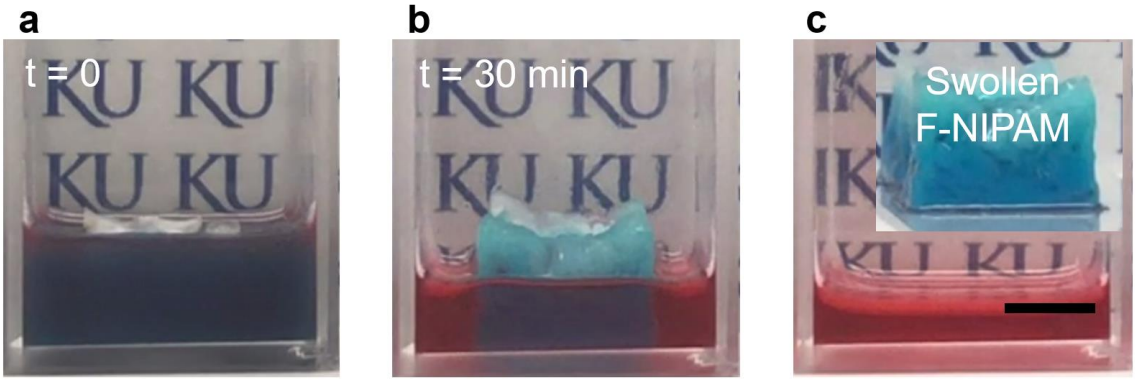

Fig. 4.29. Images showing separation of water-in-hexadecane emulsion using F-NIPAM. **(a)** F-NIPAM submerged into water-in-hexadecane (50:50 vol:vol). Water is dyed blue while hexadecane is dyed red. **(b)** After 30 minutes of submerging F-NIPAM. **(c)** After separation, almost pure hexadecane is left while our F-NIPAM became blue by absorbing water. Scale bar: 1 cm.

Fig. 4.29 shows the separation of water-in-hexadecane emulsion (50:50, vol:vol) using our F-NIPAM. Our F-NIPAM (3 cm^3) is submerged in hexadecane-in-oil emulsion (6 mL). Water is dyed blue while hexadecane is dyed red. After 30 minutes, only hexadecane (dyed red) was left in

the container. This is because of our F-NIPAM's selective absorption of water droplets from the emulsion.

We determined the separation efficiency using TGA. Fig. 4.30 shows the TGA plot for remnant after separation. We found that remnant after separation is almost same as that of pure hexadecane. From the comparison, we determined that the separation efficiency for water-in-hexadecane emulsion is greater than 99%. The separation efficiency was also determined by comparing the density of remnant after separation with the calibration curves (Fig. 3.2). We found that the density of the remnant is 0.772 g/cm^3. This is equivalent to hexadecane with less than 1 vol% water.

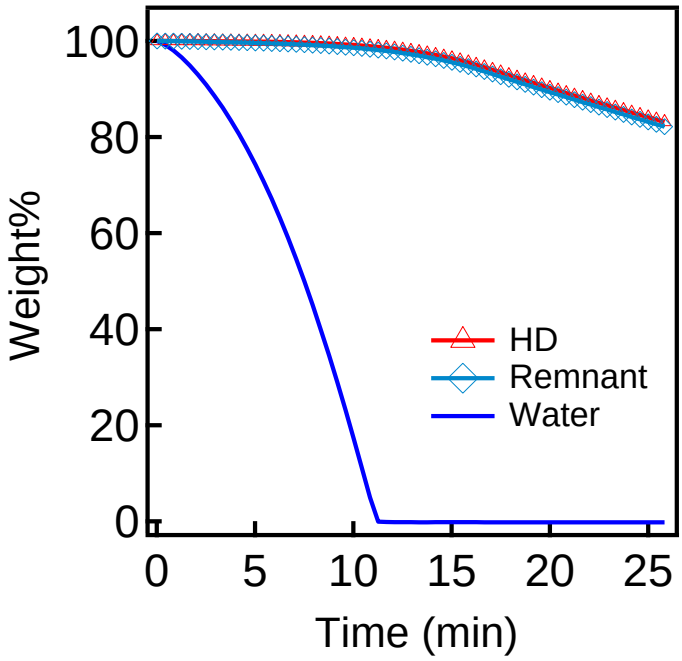

Fig. 4.30. A TGA plot for the remnant after separation of water-in-hexadecane (50:50 vol:vol) emulsion. The plots for pure hexadecane and water are also included.

Fig. 4.31 shows a plot of time dependent separation efficiency for span80-stabilized water-in-hexadecane (50:50 vol:vol) emulsion. It indicates that our F-NIPAM can effectively absorb the

water droplets although they are dispersed in the oil phase. Unlike our F-NIPAM, a neat NIPAM (HL/OL) shows very slow separation for water-in-oil emulsions (Fig. 4.31). This is because a neat NIPAM is easily fouled by oil which makes the water droplets difficult to be absorbed.

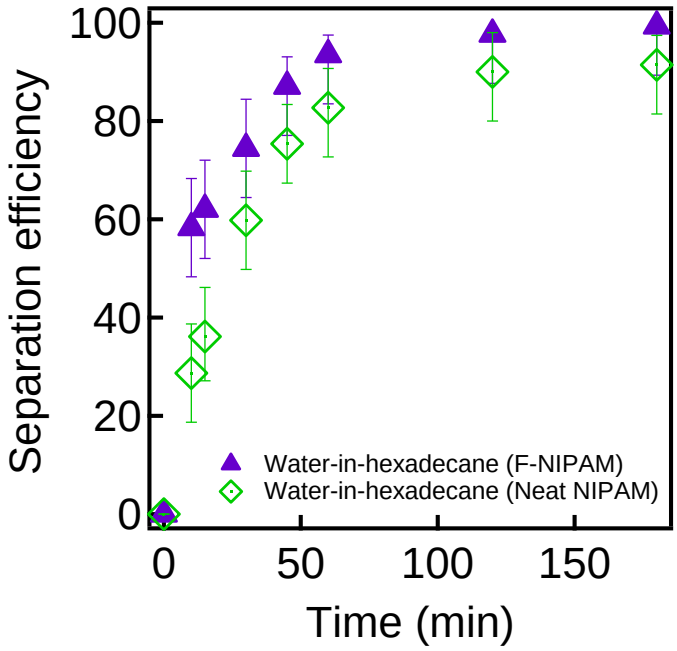

Fig. 4.31. A plot showing separation efficiency of F-NIPAM for water-in-hexadecane (50:50 vol:vol) emulsion as a function of time. The separation efficiency of F-NIPAM is higher than neat NIPAM.

4.9.2. Separation of Miscible Polar-Non-Polar Liquid Mixtures

We also tested the capability of our F-NIPAM to separate miscible liquid mixtures. First, we separate a miscible liquid mixture that consists of ethanol (polar) and heptane (non-polar). Heptane and ethanol are miscible in all ranges of compositions. Here, we used the heptane-ethanol azeotrope (54.5 vol% heptane and 45.5 vol% ethanol) to eliminate the evaporation effect during separation process.

Fig. 4.32 shows the separation of the heptane-ethanol azeotrope (6 mL) using our F-NIPAM (≈ 3 cm^3). Here, only ethanol is dyed blue while heptane is colorless. We found that

ethanol heptane azeotrope becomes colorless after 60 minutes. This is because our F-NIPAM selectively absorb ethanol (Fig. 4.32b**).** By absorbing ethanol, our F-NIPAM turns blue while the colorless heptane is left in the container (Fig. 4.32c).

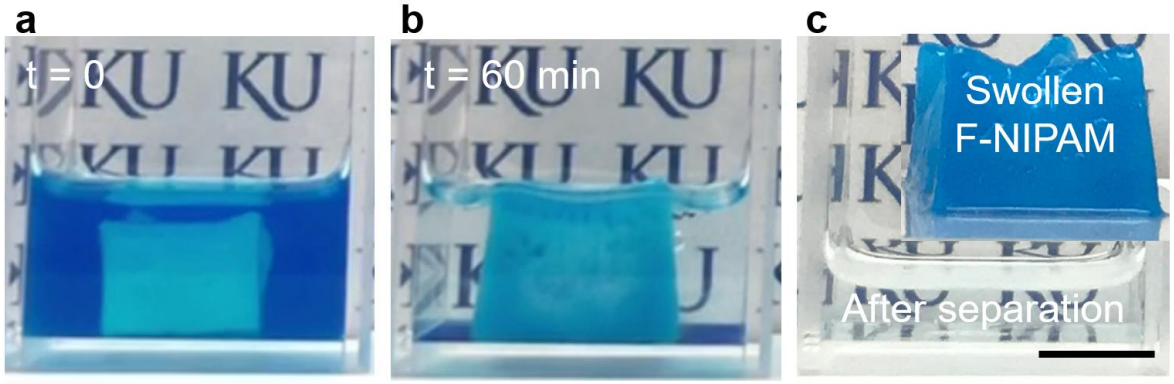

Fig. 4.32. Separation of heptane-ethanol azeotrope using our F-NIPAM. **(a)** F-NIPAM (≈ 3 cm^3) submerged into heptane-ethanol azeotrope (6 mL). Heptane is colorless while ethanol is dyed blue. **(b)** After 60 minutes of submerging F-NIPAM, the heptane-ethanol azeotrope becomes colorless. **(c)** After separation, F-NIPAM became blue by absorbing ethanol while the left liquid is colorless heptane. Scale bar: 1 cm.

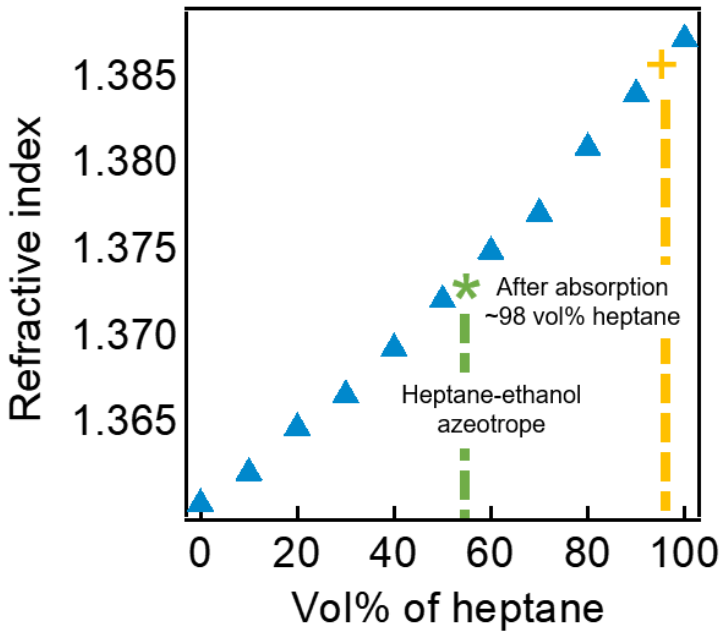

Fig. 4.33. A plot showing a refractive index of the heptane-ethanol mixture as a function of volume percentage of heptane. It indicates the refractive index of heptane-ethanol azeotrope before and after separation.

We utilized the refractive index to determine the composition of heptane-ethanol mixture after separation. Fig. 4.33 shows a plot of refractive index of heptane-ethanol mixture as a function of vol% of heptane. We found that the refractive index of the remnant after separation was 1.3864. This is equivalent to ≈ 98 vol% heptane. We also compared the volume of heptane and ethanol before and after absorption to verify the amount of ethanol (or heptane) absorbed. We found that the volume change of heptane is negligible while our F-NIPAM absorbs about 2.67 mL of ethanol. The results indicated that our F-NIPAM can selectively absorb ethanol from heptane-ethanol mixture. To our knowledge, this is the first demonstration of separation of azeotrope using selective absorption at ambient conditions (i.e. room temperature and one atmosphere).

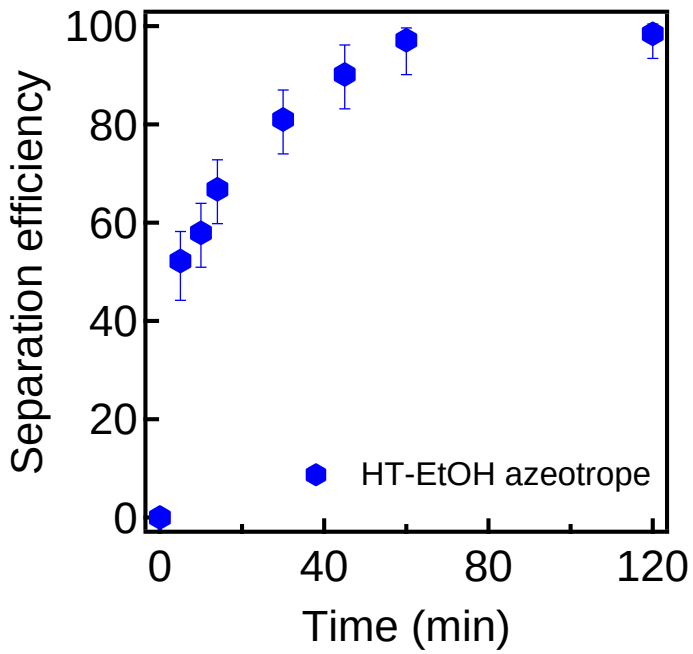

Fig. 4.34. A plot showing separation efficiency for heptane-ethanol azeotrope as a function of submerged time.

Fig. 4.34 shows the heptane-ethanol azeotrope separation efficiency as a function of submerged time. We determined the separation efficiency using the RI index measurements. Our

F-NIPAM can rapidly absorb ethanol when it is submerged. After about 30 minutes, we found that the absorption rate becomes slower. This can be due to the fact that our F-NIPAM becomes surrounded by heptane as most ethanol is absorbed.

Separation of heptane-ethanol azeotrope was further demonstrated by allowing a drop of the azeotrope to slide on our F-NIPAM surface. Our F-NIPAM surface is tilted with an angle of about 10° to the horizontal. While the azeotrope droplet slides off the surface, our F-NIPAM selectively absorbs ethanol from the droplet (Fig. 4.35). Eventually we can collect almost pure heptane droplet at the end of the surface. We attribute this to a combination of oleophobicity (Fig. 4.6) and preferential absorption (Fig. 4.32) for ethanol over heptane.

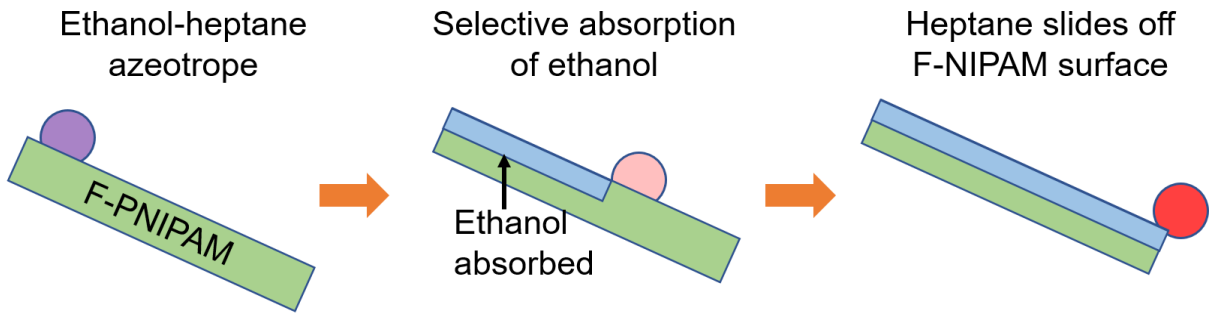

Fig. 4.35. A schematic showing the selective absorption of ethanol from heptane-ethanol mixture when sliding on the surface of F-NIPAM.

Fig. 4.36 shows the sequential images of a droplet of heptane-ethanol azeotrope sliding on our F-NIPAM surface. Here, ethanol is dyed blue while heptane is dyed red. As ethanol is selectively absorbed by our F-NIPAM, the surface of F-NIPAM turns blue while the droplet becomes heptane rich. Eventually, we can collect almost pure heptane after the droplet completes sliding the surface.

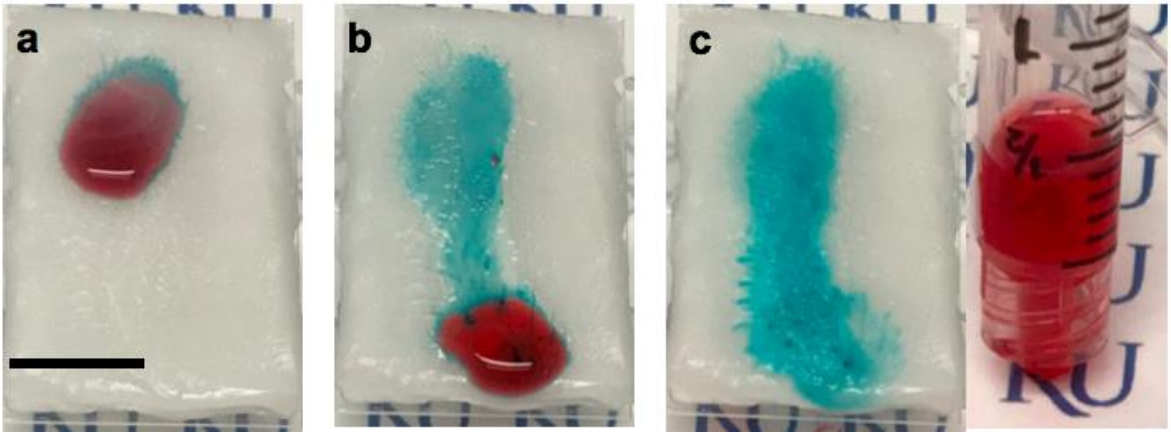

Fig. 4.36. Images showing selective absorption of ethanol while heptane-ethanol azeotrope is sliding on the surface of F-NIPAM. Here, ethanol is dyed blue while heptane is colorless. **(a)** Heptane-ethanol azeotrope droplet starting to slide on F-NIPAM surface. **(b)** Ethanol is absorbed while the azeotrope slides F-NIPAM surface. Absorption of ethanol can be identified by changing the color of F-NIPAM surface to blue. **(c)** Sliding is completed on F-NIPAM surface and pure heptane is collected. Scale bar: 1 cm.

It is worth noting that the oil repellency (oleophobicity) is important to prevent the oil fouling. This will allow for effective absorption of polar liquid (such as ethanol) while repelling oil. In fact, we found that a neat NIPAM (HL/OL) is completely wet by the ethanol-heptane mixture and eventually gets fouled.

Selective absorption of ethanol from the heptane-ethanol azeotrope can be explained by Flory-Huggins polymer-solvent interaction parameter χ[28]. The χ value of 0.5 is the limiting value for determining whether or not a polymer is miscible with solvent. If $\chi \leq 0.5$, it indicates more attractive molecular interactions between a polymer and a liquid, resulting in absorption of the liquid. If $\chi > 0.5$, the polymer cannot absorb or even release the liquid. As indicated in section 4.7, the χ values of F-NIPAM with heptane is 0.82. This indicates that our F-NIPAM repels heptane. On the other hand, the χ value for ethanol was found to be 0.432 indicating that our F-NIPAM can absorb ethanol. Consequently, our F-NIPAM can absorb ethanol while repelling heptane leading to the separation of heptane-ethanol azeotrope.

We also demonstrated the separation of miscible methanol (MeOH) and methyl oleate (MO) mixture. Methyl oleate is a representative for biodiesel whereas methanol is a byproduct that needs to be separated. We estimated that the χ value of our F-NIPAM with methanol is 0.483 ($\chi < 0.5$) whereas with methyl oleate it is 1.237 ($\chi > 0.5$). Therefore, we expect that F-NIPAM can selectively absorb methanol while repelling methyl oleate.

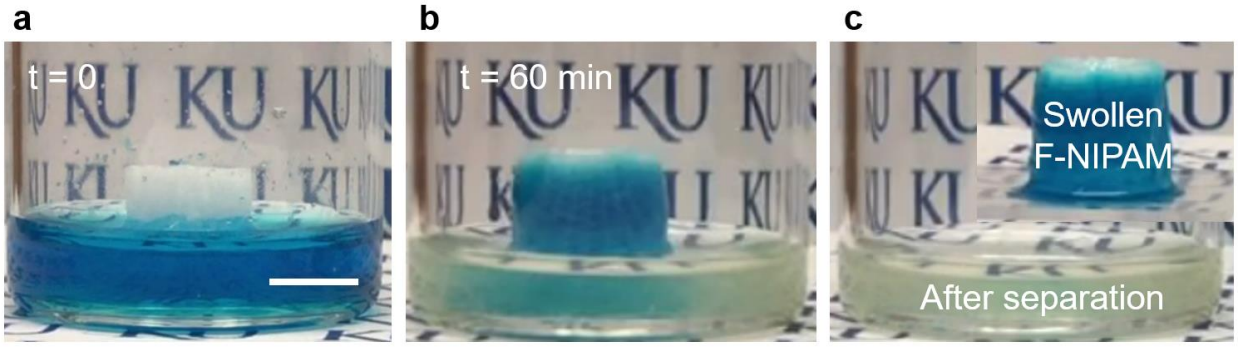

Fig. 4.37. Photographs showing separation of the miscible MeOH-MO mixture with F-NIPAM. **(a)** F-NIPAM submerged in MeOH-MO mixture of 30:70. Methanol is dyed blue while methyl oleate is intrinsically light yellow in color. **(b)** F-NIPAM selectively absorbs methanol from the mixture. **(c)** After separation, F-NIPAM becomes blue by absorbing methanol while almost pure methyl oleate is left out. Scale bar: 1 cm.

Fig. 4.37 shows the separation of the miscible MeOH-MO mixture (30:70 vol:vol) using our F-NIPAM (1 cm^3). Here, methanol is dyed blue while methyl oleate shows intrinsically light-yellow color. Once our F-NIPAM is submerged in the MeOH-MO mixture (Fig. 4.37a), it selectively absorbs methanol while repelling methyl oleate (Fig. 4.37b). After separation, our F-NIPAM becomes blue by absorbing blue-dyed methanol and almost pure methyl oleate is left (Fig. 4.37c). Fig. 4.38 shows a plot of separation efficiency for MeOH-MO mixture (30:70 vol:vol) as a function of submerging time. We found that the separation efficiency reaches about 98% within 60 minutes.

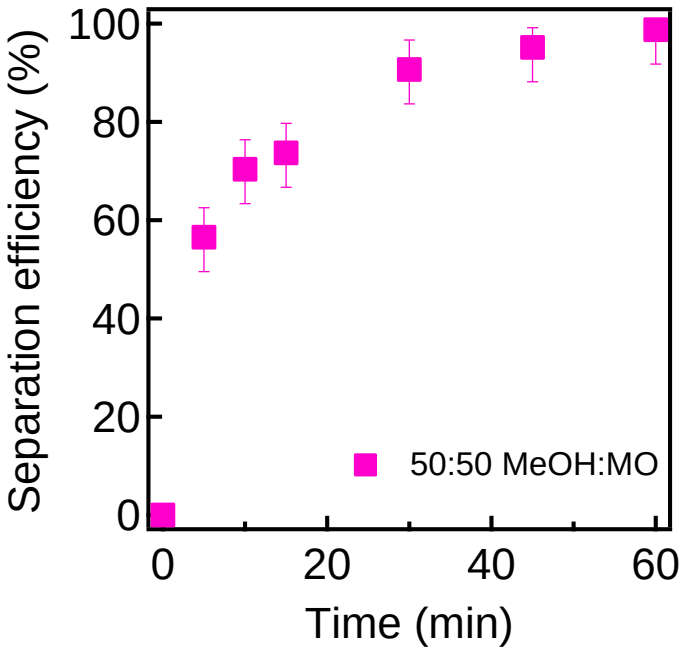

Fig. 4.38. A plot showing separation efficiency for methanol-methyl oleate mixture as a function of time. MeOH: Methanol. MO: Methyloleate.

4.9.3. Separation of Miscible Polar-Polar Liquid Mixtures

Based on the success of separating miscible polar-non-polar liquids, we tested our F-NIPAM to separate miscible polar-polar liquids. If our F-NIPAM shows $\chi > 0.5$ for one phase and $\chi \leq 0.5$ for the other phase, it can selectively absorb one over the other. Additionally, a lower value of χ implies a better miscibility of a liquid for a polymer. Based on the aforementioned criteria, polar-polar miscible liquids can be separated using our F-NIPAM if the two phases show substantially different χ values (i.e. ideally $\chi_{liquid1} \leq 0.5$ while $\chi_{liquid2} > 0.5$). From our literature survey[138], we found that the χ value for water is 0.45 when the temperature is below the LCST. On the other hand, the χ value for ethanol is 0.43 (Fig. 4.17). Since both χ values are less than 0.5, we expect that our F-NIPAM can absorb both ethanol and water. It is worth noting that $\chi_{water} > \chi_{EtOH}$ indicates less absorption of water than ethanol. In fact, we found from equilibrium swelling ratios (see

section 4.6.1), our F-NIPAM absorbs a larger amount of ethanol than water. When the temperature becomes higher than the LCST, our F-NIPAM starts to repel water and even release the absorbed liquid. This is due to the hydrophobic interaction between the isopropyl groups of F-NIPAM prevailing over the hydrophobic hydration by water molecules when the temperature is above the LCST. In fact, the χ value for water increases with increasing temperature and becomes greater than 0.5 when the temperature is higher than the LCST. On the other hand, χ value for ethanol is independent of temperature ($\chi_{EtOH} = 0.43$). Therefore, $\chi_{water} > 0.5 > \chi_{EtOH}$ can be achieved when temperature is above LCST. Guided by the above principles, we expect that our F-NIPAM can separate ethanol-water mixture at an elevated temperature (T = 40°C) above LCST.

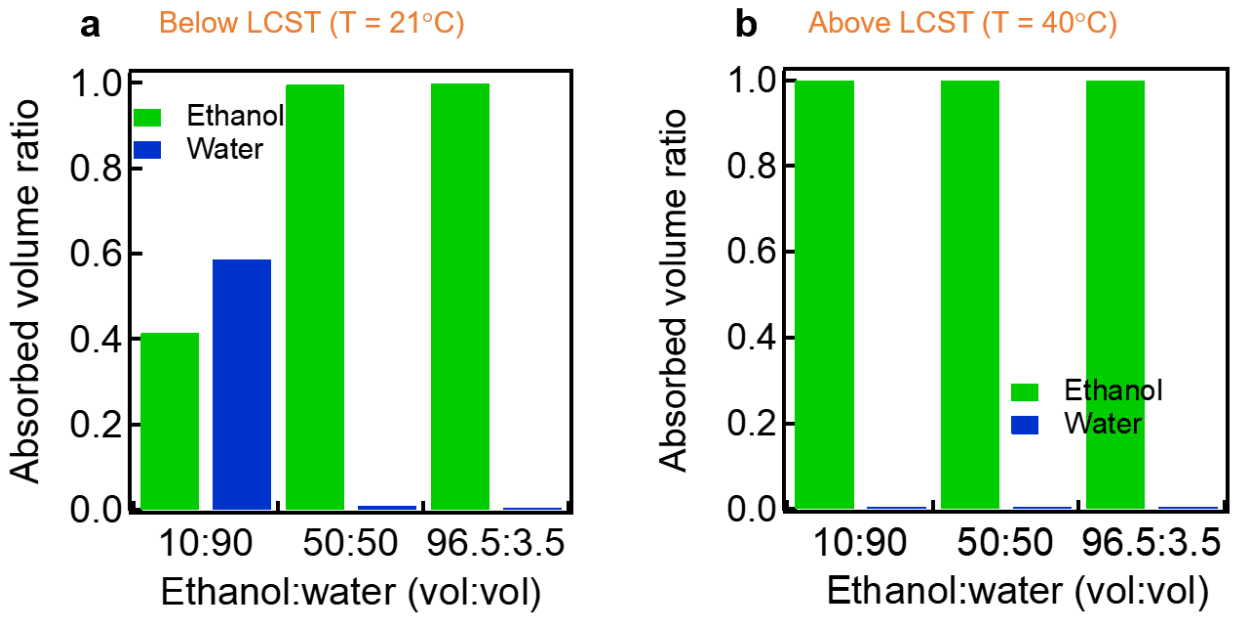

Fig. 4.39. Plots showing the volume ratio of liquid absorbed by F-NIPAM as a function of the ethanol:water (vol:vol). **(a)** Below its LCST (T = 21°C). **(b)** Above LCST (T = 40°C). Ethanol:water of 96.5:3.5 corresponds to the composition of ethanol-water azeotrope.

Fig. 4.39 shows plots of the volume ratio of the absorbed liquid at temperature below LCST (T = 21°C) and above LCST (T = 40°C). Here we used various concentrations of ethanol-water

mixture including 10:90, 50:50 and 96.5:3.5 (ethanol:water (vol:vol)). Of note, the composition 96.5: 3.5 (ethanol:water (vol:vol)) is the azeotrope of ethanol-water mixture. When the temperature is below LCST, we found that the volume ratio of ethanol in the absorbed liquid is significantly higher than the initial ethanol composition in the feed mixture. For example, the volume fraction of ethanol in the absorbed liquid is 99.59 vol% although the initial ethanol composition is 50 vol% (see Table 4.6). We attribute this to $\chi_{EtOH} < \chi_{water}$ ($\chi_{EtOH} = 0.43$ and $\chi_{water} = 0.45$). Because $\chi_{EtOH} < \chi_{water,}$ F-NIPAM absorbs higher volume of ethanol from the ethanol-water mixture.

Table 4.6. Volumes of ethanol and water absorbed by our F-NIPAM below and above LCST for various ethanol:water (vol:vol) ratio. Negative signs indicate release of the given liquid.

	Ethanol:water (vol:vol)	**10:90**	**50:50**	**96.5:3.5 (Azeotrope)**
Below LCST (T = 21°C)	Water absorbed (μL)	41	3	-360
	Ethanol absorbed (μL)	29	730	1,920
Above LCST (T = 40°C)	Water absorbed (μL)	-194	-183	-330
	Ethanol absorbed (μL)	29	785	1,840

Although our F-NIPAM is expected to selectively absorb ethanol over water, we found that our F-NIPAM can absorb a significant amount of water when the feed mixture is water-rich (i.e. ethanol:water = 10:90 (vol:vol)). This is probably because our F-NIPAM is mostly surrounded by water that prevents our F-NIPAM from contacting ethanol. When the temperature is above LCST, our F-NIPAM absorbed only ethanol while repelling water. This is probably because $\chi_{water} > 0.5 > \chi_{EtOH}$ at a temperature above LCST. Above LCST, the χ value of F-NIPAM for water becomes

greater than 0.5 indicating that F-NIPAM repels water. Moreover, the χ value of F-NIPAM for ethanol is constant (χ_{EtOH} = 0.43).

We also found that the total volume of liquid absorbed by our F-NIPAM is different for different composition of ethanol-water mixture (Table 4.6). Here, the total volume of absorbed liquid follows 10:90 < 50:50 < 96.5:3.5 for ethanol:water (vol:vol) composition. This can be explained by cononsolvency. According to cononsolvency, the absorption of NIPAM in ethanol-water mixture is changed with the composition of ethanol in ethanol-water mixture. Previous reports have demonstrated that the absorption NIPAM is minimum at 24.3 vol% (7 mol%) and increases when the vol% of ethanol is increased further.

We also tested our F-NIPAM in separating another polar-polar liquid mixture consisting of dimethylformamide (DMF) and water. We calculated the χ value of our F-NIPAM with DMF using Eqn. 8. We estimated the value as χ_{DMF} = 0.22. Since $\chi_{DMF} < \chi_{water}$ (χ_{water} = 0.45), we expect that our F-NIPAM can absorb a larger amount of DMF than water. When the temperature is above the LCST (T = 40°C), χ_{water} becomes greater than 0.5 while that for DMS remains constant (0.22). Therefore, we expect that our F-NIPAM absorbs only DMF from DMF-water mixture at an elevated temperature (i.e., above its LCST). This will lead to separation of DMF-water mixture.

Fig. 4.40 shows plots of the volume ratio of the absorbed liquid at a temperature below LCST (T = 21°C) and above LCST (T = 40°C). Here we used various compositions of DMF-water mixture including 10:90, 50:50 and 90:10 (DMF:water (vol:vol)).

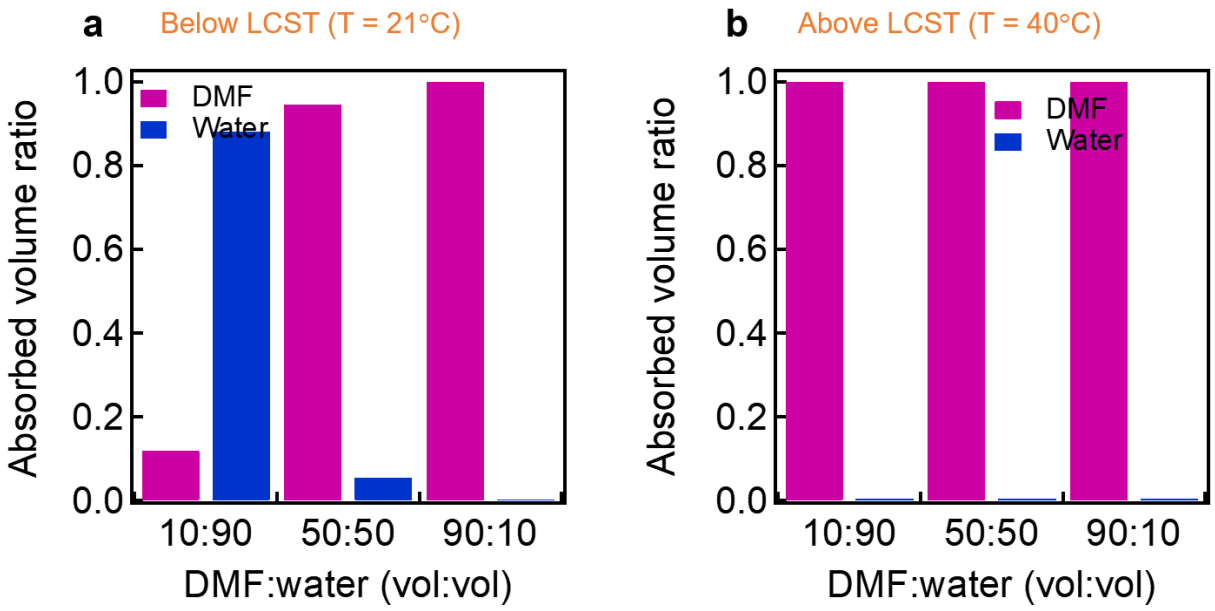

Fig. 4.40. Plots showing volume ratio of liquids absorbed by F-NIPAM as a function of DMF:water (vol:vol). **(a)** Below LCST (T = 21°C). **(b)** Above LCST (T = 40°C).

Table 4.7. Volumes of DMF and water absorbed by our F-NIPAM below and above LCST for various DMF:water (vol:vol) ratio. Negative signs indicate release of the given liquid.

	DMF:water (vol:vol)	**10:90**	**50:50**	**90:10**
Below LCST (T = 21°C)	Water absorbed (μL)	670	35	-500
	DMF absorbed (μL)	90	608	1,663
Above LCST (T = 40°C)	Water absorbed (μL)	-100	-209	-673
	DMF absorbed (μL)	91	605	1,979

When the temperature is below LCST, we found that the volume ratio of DMF in the absorbed liquid is significantly higher than that of the initial DMF composition in the feed mixture. For example, the volume fraction of DMF in the absorbed liquid is about 94% although the initial DMF composition is 50 vol% (see Table 4.7). Similar to ethanol-water separation, we attribute

this to $\chi_{DMF} < \chi_{water}$. Although our F-NIPAM is expected to selectively absorb a larger amount of DMF over water, we found that our F-NIPAM can absorb a significant amount of water when the feed mixture is water-rich (i.e., DMF:Water=10:90 vol:vol). This is probably because our F-NIPAM is mostly surrounded by water that prevents our F-NIPAM from contacting with DMF. When the temperature is above the LCST, our F-NIPAM only absorb DMF while repelling water. This is because $\chi_{DMF} < 0.5 < \chi_{water}$ at a temperature above the LCST. Therefore, we expect that DMF-Water can be completely separated using our F-NIPAM by selectively absorb DMF over water at an elevated temperature (i.e., above LCST).

4.10. Recovery of the Absorbed Liquid

In order for our separation method to be economically viable and practically feasible, it is critical to recover the absorbed liquid from our F-NIPAM after separation. Facile recovery of the absorbed liquid will allow for reusing our F-NIPAM for further separation operations.

4.10.1. Recovery of Water at a Temperature Above LCST

Due to the thermo-responsive behavior of NIPAM, our F-NIPAM can release the absorbed liquid (water) at a temperature above the LCST. It should be emphasized that the LCST for our F-NIPAM is found to be about 28°C (Fig. 4.3). This allows for water release at a mild heat treatment. Fig. 4.41 shows the recovery of water at T = 33°C. We found that our F-NIPAM can release ≈ 1,150 mg of water. This is equivalent to the recovery of about 82% of the absorbed water.

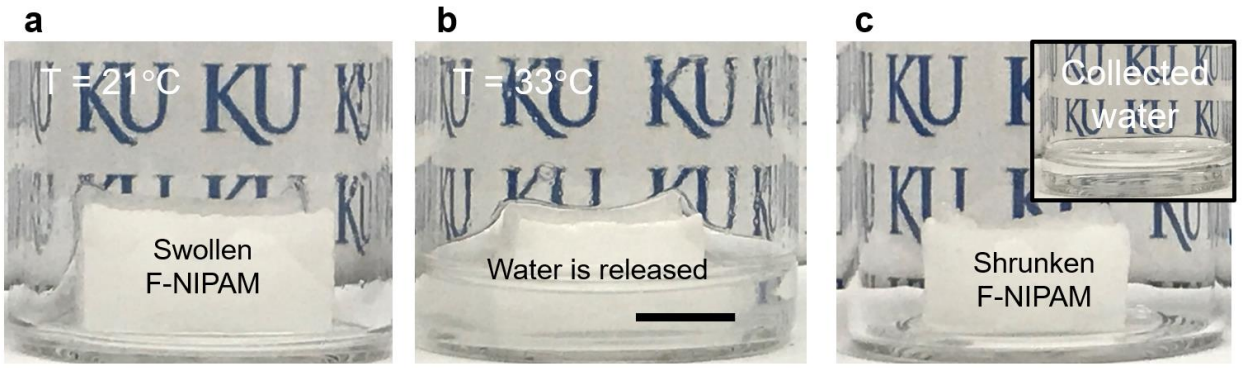

Fig. 4.41. Images showing the release of water from F-NIPAM with mild application of heat (T = 33°C). **(a)** F-NIPAM swollen to its equilibrium by absorbing water at T = 21°C. **(b)** F-NIPAM released 82% of absorbed water at a temperature of T = 33°C. **(c)** F-NIPAM is shrunken to about its as-prepared state. Inset: Released water from F-NIPAM can be collected. Scale bar: 1 cm.

It is well-documented that NIPAM can release water at a temperature above LCST because the hydrophobic interaction between the isopropyl groups in NIPAM prevails over hydrophilic hydration. NIPAM possesses the hydrophilic (HL) amide group and hydrophobic (HP) isopropyl group (Fig. 4.1). At a temperature below the LCST, water molecules hydrogen bond with the hydrophilic amide group. Moreover, the water molecules interact with isopropyl group through the hydrophobic hydration by forming a cage-like structure. This allows NIPAM to absorb water. When the temperature is above the LCST, the interaction of water molecules with isopropyl group is weakened due to an increase in entropy. Further, hydrophobic interaction between the isopropyl groups increases resulting in the collapse of the network. Consequently, the absorbed water is released. Such LCST behavior of NIPAM is reflected to the change of χ value as a function of temperature. Of note, the χ value for water at a temperature below its LCST is 0.45 indicating that NIPAM can effectively absorb water. When the temperature is above its LCST, the χ value for water becomes 0.55 indicating that NIPAM repels (and releases) water. It is worth noting that the

LCST of NIPAM can be controlled by copolymerizing with other polymers. For example, adding a low surface energy material such as F-acrylate considered in this study can lower the LCST.

4.10.2. Recovery of Water and Ethanol Using Salt Aqueous Solution

Salt ions can induce deswelling of NIPAM and consequently releasing of the absorbed liquid. It is documented[151] that anions contribute to the deswelling process. First, anions can polarize the water molecules that hydrogen bond to the amide groups. This results in the weakened hydrogen bond. In addition, anions disrupt the hydrophobic hydration of water molecules to the isopropyl groups.

We found that sodium chloride (NaCl) can effectively induce deswelling of our F-NIPAM and consequently releasing the absorbed liquid. Fig. 4.42 shows a plot of % water recovery of our F-NIPAM submerged in aqueous NaCl solution. Here we used two different concentrations (50 mg/mL and 100 mg/mL) of NaCl. We found that about 98% of the absorbed water can be recovered by submerging our F-NIPAM in NaCl solution for 120 minutes. The recovery of water using aqueous salt solution follows the first order kinetics (see section 2.8) given as Recovery% = $(1-e^{-k_r t})\times 100$. Here, k_r is the recovery rate at a given time (t). The first order kinetic model matches well with our experimental data with k_r = 0.0048 and k_r = 0.0011 for 50 mg/mL and 100 mg/mL, respectively. It is worth noting that submerging in 100 mg/mL allows for a rapid release of water. This is because higher salt concentration allows for a greater gradient between inside and outside of F-NIPAM. Consequently, it allows for rapid release of the water from our F-NIPAM.

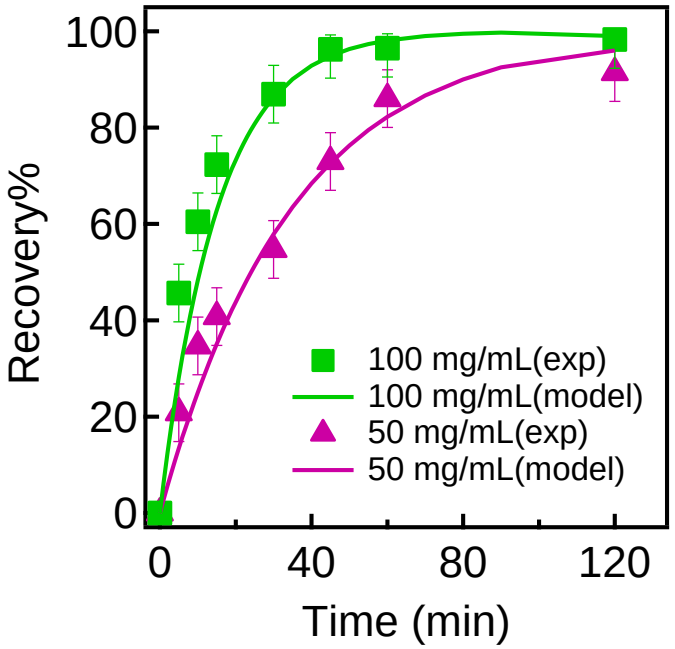

Fig. 4.42. A plot showing water recovery from F-NIPAM as a function of time in various concentration of aqueous NaCl solution. Here, the water release by F-NIPAM is described by first order kinetic model.

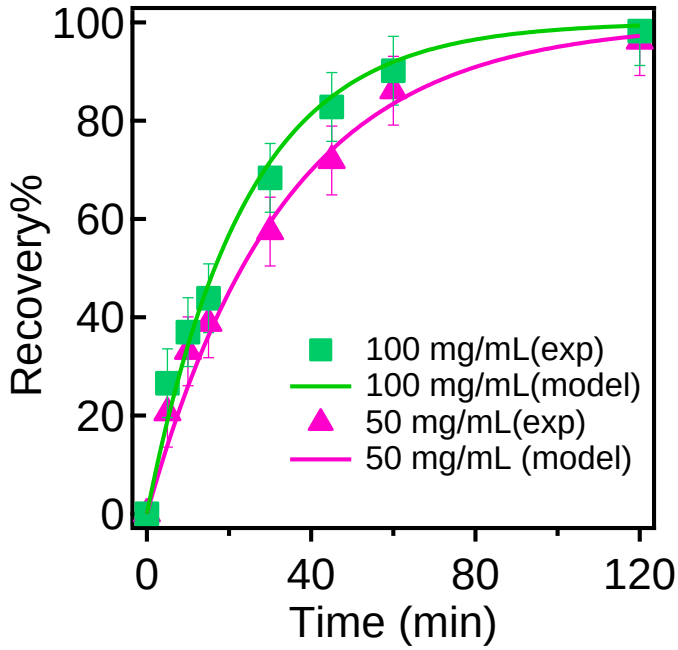

Fig. 4.43. A plot showing ethanol recovery from F-NIPAM as a function of time in various concentration of aqueous NaCl solution. Here, the ethanol release by F-NIPAM is described by first order kinetic model.

We also demonstrate that ethanol can also be released using an aqueous NaCl solution. Fig. 4.43 shows a plot of the percentage of ethanol recovery for our F-NIPAM submerged in aqueous NaCl solutions with two different concentrations (50 mg/mL and 100 mg/mL). We found that about 98% of ethanol can be recovered. The first order kinetics model can describe well our experimental data with k_r = 0.0005 for 50 mg/mL and k_r = 0.0007 for 100 mg/mL.

4.11. Continuous Separation and In-Situ Recovery of the Absorbed Liquid

We engineered an apparatus that allows for continuous separation of the liquid mixture and releasing the absorbed liquid from our F-NIPAM. In order to achieve the continuous separation and simultaneous releasing the absorbed liquid, our F-NIPAM needs to contact a liquid mixture to selectively absorb one phase over the other while contacting the salt aqueous solution to release the absorbed liquid. Fig. 4.44a shows a schematic illustrating the apparatus for continuous separation of oil-water mixture and simultaneous recovery of the absorbed water. Water is continuously absorbed by our F-NIPAM. At the same time, the absorbed water is released to the NaCl aqueous solution bath. Utilizing this apparatus, we conducted the continuous oil-water separation (Figs. 4.44b and 4.44c). Here, water is dyed blue while oil is dyed red. Upon application of oil-water mixture on top of our F-NIPAM, water is selectively absorbed while oil is repelled. Simultaneously, F-NIPAM continuously releases the absorbed water to the NaCl solution bath. Release of the absorbed water can be verified by the color change in the NaCl solution bath (Fig. 4.44c). After separation, oil remains at the top of F-NIPAM.

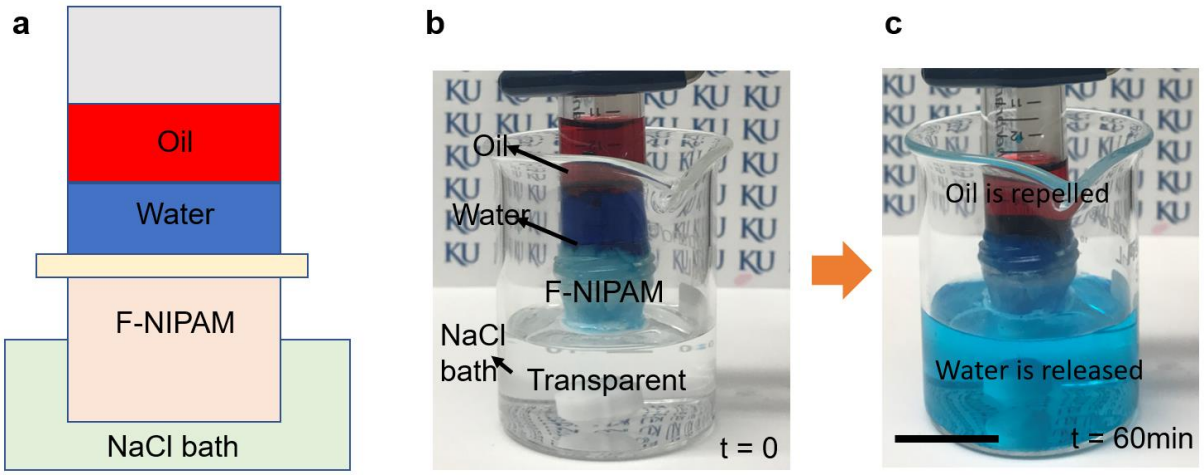

Fig. 4.44. Continuous separation of oil-water mixture and release of absorbed water. **(a)** Schematic of continuous separation setup. **(b)** F-NIPAM is placed above and in contact with NaCl bath. **(c)** When the oil-water mixture is introduced, F-NIPAM can absorb water and release to NaCl bath simultaneously. Water is dyed blue while oil is dyed red. Scale bar: 3 cm.

We further engineered the separation apparatus to continuously separate flowing oil-water mixture and to simultaneously collect both oil and water (Fig. 4.45a). F-NIPAM is prepared in the shape of a hollow cylinder (tube) such that it can contact the NaCl bath underneath it. When oil-water mixture flows through our F-NIPAM, only water is absorbed by F-NIPAM while oil slides off the surface and collected at the end of the tube. At the same time, the absorbed water will be released into the NaCl bath underneath our F-NIPAM. Figs. 4.45a and 4.45b show the continuous separation of oil-water mixture. The F-NIPAM tube is inclined slightly to allow the introduced oil-water mixture to slide through the hollow F-NIPAM. Here water was dyed blue whereas oil was dyed red. When oil-water mixture is introduced, only water is selectively absorbed by our F-NIPAM while oil is repelled. The unabsorbed oil flowed through and collected at the end of the tube. Simultaneously, our F-NIPAM releases the absorbed water into the NaCl solution bath. As the NaCl bath was colorless, the release of the absorbed water (dyed blue) can be clearly observed by the change of color (Fig. 4.45c).

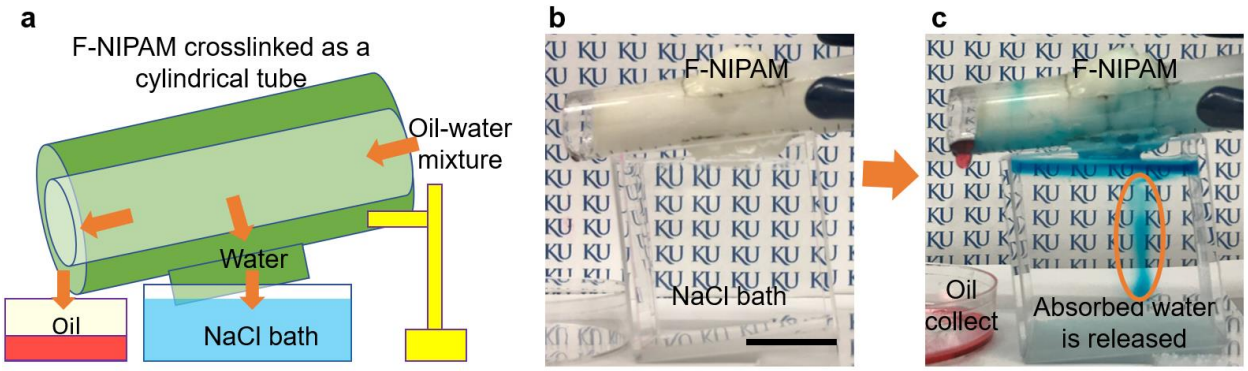

Fig. 4.45. Continuous separation of the oil-water mixture when it is flowing through F-NIPAM tube, that is in contact with aqueous NaCl solution. **(a)** Schematic of continuous separation setup. **(b)** F-NIPAM is placed over NaCl solution such that they are in contact. **(c)** After oil-water mixture slides through the F-NIPAM hollow tube, it simultaneously absorbs water and releases to the NaCl bath while repelled oil can be collected. Water is dyed blue while oil is dyed red. Scale bar: 3 cm.

5. Conclusion and Outlook

5.1. Conclusion

In this thesis, we demonstrate the separation of both immiscible and miscible liquid mixtures by using a simple absorption-based technique. First, we fabricate a hydrophilic and oleophobic (HL/OP) F-NIPAM by copolymerizing N-Isopropylacrylamide (NIPAM) with a low surface energy 1H,1H,2H,2H-Heptadecafluorodecyl acrylate (F-acrylate). The presence of acrylic groups ($-CH_2=CH-CO-$) in both NIPAM and F-acrylate allows for the copolymerization.

Our F-NIPAM can selectively absorb water while repelling oil resulting in the separation of oil-water mixtures with greater than 99% separation efficiency. In addition, our F-NIPAM can separate miscible polar-non-polar (such as heptane-ethanol or methanol-methyl oleate) liquid mixtures by selectively absorbing polar liquid over non-polar liquid. Such selective absorption behavior of our F-NIPAM can be characterized by the Flory-Huggins polymer-solvent interaction parameter (χ). The χ values of our F-NIPAM with polar liquids are ≤ 0.5 while that with non-polar liquids are greater than 0.5. This indicates that our F-NIPAM can effectively absorb polar liquids while repelling non-polar liquids.

Guided by the above principles, we demonstrate that our F-NIPAM can separate miscible polar-polar liquids by selectively making the χ value for one phase (water) greater than 0.5. Increasing the χ value for water can be achieved by increasing the temperature above the LCST.

We show that our F-NIPAM can release the absorbed liquid with the application of mild heat or submerged in an aqueous sodium chloride (NaCl) solution. Our F-NIPAM can release $\approx$

82% of the absorbed water at T = 33°C. By submerging our F-NIPAM in an aqueous sodium chloride (NaCl) solution, ≈ 98% of the absorbed water or ethanol can be released.

Finally, we engineer the separation apparatus that allows for continuous separation of liquid mixtures and in situ release of the absorbed liquid from our F-NIPAM. Utilizing the apparatus, we successfully demonstrate the separation of oil-water mixture and simultaneous recovery of the absorbed water from our F-NIPAM.

5.2. Outlook

Selective absorption of our F-NIPAM has potential applications in wastewater remediation[166], biofuel production[167], water purification and removal of contaminants from groundwater[168]. As F-NIPAM can selectively absorb polar liquids while repelling non-polar liquids, our F-NIPAM can separate a wide range of liquid mixtures including oil and water or alcohol and hydrocarbons. In addition, our F-NIPAM can be fabricated by a simple and fast photocuring method that can allow for mass production within a short period of time. Further oleophobicity of our F-NIPAM prevents the fouling by effectively repelling oils. This will enhance the lifespan of our F-NIPAM. Lastly, the absorbed liquid can be readily released either by mild heat treatment or by submerging it in an aqueous salt solution.

References

1 Energy, U. S. D. o. Bandwidth Study on Energy Use and Potential Energy Saving Opportunities in U.S. Petroleum Refining (2015).

2 Laboratory, O. R. N. Materials for Separation Technologies: Energy and Emission Reduction Opportunities. (2005).

3 Górak, A. & Sorensen, E. *Distillation: fundamentals and principles*. (Academic Press, 2014).

4 Grandison, A. S. *Separation processes in the food and biotechnology industries*. (CRC Press, 1996).

5 Hanson, C. *Recent advances in liquid-liquid extraction*. (Elsevier, 2013).

6 Zhang, J. & Seeger, S. Polyester materials with superwetting silicone nanofilaments for oil/water separation and selective oil absorption. *Advanced Functional Materials* **21**, 4699-4704 (2011).

7 Zhu, Y., Wang, D., Jiang, L. & Jin, J. Recent progress in developing advanced membranes for emulsified oil/water separation. *NPG Asia materials* **6**, e101 (2014).

8 Kiss, A. A. Distillation technology–still young and full of breakthrough opportunities. *Journal of Chemical Technology & Biotechnology* **89**, 479-498 (2014).

9 Buchaly, C., Kreis, P. & Górak, A. Hybrid separation processes—Combination of reactive distillation with membrane separation. *Chemical Engineering and Processing: Process Intensification* **46**, 790-799 (2007).

10 El-Sayed, Y. & Silver, R. Fundamentals of distillation. *Principles of desalination*, 55-109 (1980).

11 Kiss, A. A., Landaeta, S. J. F. & Ferreira, C. A. I. Towards energy efficient distillation technologies–Making the right choice. *Energy* **47**, 531-542 (2012).

12 Nature. Seven Chemical Separations to change the world. (2016).

13 Laboratory, O. R. N. *Materials for Separation Technologies: Energy and Emission Reduction Opportunities*, <https://www1.eere.energy.gov/manufacturing/industries_technologies/imf/pdfs/separationsreport.pdf> (2005).

14 Pereiro, A. B. & Rodríguez, A. Separation of ethanol− heptane azeotropic mixtures by solvent extraction with an ionic liquid. *Industrial & Engineering Chemistry Research* **48**, 1579-1585 (2008).

15 Oliveira, F. S., Pereiro, A. B., Rebelo, L. P. & Marrucho, I. M. Deep eutectic solvents as extraction media for azeotropic mixtures. *Green Chemistry* **15**, 1326-1330 (2013).

16 Pereiro, A., Araújo, J., Esperança, J., Marrucho, I. & Rebelo, L. Ionic liquids in separations of azeotropic systems–A review. *The Journal of Chemical Thermodynamics* **46**, 2-28 (2012).

17 Huddleston, J. G., Willauer, H. D., Swatloski, R. P., Visser, A. E. & Rogers, R. D. Room temperature ionic liquids as novel media for 'clean'liquid–liquid extraction. *Chemical Communications*, 1765-1766 (1998).

18 Adebajo, M. O., Frost, R. L., Kloprogge, J. T., Carmody, O. & Kokot, S. Porous materials for oil spill cleanup: a review of synthesis and absorbing properties. *Journal of Porous materials* **10**, 159-170 (2003).

19 Xue, Z., Cao, Y., Liu, N., Feng, L. & Jiang, L. Special wettable materials for oil/water separation. *Journal of Materials Chemistry A* **2**, 2445-2460 (2014).
20 Wang, C.-F. & Lin, S.-J. Robust superhydrophobic/superoleophilic sponge for effective continuous absorption and expulsion of oil pollutants from water. *ACS applied materials & interfaces* **5**, 8861-8864 (2013).
21 Su, C. Highly hydrophobic and oleophilic foam for selective absorption. *Applied Surface Science* **256**, 1413-1418 (2009).
22 Brown, P. S. & Bhushan, B. Bioinspired, roughness-induced, water and oil super-philic and super-phobic coatings prepared by adaptable layer-by-layer technique. *Scientific reports* **5**, 14030 (2015).
23 Zhou, S., Jiang, W., Wang, T. & Lu, Y. Highly hydrophobic, compressible, and magnetic polystyrene/Fe3O4/graphene aerogel composite for oil–water separation. *Industrial & Engineering Chemistry Research* **54**, 5460-5467 (2015).
24 Su, C., Yang, H., Song, S., Lu, B. & Chen, R. A magnetic superhydrophilic/oleophobic sponge for continuous oil-water separation. *Chemical Engineering Journal* **309**, 366-373 (2017).
25 Tuteja, A. *et al.* Designing superoleophobic surfaces. *Science* **318**, 1618-1622 (2007).
26 Tang, Z., Hess, D. W. & Breedveld, V. Fabrication of oleophobic paper with tunable hydrophilicity by treatment with non-fluorinated chemicals. *Journal of Materials Chemistry A* **3**, 14651-14660 (2015).
27 Xue, Z. *et al.* A novel superhydrophilic and underwater superoleophobic hydrogel-coated mesh for oil/water separation. *Advanced Materials* **23**, 4270-4273 (2011).
28 Flory, P. J. *Principles of polymer chemistry*. (Cornell University Press, 1953).
29 Huggins, M. L. Some properties of solutions of long-chain compounds. *The Journal of Physical Chemistry* **46**, 151-158 (1942).
30 Feng, X. & Jiang, L. Design and creation of superwetting/antiwetting surfaces. *Advanced Materials* **18**, 3063-3078 (2006).
31 Bico, J., Thiele, U. & Quéré, D. Wetting of textured surfaces. *Colloids and Surfaces A: Physicochemical and Engineering Aspects* **206**, 41-46 (2002).
32 Kota, A. K., Li, Y., Mabry, J. M. & Tuteja, A. Hierarchically structured superoleophobic surfaces with ultralow contact angle hysteresis. *Advanced materials* **24**, 5838-5843 (2012).
33 Li, C. *et al.* Paper-Based Surfaces with Extreme Wettabilities for Novel, Open-Channel Microfluidic Devices. *Advanced Functional Materials* **26**, 6121-6131 (2016).
34 Young, T. An assay on the cohesion of fluids. Philos. (TR Soc., 95: 65–87, 1805).
35 Zisman, W. A. Relation of the equilibrium contact angle to liquid and solid constitution. *Advan. Chem. Ser.* **43**, 1-51 (1964).
36 Kota, A. K., Kwon, G. & Tuteja, A. The design and applications of superomniphobic surfaces. *NPG Asia Materials* **6**, e109 (2014).
37 Pan, S., Kota, A. K., Mabry, J. M. & Tuteja, A. Superomniphobic surfaces for effective chemical shielding. *Journal of the American Chemical Society* **135**, 578-581 (2012).
38 Kang, S. M. *et al.* Robust superomniphobic surfaces with mushroom-like micropillar arrays. *Soft Matter* **8**, 8563-8568 (2012).
39 Kamusewitz, H., Possart, W. & Paul, D. The relation between Young's equilibrium contact angle and the hysteresis on rough paraffin wax surfaces. *Colloids and Surfaces A: Physicochemical and Engineering Aspects* **156**, 271-279 (1999).

40 Kwok, D., Gietzelt, T., Grundke, K., Jacobasch, H.-J. & Neumann, A. W. Contact angle measurements and contact angle interpretation. 1. Contact angle measurements by axisymmetric drop shape analysis and a goniometer sessile drop technique. *Langmuir* **13**, 2880-2894 (1997).
41 Joanny, J. & De Gennes, P.-G. A model for contact angle hysteresis. *The journal of chemical physics* **81**, 552-562 (1984).
42 Johnson Jr, R. E. & Dettre, R. H. Contact angle hysteresis. III. Study of an idealized heterogeneous surface. *The journal of physical chemistry* **68**, 1744-1750 (1964).
43 Nosonovsky, M. & Bhushan, B. Superhydrophobic surfaces and emerging applications: non-adhesion, energy, green engineering. *Current Opinion in Colloid & Interface Science* **14**, 270-280 (2009).
44 Dufour, R., Harnois, M., Thomy, V., Boukherroub, R. & Senez, V. Contact angle hysteresis origins: Investigation on super-omniphobic surfaces. *Soft Matter* **7**, 9380-9387 (2011).
45 Gao, L. & McCarthy, T. J. Contact angle hysteresis explained. *Langmuir* **22**, 6234-6237 (2006).
46 Wang, W. *et al.* Superhydrophobic coatings with edible materials. *ACS applied materials & interfaces* **8**, 18664-18668 (2016).
47 Yun, S. Bouncing of an ellipsoidal drop on a superhydrophobic surface. *Scientific reports* **7**, 17699 (2017).
48 Zhi, J. & Zhang, L.-Z. Durable superhydrophobic surfaces made by intensely connecting a bipolar top layer to the substrate with a middle connecting layer. *Scientific reports* **7**, 9946 (2017).
49 Kota, A. K., Mabry, J. M. & Tuteja, A. Superoleophobic surfaces: design criteria and recent studies. *Surface Innovations* **1**, 71-83 (2013).
50 Howarter, J. A., Genson, K. L. & Youngblood, J. P. Wetting behavior of oleophobic polymer coatings synthesized from fluorosurfactant-macromers. *ACS applied materials & interfaces* **3**, 2022-2030 (2011).
51 Kota, A. K., Choi, W. & Tuteja, A. Superomniphobic surfaces: design and durability. *MRS bulletin* **38**, 383-390 (2013).
52 Kwon, G., Post, E. & Tuteja, A. Membranes with selective wettability for the separation of oil–water mixtures. *MRS Communications* **5**, 475-494 (2015).
53 Kota, A. K., Kwon, G., Choi, W., Mabry, J. M. & Tuteja, A. Hygro-responsive membranes for effective oil–water separation. *Nature communications* **3**, 1025 (2012).
54 Brown, P., Atkinson, O. & Badyal, J. Ultrafast oleophobic–hydrophilic switching surfaces for antifogging, self-cleaning, and oil–water separation. *ACS applied materials & interfaces* **6**, 7504-7511 (2014).
55 Yang, J. *et al.* Superhydrophilic–superoleophobic coatings. *Journal of Materials Chemistry* **22**, 2834-2837 (2012).
56 Wang, Y., Dugan, M., Urbaniak, B. & Li, L. Fabricating Nanometer-Thick Simultaneously Oleophobic/Hydrophilic Polymer Coatings via a Photochemical Approach. *Langmuir* **32**, 6723-6729 (2016).
57 Wang, Y. & Gong, X. Special oleophobic and hydrophilic surfaces: approaches, mechanisms, and applications. *Journal of Materials Chemistry A* **5**, 3759-3773 (2017).
58 Tuteja, A., Choi, W., Mabry, J. M., McKinley, G. H. & Cohen, R. E. Robust omniphobic surfaces. *Proceedings of the National Academy of Sciences* **105**, 18200-18205 (2008).

59 Hare, E., Shafrin, E. & Zisman, W. Properties of films of adsorbed fluorinated acids. *The Journal of physical chemistry* **58**, 236-239 (1954).
60 Schulman, F. & Zisman, W. The spreading of liquids on low-energy surfaces. V. Perfluorodecanoic acid monolayers. *Journal of Colloid Science* **7**, 465-481 (1952).
61 Fox, H. & Zisman, W. The spreading of liquids on low energy surfaces. I. polytetrafluoroethylene. *Journal of Colloid Science* **5**, 514-531 (1950).
62 Fox, H. & Zisman, W. Some advances in techniques for the study of adsorbed monolayers at the liquid-air interface. *Review of Scientific Instruments* **19**, 274-274 (1948).
63 Nishino, T., Meguro, M., Nakamae, K., Matsushita, M. & Ueda, Y. The lowest surface free energy based on− CF3 alignment. *Langmuir* **15**, 4321-4323 (1999).
64 Wang, X. *et al*. Fluorinated polyhedral oligomeric silsesquioxanes. *RSC Advances* **5**, 4547-4553 (2015).
65 Patankar, N. A. On the modeling of hydrophobic contact angles on rough surfaces. *Langmuir* **19**, 1249-1253 (2003).
66 Marmur, A. Wetting on hydrophobic rough surfaces: to be heterogeneous or not to be? *Langmuir* **19**, 8343-8348 (2003).
67 Wenzel, R. N. Resistance of solid surfaces to wetting by water. *Industrial & Engineering Chemistry* **28**, 988-994 (1936).
68 Cassie, A. & Baxter, S. Wettability of porous surfaces. *Transactions of the Faraday society* **40**, 546-551 (1944).
69 Owens, D. K. & Wendt, R. Estimation of the surface free energy of polymers. *Journal of applied polymer science* **13**, 1741-1747 (1969).
70 Fowkes, F. M. Attractive forces at interfaces. *Industrial & Engineering Chemistry* **56**, 40-52 (1964).
71 Zhang, X., Li, Z., Liu, K. & Jiang, L. Bioinspired multifunctional foam with self-cleaning and oil/water separation. *Advanced Functional Materials* **23**, 2881-2886 (2013).
72 Cheryan, M. & Rajagopalan, N. Membrane processing of oily streams. Wastewater treatment and waste reduction. *Journal of membrane science* **151**, 13-28 (1998).
73 Lee, M.-H., Oh, S.-G., Moon, S.-K. & Bae, S.-Y. Preparation of silica particles encapsulating retinol using O/W/O multiple emulsions. *Journal of colloid and interface science* **240**, 83-89 (2001).
74 Matsumoto, S., Kita, Y. & Yonezawa, D. An attempt at preparing water-in-oil-in-water multiple-phase emulsions. *Journal of Colloid and Interface Science* **57**, 353-361 (1976).
75 Program, H. S. R. C. S. S. O. Environmental Impact of the Petroleum Industry. (2003).
76 Atadashi, I., Aroua, M. & Aziz, A. A. Biodiesel separation and purification: a review. *Renewable Energy* **36**, 437-443 (2011).
77 Bournay, L., Casanave, D., Delfort, B., Hillion, G. & Chodorge, J. New heterogeneous process for biodiesel production: a way to improve the quality and the value of the crude glycerin produced by biodiesel plants. *Catalysis Today* **106**, 190-192 (2005).
78 Hong, Y. K. & Hong, W. H. Removal of acetic acid from aqueous solutions containing succinic acid and acetic acid by tri-n-octylamine. *Separation and purification technology* **42**, 151-157 (2005).
79 Falconer, A. Gravity separation: old technique/new methods. *Physical Separation in Science and Engineering* **12**, 31-48 (2003).

80 Al-Shamrani, A., James, A. & Xiao, H. Separation of oil from water by dissolved air flotation. *Colloids and Surfaces A: Physicochemical and Engineering Aspects* **209**, 15-26 (2002).
81 Verma, S., Prasad, B. & Mishra, I. M. Pretreatment of petrochemical wastewater by coagulation and flocculation and the sludge characteristics. *Journal of Hazardous materials* **178**, 1055-1064 (2010).
82 Yu, L., Han, M. & He, F. A review of treating oily wastewater. *Arabian journal of chemistry* **10**, S1913-S1922 (2017).
83 Luyben, W. L. Comparison of extractive distillation and pressure-swing distillation for acetone− methanol separation. *Industrial & Engineering Chemistry Research* **47**, 2696-2707 (2008).
84 Huang, Y., Baker, R. W. & Vane, L. M. Low-energy distillation-membrane separation process. *Industrial & Engineering Chemistry Research* **49**, 3760-3768 (2010).
85 Nature. *Seven chemical separations to change the world*, <https://www.nature.com/news/seven-chemical-separations-to-change-the-world-1.19799> (2016).
86 Laroche, L., Bekiaris, N., Andersen, H. W. & Morari, M. The curious behavior of homogeneous azeotropic distillation—implications for entrainer selection. *AIChE journal* **38**, 1309-1328 (1992).
87 Knapp, J. P. & Doherty, M. F. A new pressure-swing-distillation process for separating homogeneous azeotropic mixtures. *Industrial & engineering chemistry research* **31**, 346-357 (1992).
88 Li, G. & Bai, P. New operation strategy for separation of ethanol–water by extractive distillation. *Industrial & Engineering Chemistry Research* **51**, 2723-2729 (2012).
89 Huang, H.-J., Ramaswamy, S., Tschirner, U. & Ramarao, B. A review of separation technologies in current and future biorefineries. *Separation and purification technology* **62**, 1-21 (2008).
90 Reboredo-Rodríguez, P. *et al.* Ultrasound-assisted emulsification–microextraction for the determination of phenolic compounds in olive oils. *Food chemistry* **150**, 128-136 (2014).
91 Gabelman, A. & Hwang, S.-T. Hollow fiber membrane contactors. *Journal of Membrane Science* **159**, 61-106 (1999).
92 Zhang, Y. & Lee, H. K. Low-density solvent-based vortex-assisted surfactant-enhanced-emulsification liquid–liquid microextraction combined with gas chromatography–mass spectrometry for the fast determination of phthalate esters in bottled water. *Journal of Chromatography A* **1274**, 28-35 (2013).
93 Kralj, J. G., Schmidt, M. A. & Jensen, K. F. Surfactant-enhanced liquid–liquid extraction in microfluidic channels with inline electric-field enhanced coalescence. *Lab on a Chip* **5**, 531-535 (2005).
94 Nath, K. *Membrane separation processes*. (PHI Learning Pvt. Ltd., 2017).
95 Cheryan, M. *Ultrafiltration and microfiltration handbook*. (CRC press, 1998).
96 Petersen, R. J. Composite reverse osmosis and nanofiltration membranes. *Journal of membrane science* **83**, 81-150 (1993).
97 Rohrbach, K. *et al.* A cellulose based hydrophilic, oleophobic hydrated filter for water/oil separation. *Chemical Communications* **50**, 13296-13299 (2014).

98 Feng, L. *et al.* A super-hydrophobic and super-oleophilic coating mesh film for the separation of oil and water. *Angewandte Chemie* **116**, 2046-2048 (2004).
99 Zhang, F. *et al.* Nanowire-haired inorganic membranes with superhydrophilicity and underwater ultralow adhesive superoleophobicity for high-efficiency oil/water separation. *Advanced Materials* **25**, 4192-4198 (2013).
100 Zhu, X., Tu, W., Wee, K.-H. & Bai, R. Effective and low fouling oil/water separation by a novel hollow fiber membrane with both hydrophilic and oleophobic surface properties. *Journal of Membrane Science* **466**, 36-44 (2014).
101 Chen, P.-C. & Xu, Z.-K. Mineral-coated polymer membranes with superhydrophilicity and underwater superoleophobicity for effective oil/water separation. *Scientific reports* **3**, 2776 (2013).
102 Zhou, C. *et al.* Nature-inspired strategy toward superhydrophobic fabrics for versatile oil/water separation. *ACS applied materials & interfaces* **9**, 9184-9194 (2017).
103 Wang, J., Han, F., Liang, B. & Geng, G. Hydrothermal fabrication of robustly superhydrophobic cotton fibers for efficient separation of oil/water mixtures and oil-in-water emulsions. *Journal of Industrial and Engineering Chemistry* **54**, 174-183 (2017).
104 Ma, Q., Cheng, H., Fane, A. G., Wang, R. & Zhang, H. Recent development of advanced materials with special wettability for selective oil/water separation. *Small* **12**, 2186-2202 (2016).
105 Radetić, M. M., Jocić, D. M., Jovančić, P. M., Petrović, Z. L. & Thomas, H. F. Recycled wool-based nonwoven material as an oil sorbent. *Environmental science & technology* **37**, 1008-1012 (2003).
106 Annunciado, T., Sydenstricker, T. & Amico, S. Experimental investigation of various vegetable fibers as sorbent materials for oil spills. *Marine pollution bulletin* **50**, 1340-1346 (2005).
107 Gupta, R. K., Dunderdale, G. J., England, M. W. & Hozumi, A. Oil/water separation techniques: a review of recent progresses and future directions. *Journal of Materials Chemistry A* **5**, 16025-16058 (2017).
108 Gu, J. *et al.* Functionalization of biodegradable PLA nonwoven fabric as superoleophilic and superhydrophobic material for efficient oil absorption and oil/water separation. *ACS applied materials & interfaces* **9**, 5968-5973 (2017).
109 Li, Y., Zhang, Z., Wang, M., Men, X. & Xue, Q. One-pot fabrication of nanoporous polymer decorated materials: from oil-collecting devices to high-efficiency emulsion separation. *Journal of Materials Chemistry A* **5**, 5077-5087 (2017).
110 Lei, Z., Deng, Y. & Wang, C. Ambient-temperature fabrication of melamine-based sponges coated with hydrophobic lignin shells by surface dip adsorbing for oil/water separation. *RSC Advances* **6**, 106928-106934 (2016).
111 Zhang, L., Zhang, Z. & Wang, P. Smart surfaces with switchable superoleophilicity and superoleophobicity in aqueous media: toward controllable oil/water separation. *NPG Asia Materials* **4**, e8 (2012).
112 Kwon, G. *et al.* On-demand separation of oil-water mixtures. *Advanced materials* **24**, 3666-3671 (2012).
113 Wu, L., Li, L., Li, B., Zhang, J. & Wang, A. Magnetic, durable, and superhydrophobic polyurethane@ Fe3O4@ SiO2@ fluoropolymer sponges for selective oil absorption and oil/water separation. *ACS applied materials & interfaces* **7**, 4936-4946 (2015).

114 Kulawardana, E. U. & Neckers, D. C. Photoresponsive oil sorbers. *Journal of Polymer Science Part A: Polymer Chemistry* **48**, 55-62 (2010).
115 Kopeček, J. Polymer chemistry: swell gels. *Nature* **417**, 388 (2002).
116 Hoare, T. R. & Kohane, D. S. Hydrogels in drug delivery: Progress and challenges. *Polymer* **49**, 1993-2007 (2008).
117 Bhattarai, N., Gunn, J. & Zhang, M. Chitosan-based hydrogels for controlled, localized drug delivery. *Advanced drug delivery reviews* **62**, 83-99 (2010).
118 Feil, H., Bae, Y. H., Feijen, J. & Kim, S. W. Molecular separation by thermosensitive hydrogel membranes. *Journal of membrane science* **64**, 283-294 (1991).
119 Stapleton, F., Stretton, S., Papas, E., Skotnitsky, C. & Sweeney, D. F. Silicone hydrogel contact lenses and the ocular surface. *The ocular surface* **4**, 24-43 (2006).
120 Kabiri, K., Omidian, H., Zohuriaan-Mehr, M. & Doroudiani, S. Superabsorbent hydrogel composites and nanocomposites: a review. *Polymer Composites* **32**, 277-289 (2011).
121 Kamoun, E. A., Kenawy, E.-R. S. & Chen, X. A review on polymeric hydrogel membranes for wound dressing applications: PVA-based hydrogel dressings. *Journal of advanced research* **8**, 217-233 (2017).
122 Hoffman, A. S. Hydrogels for biomedical applications. *Advanced drug delivery reviews* **64**, 18-23 (2012).
123 Ahmed, E. M. Hydrogel: Preparation, characterization, and applications: A review. *Journal of advanced research* **6**, 105-121 (2015).
124 Park, T. G. & Hoffman, A. S. Synthesis and characterization of pH-and/or temperature-sensitive hydrogels. *Journal of Applied Polymer Science* **46**, 659-671 (1992).
125 Crespy, D. & Rossi, R. M. Temperature-responsive polymers with LCST in the physiological range and their applications in textiles. *Polymer International* **56**, 1461-1468 (2007).
126 Fujishige, S., Kubota, K. & Ando, I. Phase transition of aqueous solutions of poly (N-isopropylacrylamide) and poly (N-isopropylmethacrylamide). *The Journal of Physical Chemistry* **93**, 3311-3313 (1989).
127 Otake, K., Inomata, H., Konno, M. & Saito, S. Thermal analysis of the volume phase transition with N-isopropylacrylamide gels. *Macromolecules* **23**, 283-289 (1990).
128 Jiang, S., Liu, F., Lerch, A., Ionov, L. & Agarwal, S. Unusual and superfast temperature-triggered actuators. *Advanced materials* **27**, 4865-4870 (2015).
129 Winnik, F. M. Fluorescence studies of aqueous solutions of poly (N-isopropylacrylamide) below and above their LCST. *Macromolecules* **23**, 233-242 (1990).
130 Hirotsu, S., Hirokawa, Y. & Tanaka, T. Volume-phase transitions of ionized N-isopropylacrylamide gels. *The Journal of chemical physics* **87**, 1392-1395 (1987).
131 Katsumoto, Y., Tanaka, T., Sato, H. & Ozaki, Y. Conformational change of poly (N-isopropylacrylamide) during the Coil− Globule transition investigated by attenuated total reflection/infrared spectroscopy and density functional theory calculation. *The Journal of Physical Chemistry A* **106**, 3429-3435 (2002).
132 Lin, S.-Y., Chen, K.-S. & Liang, R.-C. Thermal micro ATR/FT-IR spectroscopic system for quantitative study of the molecular structure of poly (N-isopropylacrylamide) in water. *Polymer* **40**, 2619-2624 (1999).

133 Bischofberger, I., Calzolari, D., De Los Rios, P., Jelezarov, I. & Trappe, V. Hydrophobic hydration of poly-N-isopropyl acrylamide: a matter of the mean energetic state of water. *Scientific reports* **4**, 4377 (2014).
134 Tamai, Y., Tanaka, H. & Nakanishi, K. Molecular dynamics study of polymer− water interaction in hydrogels. 1. Hydrogen-bond structure. *Macromolecules* **29**, 6750-6760 (1996).
135 Feil, H., Bae, Y. H., Feijen, J. & Kim, S. W. Effect of comonomer hydrophilicity and ionization on the lower critical solution temperature of N-isopropylacrylamide copolymers. *Macromolecules* **26**, 2496-2500 (1993).
136 Milner, S. T., Lacasse, M.-D. & Graessley, W. W. Why χ is seldom zero for polymer− solvent mixtures. *Macromolecules* **42**, 876-886 (2009).
137 Hansen, C. M. *Hansen solubility parameters: a user's handbook*. (CRC press, 2007).
138 Hirotsu, S. Phase transition of a polymer gel in pure and mixed solvent media. *Journal of the Physical Society of Japan* **56**, 233-242 (1987).
139 Yagi, Y., Inomata, H. & Saito, S. Solubility parameter of an N-isopropylacrylamide gel. *Macromolecules* **25**, 2997-2998 (1992).
140 Hoftyzer, P. & Van Krevelen, D. Properties of polymers. *Elsevier, New York* (1976).
141 Van Krevelen, D. W. & Te Nijenhuis, K. *Properties of polymers: their correlation with chemical structure; their numerical estimation and prediction from additive group contributions*. (Elsevier, 2009).
142 Patel, A. & Mequanint, K. in *Biomedical engineering-frontiers and challenges* (InTech, 2011).
143 Bouklas, N. & Huang, R. Swelling kinetics of polymer gels: comparison of linear and nonlinear theories. *Soft Matter* **8**, 8194-8203 (2012).
144 Li, Y. & Tanaka, T. Kinetics of swelling and shrinking of gels. *The Journal of chemical physics* **92**, 1365-1371 (1990).
145 Díez-Peña, E., Quijada-Garrido, I. & Barrales-Rienda, J. Analysis of the Swelling Dynamics of Cross-Linked P (N-iPAAm-c o-MAA) Copolymers and Their Homopolymers under Acidic Medium. A Kinetics Interpretation of the Overshooting Effect. *Macromolecules* **36**, 2475-2483 (2003).
146 Wu, C. & Yan, C.-Y. Studies of the swelling and drying kinetics of thin gelatin gel films by in situ interferometry. *Macromolecules* **27**, 4516-4520 (1994).
147 Yılmaz, Y. & Pekcan, Ö. In situ fluorescence experiments to study swelling and slow release kinetics of disc-shaped poly (methyl methacrylate) gels made at various crosslinker densities. *Polymer* **39**, 5351-5357 (1998).
148 Schott, H. Kinetics of swelling of polymers and their gels. *Journal of pharmaceutical sciences* **81**, 467-470 (1992).
149 Park, T. G. & Hoffman, A. S. Sodium chloride-induced phase transition in nonionic poly (N-isopropylacrylamide) gel. *Macromolecules* **26**, 5045-5048 (1993).
150 Lopez-Leon, T. & Fernandez-Nieves, A. Macroscopically probing the entropic influence of ions: Deswelling neutral microgels with salt. *Physical Review E* **75**, 011801 (2007).
151 Zhang, Y., Furyk, S., Bergbreiter, D. E. & Cremer, P. S. Specific ion effects on the water solubility of macromolecules: PNIPAM and the Hofmeister series. *Journal of the American Chemical Society* **127**, 14505-14510 (2005).

152 Ruel-Gariepy, E. & Leroux, J.-C. In situ-forming hydrogels—review of temperature-sensitive systems. *European Journal of Pharmaceutics and Biopharmaceutics* **58**, 409-426 (2004).
153 Sun, S., Zhang, W., Zhang, W., Wu, P. & Zhu, X. Dynamic self-aggregation behavior of a PNIPAM-based nonlinear multihydrophilic block copolymer revealed by two-dimensional correlation spectroscopy. *Soft Matter* **8**, 3980-3987 (2012).
154 Rivero, R. *et al.* Physicochemical properties of ionic and non-ionic biocompatible hydrogels in water and cell culture conditions: Relation with type of morphologies of bovine fetal fibroblasts in contact with the surfaces. *Colloids and Surfaces B: Biointerfaces* **158**, 488-497 (2017).
155 Futscher, M. H., Philipp, M., Müller-Buschbaum, P. & Schulte, A. The Role of Backbone Hydration of Poly (N-isopropyl acrylamide) Across the Volume Phase Transition Compared to its Monomer. *Scientific reports* **7**, 17012 (2017).
156 Gupta, M. & Gleason, K. K. Initiated chemical vapor deposition of poly (1H, 1H, 2H, 2H-perfluorodecyl acrylate) thin films. *Langmuir* **22**, 10047-10052 (2006).
157 Fei, R., George, J. T., Park, J. & Grunlan, M. A. Thermoresponsive nanocomposite double network hydrogels. *Soft Matter* **8**, 481-487 (2012).
158 Kanai, T., Ohtani, K., Fukuyama, M., Katakura, T. & Hayakawa, M. Preparation of monodisperse PNIPAM gel particles in a microfluidic device fabricated by stereolithography. *Polymer journal* **43**, 987 (2011).
159 Deen, G. R. & Chua, V. Synthesis and properties of new "stimuli" responsive nanocomposite hydrogels containing silver nanoparticles. *Gels* **1**, 117-134 (2015).
160 Diehl, C. & Schlaad, H. Thermo-responsive polyoxazolines with widely tuneable LCST. *Macromolecular bioscience* **9**, 157-161 (2009).
161 Kumar, V. *et al.* Fluorocarbon Coatings Via Plasma Enhanced Chemical Vapor Deposition of 1H, 1H, 2H, 2H-perfluorodecyl Acrylate-2, Morphology, Wettability and Antifouling Characterization. *Plasma Processes and Polymers* **7**, 926-938 (2010).
162 Chen, L. *et al.* Thermal-responsive hydrogel surface: tunable wettability and adhesion to oil at the water/solid interface. *Soft Matter* **6**, 2708-2712 (2010).
163 Xia, F. *et al.* Dual-responsive surfaces that switch between superhydrophilicity and superhydrophobicity. *Advanced Materials* **18**, 432-436 (2006).
164 Sun, T. *et al.* Reversible switching between superhydrophilicity and superhydrophobicity. *Angewandte Chemie International Edition* **43**, 357-360 (2004).
165 Hansen, C. & Parameters, H. S. (CRC Press, 2007).
166 Fakhru'l-Razi, A. *et al.* Review of technologies for oil and gas produced water treatment. *Journal of hazardous materials* **170**, 530-551 (2009).
167 Atadashi, I. Purification of crude biodiesel using dry washing and membrane technologies. *Alexandria Engineering Journal* **54**, 1265-1272 (2015).
168 Xiao, F., Simcik, M. F. & Gulliver, J. S. Mechanisms for removal of perfluorooctane sulfonate (PFOS) and perfluorooctanoate (PFOA) from drinking water by conventional and enhanced coagulation. *Water research* **47**, 49-56 (2013).